Welding Research

SPONSORED BY THE WELDING RESEARCH COUNCIL OF THE ENGINEERING FOUNDATION

W. SPRARAGEN, DIRECTOR

SUPPLEMENT TO THE WELDING JOURNAL, AUGUST, 1956

THE EFFECT OF ALUMINUM ADDITIONS TO MILD-STEEL WELD METAL

Aluminized steel electrodes for gas-shielded welding processes found to have a number of advantages over bare and copper-flashed electrodes containing the normal amount of deoxidizers

BY CRAIG R. SIBLEY

ABSTRACT. The mild and low-alloy steel electrodes presently used in gas-shielded arc welding are usually supplied with a bright-bare or copper-flashed surface. When these finishes are replaced by a particular coating of aluminum or aluminum-silicon alloy, two of the advantages which are achieved are improved corrosion resistance of the electrode during storage and elimination of weld-metal porosity because a large amount of aluminum can be made available for deoxidation.

Four samples of aluminum-coated steel wire welding electrodes were prepared for evaluation and comparison with bare and copper-flashed electrodes. These aluminized electrodes can be fed through standard manual or automatic welding equipment which is adapted for steel applications.

The results indicate that aluminized-steel electrodes have an advantage over bare and copper-flashed electrodes containing the normal amount of deoxidizers in the reduction of weld-metal porosity, especially in plug type deposits. In addition, the aluminized electrodes produce less spatter and better fillet-weld shape than bare and copper-flashed electrodes when carbon dioxide shielding is used. The aluminized electrodes developed less notch toughness in the as-welded metal; the fracture-transition temperature was increased above that of deposits made with bare and copper-flashed wire.

Rather large amounts of metallic aluminum were recovered in the weld metal with all the aluminized electrodes tested, and it is felt that such amounts of alloyed aluminum are beyond the range where decided benefit to the mechanical properties, specifically impact strength, might be expected.

Craig R. Sibley is associated with the Air Reduction Company, Inc., Research and Engineering Dept., Murray Hill, N. J.

Presented at the AWS National Fall Meeting held in Philadelphia, Pa., Oct. 17–21, 1955.

Introduction

The bare and copper-flashed steel electrodes currently used in gas-shielded welding processes are usually deoxidized with silicon and/or aluminum, and the finished wire generally contains a generous amount of residual deoxidizers. On occasion, weld metal porosity is encountered with these electrodes, which is believed to be caused by a lack of available deoxidizers. It has been discovered that a particular aluminum-coated steel wire eliminates or controls the formation of porosity in steel weld metal and this invention is embodied in a pending patent application. A recent article describes one method for coating in order to obtain a uniform continuous coating of aluminum.[1]

Although either silicon or aluminum can be used to control porosity arising from the rimming reaction, only aluminum would be able to reduce nitrogen porosity, because it forms a stable nitride which can be retained in steel upon solidification. Nitrogen porosity results from nitrogen pickup from air entrained in the shielding gas or from air entrapped in certain joint types. The tolerance limit for nitrogen in the deposit made with the aluminized electrode could reduce the amount of gas necessary to shield the weld. However, too much nitrogen pickup is undesirable because aluminum nitride hardens and embrittles steel and results in inferior weld metal properties.

Other effects result by the use of aluminum coated electrodes; the effective weld-metal fluidity is decreased because an aluminum oxide skin forms on the surface of the deposit to prevent wetting and good corrosion resistance is provided during storage.

Samples of various aluminum coatings were placed on a mild-steel welding-quality core wire by a hot dipping technique. The effect of these coatings on the electrode welding characteristics and the mechanical properties of the weld metal were investigated and the results of this investigation are presented herein.

Electrodes

The mild-steel wire used for the aluminum-coated electrodes in this investigation was obtained from one heat having the following chemical analysis:

C, %	0.12
Mn, %	0.63
P, %	0.027
S, %	0.020
Si, %	0.45
Ti, %	0.004
Al + Alumina, %	0.13

This wire, with a bright-bare finish, was used as a reference electrode (electrode 1) to measure the changes caused by the aluminum coating. The coated

electrodes were prepared by hot dipping in either aluminum or an aluminum-silicon alloy. The coatings on these electrodes were reported as follows:

Electrode 2—Al-3% Si alloy, 0.19 oz/sq ft
Electrode 3—Al-3% Si alloy, 0.21 oz/sq ft
Electrode 4—Pure Al, 0.22 oz/sq ft
Electrode 5b—Al-3% Si alloy, 0.21 oz/sq ft

Each electrode was finished to an approximate diameter of 0.093 in. and supplied in coil form.

Electrode 1, the bare wire, was hard drawn to finish size of 0.093 in. using a water-soluble soap lubricant with residual lubricant removed by steam cleaning.

Electrode 2 was representative of a thinner coating of aluminum-3% silicon alloy drawn 32% after coating to finish size of 0.093 in. A water-soluble lubricant and steam cleaning were used.

Electrode 3 was coated with an aluminum-3% silicon alloy at 0.093 in. size and shipped as coated; there was no sizing draft.

Electrode 4 was coated at 0.095 in. size with pure aluminum and drawn 6% by sizing to 0.092 in. A water-soluble lubricant followed by steam cleaning was used.

Electrode 5b was coated at 0.095 in. size with an aluminum-3% silicon alloy and drawn a light sizing draft to 0.093 in. in oil and was not cleaned after sizing.

Table 1—Porosity Count Taken on Bead Welds

Plate Condition		*Electrode* 1	2	3	4	5
		Welding speed, 10 ipm				
Rimmed						
Scale	(a)	2	0	0	3	4
Ground	(b)	5	2	11	11	6
Sandblast	(c)	4	4	4	5	6
Killed						
Scale	(d)	4	4	0	2	4
Ground	(e)	0	2	2	1	2
Sandblast	(f)	2	6	3	2	1
Killed						
Heavy oxide	(g)	6	0	0	0	1
Heavy + grease	(h)	1	0	0	0	3
Heavy + paint	(i)	3	0	0	0	1
		Welding speed, 30 ipm				
Rimmed						
Scale	(a)	6	2	2	0	9
Ground	(b)	7	2	1	5	7
Sandblast	(c)	10	6	10	7	4
Killed						
Scale	(d)	3	1	0	3	2
Ground	(e)	18	8	8	7	6
Sandblast	(f)	6	1	16	11	1
Killed						
Heavy oxide	(g)	1	1	0	4	5
Heavy + grease	(h)	12	1	0	0	2
Heavy + paint	(i)	8	1	0	0	1

Procedure

During the first portion of this investigation, an evaluation was made of the effect of aluminum-coated steel wire on weld-metal soundness. Bead welds were deposited on $^1/_2$-in. rimmed and killed-steel plates having surfaces that were either oxidized, sandblasted or ground. Killed-steel plates, $^3/_4$ in., also were used, having surfaces coated with iron oxide, paint or grease. The welds were made with the five 0.093-in. diam electrodes at two welding speeds, 10 ipm to represent a typical manual operation with a large molten pool and 30 ipm to represent mechanized welding in which rapid freezing of the molten pool occurs. Reverse-polarity direct current of 420–440 amp and pure argon shielding were used. Pure argon was selected as the shielding gas to eliminate possible confusion in the results arising from the composition of the shield gas. It is known that oxygen addition to argon tends to eliminate bead irregularities, which are noted on some surfaces when pure argon shielding is used.

The bead welds were radiographed to 2% sensitivity, and the number of holes occurring in each bead were counted. Typical bead weld surfaces and etched cross sections of the deposits were examined to determine uniformity of the deposit and the presence of undercutting.

Plug welds also served to evaluate the relative ability of bare and aluminum-coated electrodes to produce sound weld metal in an argon shield. A

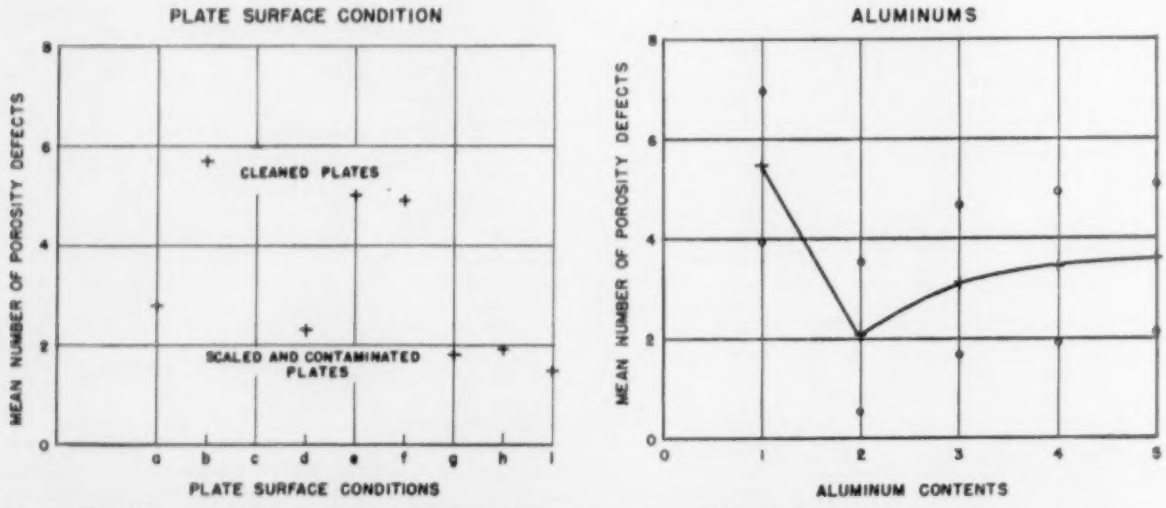
PLATE SURFACE CONDITION
MEAN NUMBER OF POROSITY DEFECTS
CLEANED PLATES
SCALED AND CONTAMINATED PLATES
a b c d e f g h i
PLATE SURFACE CONDITIONS
ALUMINUMS
MEAN NUMBER OF POROSITY DEFECTS
0 1 2 3 4 5
ALUMINUM CONTENTS

Fig. 1 Plot of mean number of porosity defects vs. aluminum contents and plate surfaces

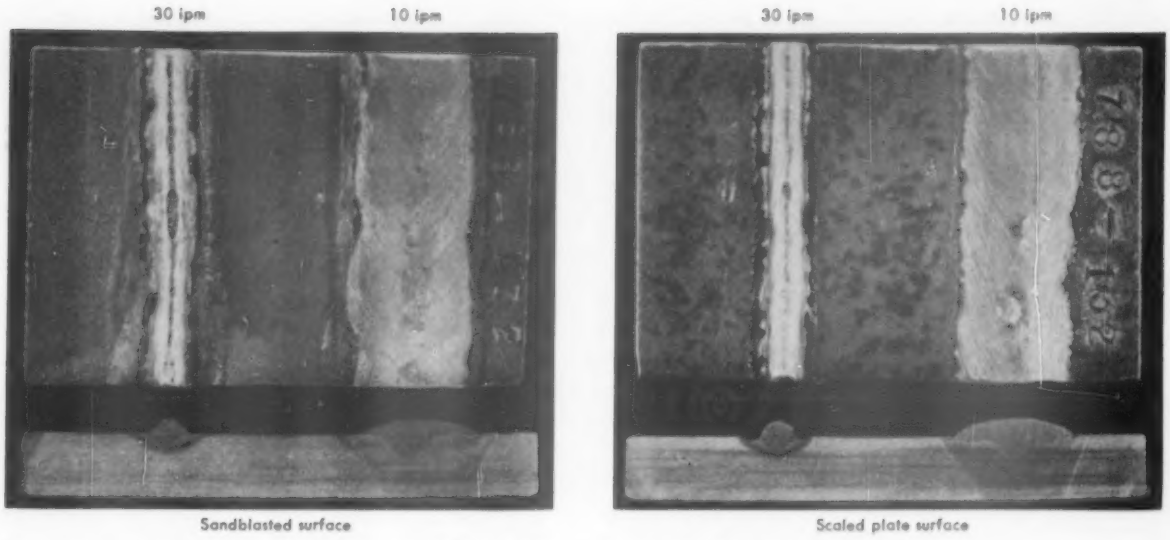

Fig. 2 Bare-electrode bead-we'd deposits at 10 and 30 ipm on scaled and sandblasted surfaces

hole 1½ in. in diameter was drilled through a 1½-in. thick plate, and the deposit was made with a steel backing by rotating the plate without interrupting the arc until the hole was filled.

To provide weld-metal specimens for mechanical property testing, all-weld-metal deposits from each electrode were made in 1-in. plate having a groove with a 45-deg included angle and a ½-in. root opening. Tensile properties in the as-welded and furnace stress-relieved (1150° F for 1 hr) conditions were obtained from 0.505-in. weld-metal tensile bars. Transverse Charpy-type impact specimens were machined from each deposit with an Izod notch centered in the weld metal. Impact testing of as-welded specimens was conducted over a range of temperature so that the fracture-transition and ductility-transition behavior could be observed.

Metallographic examination of the weld metal from each electrode was made on as-polished and etched surfaces to determine the amount of nonmetallic inclusions and the characteristic macrostructure and microstructure of each deposit.

Carbon-dioxide shielding also was used to make all-weld-metal deposits, and these results were compared to those obtained with argon shielding described above. Two of the aluminized electrodes were selected as representative to limit the production of samples.

Results of Bead Weld Tests

Soundness

Despite the fact that widely varying conditions of plate surface were used for the bead weld tests, the variations in porosity were only minor. The number of holes present in each of the bead weld deposits is listed in Table 1. Since the significance of the data illustrated in Table 1 is not readily apparent, these test data were treated statistically as a factorial experiment for which an analysis of variance could be determined. The analysis indicates that the risk of a difference being established when it does not actually exist is 5%.

The results of this experiment show that in these tests only Electrode 2 varied significantly in porosity from the uncoated Electrode 1. No significant variation exists between Electrodes 1, 3, 4, and 5b. A plot of the column mean values of the number of porosity defects for the variables, aluminum content and plate surface condition was made and is illustrated in Fig. 1.

Because only Electrode 2 was significantly different from Electrode 1, it was necessary to compare the aluminized electrodes as a group with Electrode 1 to determine if a significant reduction in porosity was brought about by the aluminum addition. The results

Table 2—Appearance of Bead Welds

Plate condition		*Electrode* 1	2	3	4	5
		10 ipm				
Rimmed						
Scale	(a)	*a, b*	*a, b*	*a, b*	*a, b*	*a, b*
Ground	(b)	*c*	*c*	*c*	*a, c*	*c*
Sandblast	(c)	*c*	*c*	*c*	*c*	*c*
Killed						
Scale	(d)	*b*	*a, b*	*a, b*	*a, b*	*a, b*
Ground	(e)	*c*	*c*	*c*	*c*	*c*
Sandblast	(f)	*c*	*c*	*c*	*c*	
Killed						
Heavy oxide	(g)	*c*	*a, b*	*a, b*	*a, b*	*a, b*
Heavy + grease	(h)	*b*	*a, b*	*a, b*	*a, b*	*a, b*
Heavy + paint	(i)	*b*	*a, b*	*a, b*	*a, b*	*a, b*
		30 ipm				
Rimmed						
Scale	(a)	*a, b*	*a, b*	*a, b*	*a, b*	*a, b*
Ground	(b)	*c, d*	*c, e*	*c, e*	*c, e*	*c, e*
Sandblast	(c)	*c, d*	*c, e*	*c, e*	*e*	*c, e*
Killed						
Scale	(d)	*a, b*	*a, b*	*a, b*	*a, b*	*a, b*
Ground	(e)	*c*	*c, e*	*c, d*	*c, e*	*c, d*
Sandblast	(f)	*c*	*b, d*	*b, d*	*b, d*	*c, e*
Killed						
Heavy oxide	(g)	*a, b*	*a, b*	*a, b*	*a, b*	*a, b*
Heavy + grease	(h)	*a, b*	*a, b*	*a, b*	*a, b*	*a, b*
Heavy + paint	(i)	*a, b*	*a, b*	*a, b*	*a, b*	*a, b*

a = Undercut. *b* = Even bead shape. *c* Uneven bead shape. *d* = Humped. *e* = Skips.

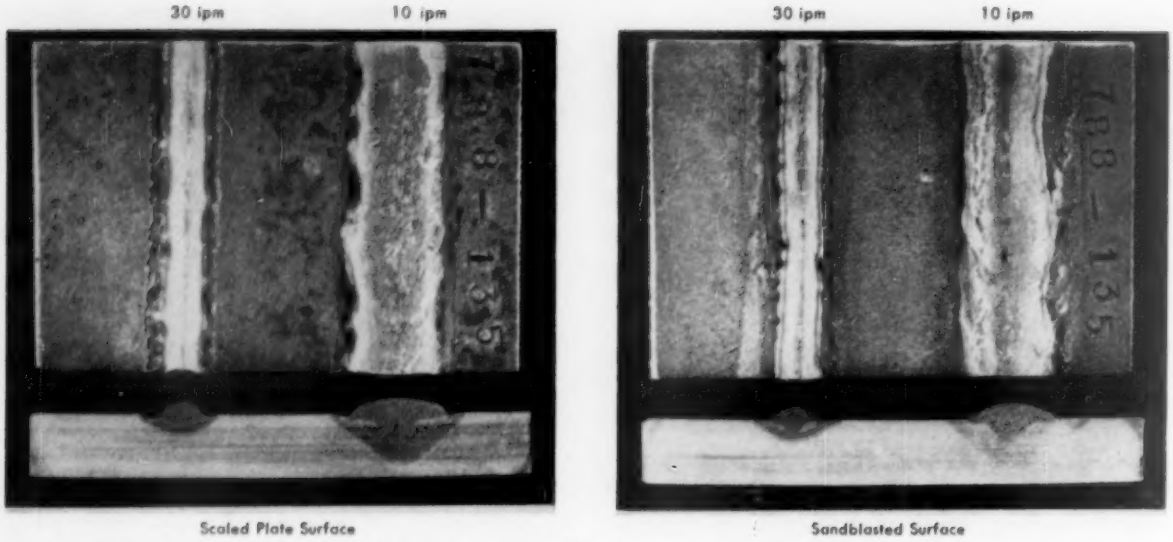

Fig. 3 Aluminized-electrode bead-weld deposits at 10 and 30 ipm on scaled and sandblasted surfaces

of this comparison indicate a significant variation in porosity between the aluminized and bare electrodes. Since the mean values of the number of porosity defects for cleaned plates were much higher than for scaled plates, as shown in Fig. 1, the two types of plates were considered together, and a significant variation was found between cleaned and scaled plate. Another question arising from the data concerned the ability of the aluminized wire to reduce porosity on the cleaned plate. Analysis proved that a significant variation between the aluminum-coated and bare wires only exists in the case of scaled plate.

Since with all the electrodes less porosity was found in welds made on scaled plate, iron oxide on the plate surface is evidently beneficial, as is the case with a shield of argon containing oxygen. If a shield of argon containing oxygen had been used, this difference in porosity probably would not have occurred. Further, it is evident that the porosity of the bead welds on the cleaned plates could be lowered by adding oxygen to the shield gas.

Shape

The surface appearance of bead welds was affected by the presence of the aluminum coating on the electrode as well as scale or other contaminants on the plate surface. An appraisal of each bead weld for undercut and shape appears in Table 2. Typical bead weld deposits made with the bare electrode at the two welding speeds on scaled and sandblasted plate surfaces are shown in Fig. 2.

The argon-shielded arc formed a deep, uniform crater on the scaled surface which advanced ahead of the deposit and was particularly evident with the 30 ipm welding speed. Serious undercut develops at this travel speed, since either the weld metal solidifies too rapidly or there is inadequate weld metal present to fill out the crater depression. The thought that inadequate weld metal exists for this condition of welding stems from the fact that quality deposits have been made using a 0.0625-in. electrode with about 350 amp, which results in a higher melting rate than that obtained with the 0.093-in. electrode deposit described herein. Also, the magnitude of the current affects the geometry of the crater depression. A similar crater was encountered at the 10 ipm travel speed, but the larger molten pool remains fluid longer and permits uniform filling of the crater, thus virtually eliminating undercut.

A wide sputtered area formed on the sandblast surface, and a depression occurred only directly below the arc. At a welding speed of 30 ipm, the bead weld varied in width without forming appreciable undercut; at 10 ipm, the weld metal wetted a large portion of the sputtered area. The cross section of

Table 3—All-Weld-Metal Tensile Test Results*

	Argon									
	As-welded					Furnace Stress Relieved (1150° F)				
Electrode No.	Yield strength, psi	Tensile strength, psi	Elongation in 2 in., %	Reduction of area, %	Fracture type	Yield strength, psi	Tensile strength, psi	Elongation in 2 in., %	Reduction of area, %	Fracture type
1	70,000	81,750	28.0	71.0	Cup-cone	55,300	70,300	32.0	66.0	Cup-cone
2	69,200	82,200	21.0	44.3	Shear	59,700	76,750	25.0	52.0	Shear
3	62,800	78,300	25.0	50.3	Shear	53,100	72,700	31.0	66.6	Cup-cone
4	59,400	76,300	26.0	62.2	Cup-cone	48,500	69,800	32.0	65.2	Cup-cone
5b	56,750	75,000	27.5	49.2	Shear	50,800	71,500	31.0	67.7	Cup-cone

	Carbon dioxide				
	As-welded				
Electrode No.	Yield strength, psi	Tensile strength, psi	Elongation in 2 in., %	Reduction of area, %	Fracture type
2	63,200	75,300	24.0	60.0	Cup-cone
4	65,600	76,100	26.0	59.0	Cup-cone

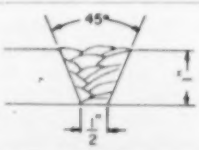

* 0.505-in. tensile specimens; multipass deposits in 1-in. plate; 0.093-in. electrodes; average of two specimens.

the bead weld reveals a lack of symmetry resulting from uneven wetting. The improved ability of the molten metal to wet the sputtered surface resulted in a greater flow of metal away from the weld centerline and a consequent reduction in reinforcement.

The arc is affected by oxides on the plate surface due to changes in the emissive phenomenon at this surface when oxides are present. Oxide films on the molten weld metal alter the wetting characteristics, which prevent the deposit spreading out. In the absence of surface films, as in the case of the deposits made on cleaned surfaces with Electrode 1, the weld metal exhibits better fluidity, thus minimizing undercut and skipping. The humping of the deposits made on the cleaned rimmed plate with Electrode 1 at the 30 ipm welding speed is unique to this condition and probably results from a number of effects, including arc action and weld-metal fluidity.

A bead weld of symmetrical cross section could be deposited on the cleaned plate if a small percentage of oxygen were mixed with the argon to form iron oxide on the plate surface, minimizing wide sputtering.

Bead welds deposited with an aluminum-coated steel electrode are shown in Fig. 3. These deposits have characteristics similar to those of the bare-wire deposits, except that the poorer weld-metal fluidity caused undercutting on the scaled surface at both welding speeds.

Undercut

The data of Table 2 clearly outline the effects of surface oxides and contamination on bead weld undercutting. Undercut is affected by the arc action on the plate surface and the wettability of the weld metal. If the arc forms a wide gouge on the plate surface, as occurred with the scaled surfaces, the weld metal must have excellent fluidity and wettability if the gouge is to be filled. On the other hand, if the arc action covers a large area of plate surface, as occurred with the cleaned surfaces, the weld metal does not have to fill a wide gouge, and undercut is minimized. The pronounced undercutting that occurs with the aluminum-coated electrodes at the 10 ipm welding speed strongly indicates that the slag formed on these deposits increases the surface tension of the weld metal. This difference in undercutting between the bare and aluminized electrodes does not exist at the 30 ipm welding speed, where undercutting occurred on all surfaces that were not cleaned. The complete absence of undercutting on cleaned surfaces at the 30 ipm welding speed for all five electrodes demonstrates the dominating effect of the plate surface condition at this speed. Bead welds which were not undercut had uneven shapes, and at the high welding speed they were prone to being humped or discontinuous. The unevenly shaped beads had good weld metal fluidity, but wet the plate surface irregularly. The discontinuity of a bead weld resulted from an oxide build-up on the surface, which caused intermittent skips to occur. The phenomenon of bead weld humping occurs during the formation of the bead and is undoubtedly affected by surface oxides on the plate as well as arc characteristics and weld-metal fluidity.

Results of Weld Metal Tests

Mechanical test results were obtained from multipass deposits made in an argon atmosphere with each of the five

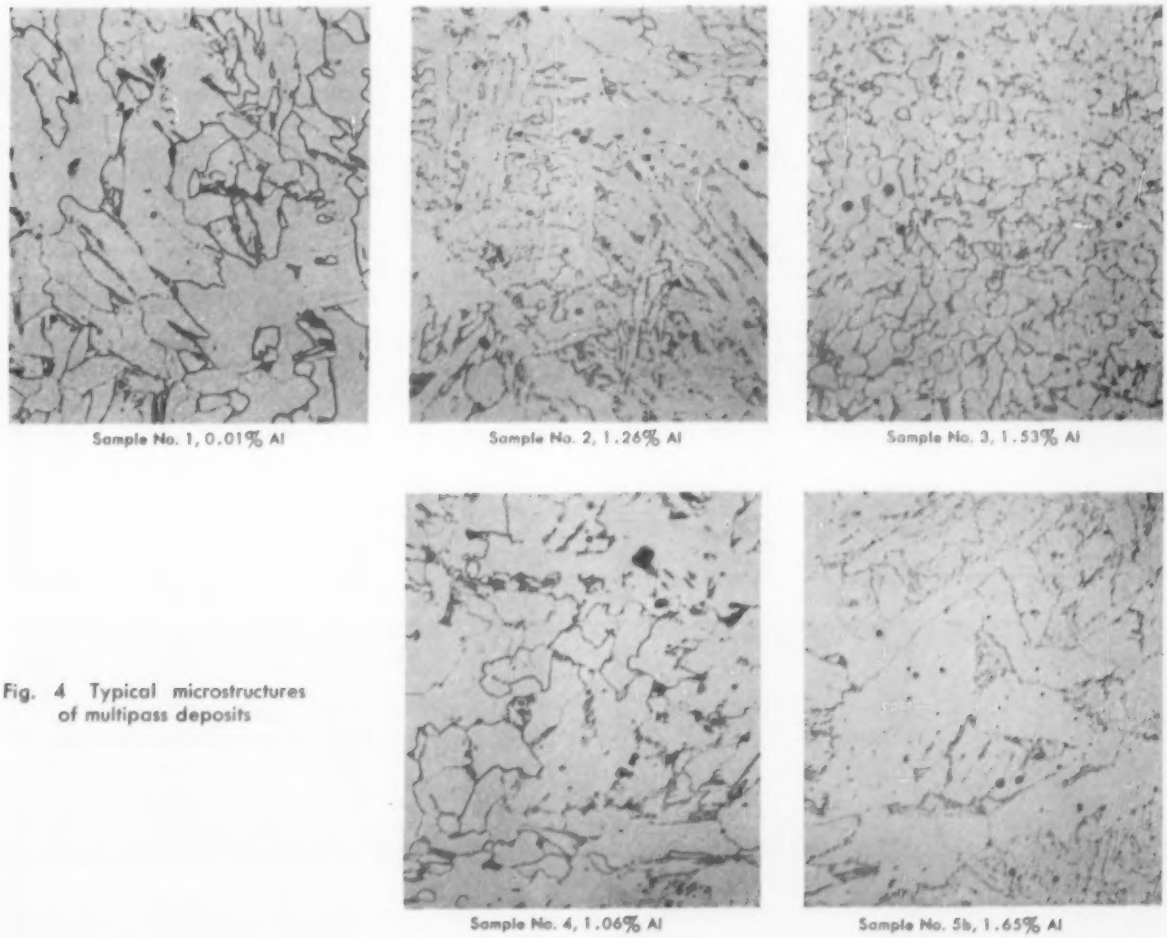

Fig. 4 Typical microstructures of multipass deposits

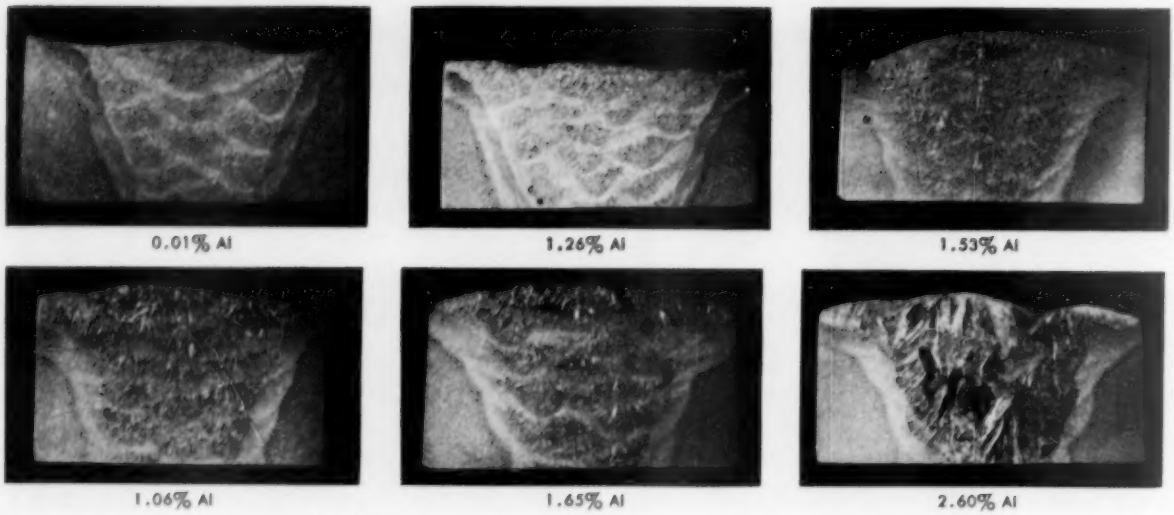

Fig. 5 Typical macrostructures of multipass deposits

electrodes. Two electrodes also were tested in a shield of carbon dioxide. The deposits were produced by machine welding with current, number of passes and welding speed being held as constant as possible throughout. No preheating was used, and the deposits were air-cooled between passes to maintain an interpass temperature below 150° F.

Tensile test data are summarized in Table 3 for both the as-welded and furnace stress-relieved deposits made in argon and the as-welded deposits made in carbon dioxide. From the as-welded results for the argon-shielded deposits it is evident that Electrode 1 has the best ductility and that the presence of aluminum coating lowers the ductility and yield strength. Furnace stress-relieving the weld metal at 1150° F lowers the tensile and yield strengths but increases the ductility. All of the deposits in the as-welded condition meet the tensile requirements of the AWS specifications for E60XX electrodes. The only deposit meeting the filler metal requirement of the AWS specification for E70XX electrodes is Electrode 2. Carbon-dioxide shielding definitely increases the as-welded ductility of the weld metal above the values obtained for argon. The differences in the yield and tensile strengths of the various deposits are much greater with argon shielding than with carbon dioxide. The greatest difference occurred with Electrode 4, which has a higher yield strength with carbon dioxide than with argon shielding.

The microstructure of a typical area of each argon-shielded deposit as seen at 500 × is shown in Fig. 4. Pronounced variations in the microstructure result from the various amounts of metallic aluminum present in the deposits. The deposits containing the most aluminum exhibit a coarsening of the dendritic grains. The photomacrographs of Fig. 5 illustrate this grain growth best since the entire dendrites are visible. To further illustrate this grain coarsening effect of aluminum, the structure of a deposit containing 2.6%

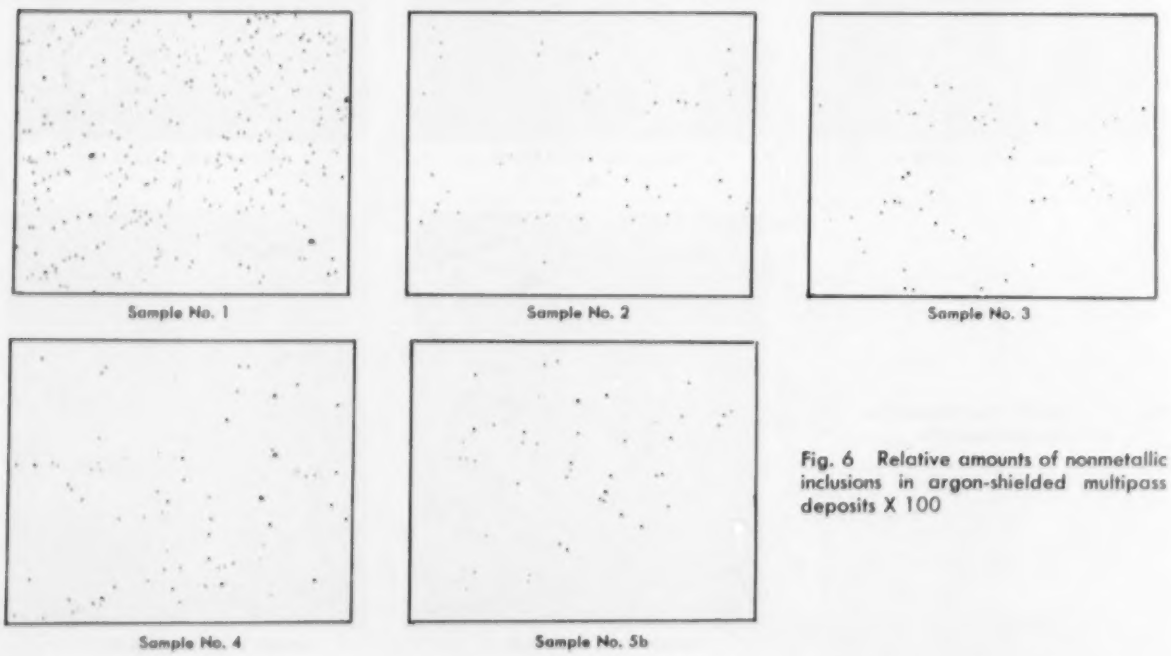

Fig. 6 Relative amounts of nonmetallic inclusions in argon-shielded multipass deposits X 100

aluminum which was made from a heavily-aluminum-coated wire is included in Fig. 5.

Each multipass deposit contained layers of coarse and fine grains, but the relative amounts of coarse and fine grains varied. In general, the alloying of aluminum caused a widening of the coarse-grained regions in the deposits. The stress-relieved deposits had microstructures similar to the as-welded, with the exception of some carbide spheroidization. The relative amounts of nonmetallic inclusions in each multipass deposit are shown in Fig. 6.

Since the behavior of steels in impact testing is affected by grain size and microstructural changes, one would expect a variation in impact performance for the structures shown in Figs. 4 and 5. A summary of the impact testing data obtained from as-welded samples of the five deposits appears in Fig. 7, where the absorbed energy is plotted against the temperature of testing. The variations exhibited are generally in accord with those expected from the structures present in the deposits. In order to evaluate the alloying effect of aluminum on the impact performance, each structure would have to be standardized in grain size through heat treatment. Such an evaluation is not of interest here since the conditions of welding are subject to change, and the resultant deposit structure would be affected by these changes.

Since the ductility in the tensile tests was increased by stress-relieving the deposits, a few exploratory checks were made to see if the impact performance changed. The results of these tests indicated no variation in impact strength due to stress relieving. Likewise, no improvement in impact performance was noted when carbon dioxide replaced argon as the shield gas.

The data of Fig. 7 apply to one condition of welding, and these results could certainly be altered by variations in welding procedures and techniques. The data for the argon-shielded deposits indicate that the alloying of aluminum in mild steel weld metal in the range of 1.06 to 1.65% causes the impact transition to shift toward higher temperatures. Its action duplicates that of phosphorus

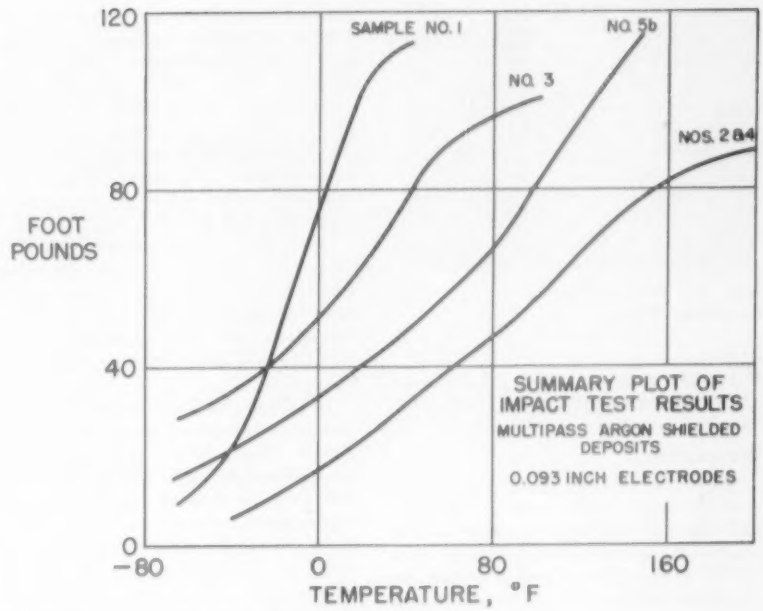

Fig. 7 Summary plot of impact test results

in wrought steels, since the upper and lower energy absorption values do not change greatly. In addition, the data indicate sharp variations in transition temperatures for small changes in aluminum content within the range of alloys tested.

Results of Plug Weld Tests

The pronounced difference in porosity of plug welds made with bare and aluminized electrodes is shown in Fig. 8. The two small defects evident in the deposit from the aluminized wire are caused by lack of fusion, a condition which was common to multipass aluminized wire deposits. Prior to establishing the arc, the hole was purged with argon in an attempt to exclude the air. The heavy porosity produced in the bare wire deposit is believed to have resulted from air entering the argon shield. Due to a fault in the setup, part of the gas nozzle was over the plate surface at the start, which gave a condition of possible turbulence. As the hole became filled, the possibility of entraining air in the shield diminished, since the gas nozzle was raised above the plate surface during welding. Since the bare electrode may not have had sufficient deoxidants to prevent the rimming reaction, the oxygen component of the air could have been responsible for the holes. However, when welding with the aluminized wire, the soundness of the deposit could result from the aluminum forming a stable nitride and thus preventing the formation of porosity by nitrogen. If this postulate were true, then one would expect to find evidence of aluminum nitride in the sound plug welds. Samples were taken from such welds and subjected to a heat treatment designed to precipitate aluminum nitride in the structure. Examination of these samples revealed positive evidence of nitride needles of the type found in nitrided steels. The photomicrograph of Fig. 9 illustrates the nitride needles present in a typical field of view.

The important implication to be drawn from these results is that perhaps less shielding gas would be required to obtain sound deposits with aluminized steel electrodes. However, the presence

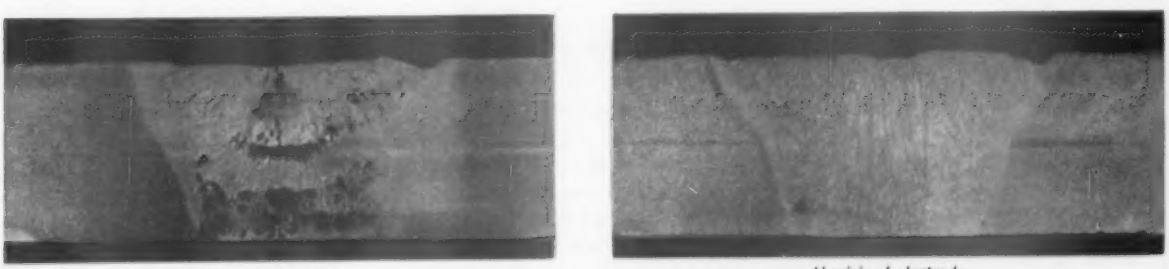

Bare electrode

Aluminized electrode

Fig. 8 Plug welds: bare wire vs. aluminized wire

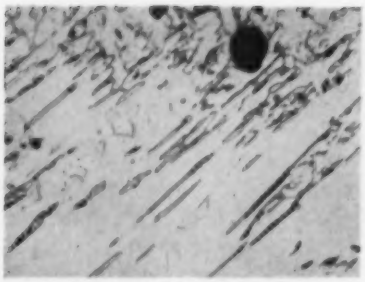

Fig. 9 Photomicrograph of nitride needles

of nitrogen in steel, whether as a gas or in combined form, generally alters adversely its mechanical properties.

Discussion

Since the use of aluminum-coated steel electrodes could cause mechanical difficulties in feeding, such as those encountered in aluminum welding, the ability to feed these electrodes through standard welding equipment was evaluated.

During the production of the bead welds and multipass deposits for mechanical testing, approximately 30 lb of each of the 0.093-in. electrodes were fed through automatic welding equipment without difficulty. Two of the 0.093-in. electrodes, No. 2 and No. 4, were fed through manual equipment adapted for heavy-duty steel welding and having a serrated drive roll. A continuous welding arc was maintained for five minutes as a feeding test.

The conclusion resulting from the feeding tests is that aluminized electrodes of the types tested can be fed through automatic and manual welding equipment adapted for steel electrodes.

Summary

The aluminum-coated steel wires used in this investigation were processed to welding electrodes by various coating and drawing techniques. Data were obtained with these electrodes to evaluate their performance in welding over a range of applications characteristic of welding steel by the gas-shielded arc processes. The standard performance was determined with an uncoated electrode.

Mechanical test results reported herein for the case of argon shielding indicate that when these aluminized wires are used as welding electrodes, the deposited weld metal is somewhat inferior to that deposited with bare electrodes.

Metallographic examination of multipass deposits revealed coarse dendrites in certain cases where the aluminized electrodes were used. These dendrites were prone to growing across individual pass boundaries and caused some loss of pass detail in the cross-sectional macrostructure. Variations in the microstructure also existed which affected the mechanical properties, especially in the impact strength.

Porosity formed in argon-shielded bead weld deposits made on several types of plate surface was reduced when the aluminized electrodes replaced the bare electrode. This reduction in porosity was significant, but the number of holes per inch involved in both cases was small and within the scope of serviceable weld metal density. In the case of a plug weld, the reduction in porosity was marked when the aluminized electrode replaced the bare one.

The amount of metallic aluminum recovered in multipass deposits constitutes a considerable alloy addition to the mild-steel weld metal, and the resultant effects on the constitution of the alloys caused changes in the kinetics of nucleation and grain growth.

The changes which occurred over the narrow range of aluminum content present in the deposits caused a large shift in the mechanical behavior of the weld metal. Since it is impossible to predict the exact amount of aluminum which would be recovered with a given aluminized electrode, the prediction of mechanical behavior would be uncertain.

A serious gap in the data exists between 0.01 and 1.06% aluminum which prevents anything but conjecture being applied to the behavior in this region. It might be that aluminum alloyed below 1.06% could have a beneficial effect on the mechanical properties. Some investigators[2] have shown small additions of aluminum (0.10%) to be beneficial in lowering the Tear-Test transition temperature of wrought steels. It is believed that similar effects in steel weld metal are brought about by 0.5% aluminum in the deposit.

Carbon-dioxide shielding has a leveling effect on the tensile properties obtained with bare and aluminized electrode deposits. The amount of aluminum recovered in these deposits would be less than in argon-shielded deposits since the oxygen from dissociated carbon dioxide can form considerable aluminum oxide during welding. However, this reduction in alloyed aluminum did not cause improvements in the impact test performance.

The porosity of carbon-dioxide-shielded bead weld and multipass deposits was generally less than for similar argon-shielded deposits.

References

1. Westerman, B. S., "New Aluminizing Process for Steel Wire." *Wire and Wire Products*, 30 (4), 419 (1955).

2. Boulger, F. W., and Frazier, R. H., "Some Metallurgical Aspects of Low-Temperature Behavior of Metals." Conference on Materials and Design for Low-Temperature Service, 1955. Fort Belvoir, Va., Department of the Army Corps of Engineers.

Weldability of Steels

Copies of the monograph entitled "WELDABILITY OF STEELS" by Robert D. Stout and W. D'O. Doty, who were commissioned by the Weldability Committee of the WELDING RESEARCH COUNCIL to prepare this book, are still available for distribution. This monograph consists of 381 pages, handsomely bound and copiously illustrated. A limited edition of this book has been published. The list price is $6.50. Special arrangements with the American Welding Society are such that Members of the Council and the American Welding Society receive a 20% discount from the list price. The distribution of four or more copies will be handled by the WELDING RESEARCH COUNCIL. Less than four copies may be ordered from the American Welding Society, 33 West 39th Street, New York 18, N. Y.

INFLUENCE OF OXYGEN ON SOUNDNESS AND DUCTILITY OF MOLYBDENUM WELDS

Oxygen in the base metal or in the welding atmosphere is found to cause hot cracking, porosity and low ductility

BY W. N. PLATTE

ABSTRACT. The effects of oxygen in the base metal and in the welding atmosphere on the occurrence of hot cracks, porosity and low ductility are discussed. The necessity for deoxidization of the base metal is shown and the effectiveness of several deoxidizing agents, including carbon, titanium, tantalum, niobium and aluminum, is examined.

The harmful effects of small quantities of oxygen in the welding atmosphere are shown. Oxygen limits are established for hot cracking in the weld beads and for maximum ductility in bending.

Introduction

The formation of molybdenum welds which are sound and have a satisfactory degree of ductility is an involved problem. However, the ultimate solution of this problem may have applications that are not limited to molybdenum alone. Many of the difficulties encountered in joining of molybdenum are also found in varying degrees of complexity in other body-centered cubic materials, such as Fe, W, and Cr, which show an increase in yield strength with decreasing temperature. Problems of base metal quality, welding techniques, and evaluation methods are all involved in the solution of joining problems in these materials, and must be approached simultaneously.

In the past, welds in molybdenum have been made using both electrical-resistance and arc-welding techniques. A number of inherent disadvantages exist in each of these methods. Low ductility has been characteristic of all types of welds with the exception of percussive welds.[1, 2] Porosity and hot cracking are prevalent in welds formed using the shielded-electric-arc process. Excessive electrode sticking and material contamination occur in the spot- and seam-welding processes. The resistance-butt and flash-butt welding processes both require shielding during welding or special high-speed equipment to prevent oxidization and are limited in application to particular types and sizes of joints.[2, 3] The latter limitation is especially applicable to the use of percussive welding which, while it produces fairly ductile welds, is limited to small sections. Of the welding methods available, the inert-gas arc is the most versatile; it can be used to produce most types of joints. Because of this wide field of potential usefulness work was undertaken in using the inert-gas-shielded tungsten-arc process for welding molybdenum.

Welds made using any of the fusion-welding processes are subject to the same basic problems inherent in any cast structure, complicated by the fact that weld metals are bonded to the mold and subjected to all the restraint implied by this condition. Large dendritic grains and ingot characteristics are present. Trapped or combined gases in the original material or dissolved in the molten puddle during welding tend to be released either while the metal is molten or on cooling. This may cause weld porosity. Impurities segregating in the grain boundaries may cause either hot short cracking or low ductility at room temperature. The effects of porosity and segregation are emphasized by the restraint imposed on the weld during solidification. Welds in molybdenum involve no exceptions to these phenomena.

Molybdenum and most other body-centered-cubic materials are subject to a rise in the yield strength when the temperature is decreased. Brittle fracture occurs when the yield strength reaches the fracture strength of the material. Bechtold[4] has shown that the fracture strength is dependent upon the grain size. His work explains in part the difficulties encountered in fusion welding molybdenum. Perry, Spacil and Wulff[5] suggest that the grain boundaries of molybdenum are wet by a eutectic of MoO_3 and Mo at temperatures in the welding range. They also show that MoO_3 is sufficiently volatile above 3800° F to cause porosity. The combination of large grain size and grain boundary precipitates may explain the low ductility found in molybdenum fusion welds. Porosity and hot cracking can also be explained by oxides in the weld metal. The work of Battelle investigators[6,7] showed that the impurity content of cast molybdenum must be held at a minimum if a ductile material is to be obtained. It is apparent that if sound ductile weld metal is to be produced the material must have a low initial impurity content and the acquisition of impurities must be minimized.

Exploratory weld beads made in molybdenum under an inert-gas shield showed that commercially available molybdenum without deoxidization was inferior to the deoxidized material. Radiographs of arc welds made in a chamber containing high-purity helium are shown in Figs. 1 and 2. The gross cracking and porosity demonstrated in Fig. 1 are representative of commercial molybdenum without deoxidizer additions. Only one small crater crack was observed in the carbon-deoxidized material. Since commercial arc-cast molybdenum is made with deoxidizer additions and commercial sintered molybdenum is not usually deoxidized, these two materials were used in different phases of the investigation. Sintered molybdenum was used to determine the effects of deoxidizer additions on welding properties and arc-cast carbon deoxidized molybdenum was used to investigate the effects of contamination of the welding atmosphere with oxygen.

The improvement of the sintered

W. N. Platte is associated with the Metals Joining Section, Westinghouse Electric Corp., Pittsburgh, Pa.

Presented at 1955 AWS National Fall Meeting in Philadelphia, Pa., Oct. 17-21.

Fig. 1 Radiograph of weld in nondeoxidized molybdenum made under helium atmosphere

Fig. 2 Radiograph of weld in carbon-deoxidized molybdenum made under helium atmosphere

materials through the use of deoxidizers was accomplished by additions of carbon, aluminum, niobium, tantalum, and titanium in varying amounts. Weld bends were made in plates rolled from sintered compacts containing these materials.

Prevention of contamination of the weld metal during fusion was accomplished by the use of a welding chamber which contained an inert gas of high purity. The effects of oxygen were examined by controlled additions of this contaminating gas to the atmosphere in the chamber.

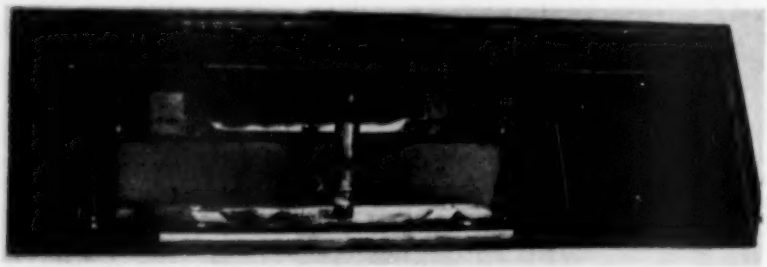

Fig. 3 Arc chamber

The selection of the proper testing procedure for molybdenum is determined by the properties of the material. Tests involving brittle materials impose restrictions on the testing method. When the degree of ductility is low, it is necessary that undue stress concentrations be avoided outside the area to be tested. The effects of temperature upon the ductility also must be taken into consideration. These restrictions were carefully examined in the selection and design of bend test fixtures for use in constant strain rate equipment. Provisions were made for testing over a range of temperatures both above and below ambient.

Welding Method, Materials and Test Equipment

The welding chamber used to explore the effects of the purity of the welding atmosphere on the quality and ductility of molybdenum welds was constructed so that consistent high-purity atmospheres could be obtained. This welding chamber and auxiliary equipment are shown in Figs. 3–5. The chamber operates at a positive pressure of approximately 30 mm of Hg. The system consists of a gas-shielded arc operating in an atmosphere of the same gas. This is accomplished by causing the welding atmosphere to enter around the tungsten electrode during purging and during welding. Gases liberated during welding are continually removed by the incoming atmosphere. This system is advantageous in welding materials, such as molybdenum, which have volatile oxides. Any oxide formed or liberated is swept away by the welding atmosphere entering around the electrode.

The composition of the atmosphere supplied to the chamber may be varied as desired. A gas-mixing system is used to pre-mix the gases before they enter the chamber. A schematic drawing of the mixing system as used for two gases is shown in Fig. 4.

The chamber is purged by passing gas of the desired composition from the mixing system into the chamber. When the pressure in the chamber reaches 30 mm of Hg, the gas supply is automatically stopped and the chamber is evacuated to a pressure slightly below atmospheric. At the end of the pumping period the gas flow is resumed. This process is repeated 30 times. The atmosphere was sampled using the system shown in Fig. 5. Gas samples were analyzed by means of a mass spectrometer, and it was found that the atmosphere in the chamber was equivalent to the atmosphere supplied from the gas-mixing unit.

Welding was accomplished by use of a direct-current tungsten arc. The molybdenum plate was used as the anode and the welding current was maintained at 180 amperes for the 0.060-in. thick molybdenum plate. A spark-gap oscillator was used to provide a high-frequency

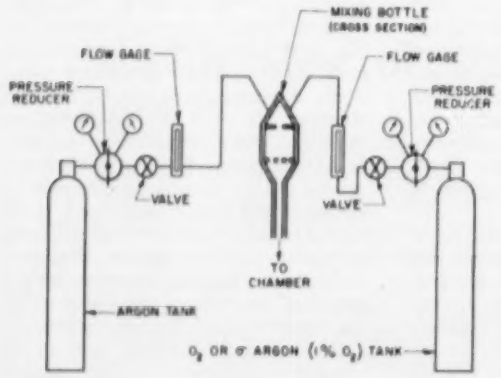

Fig. 4 Schematic of gas mixing system

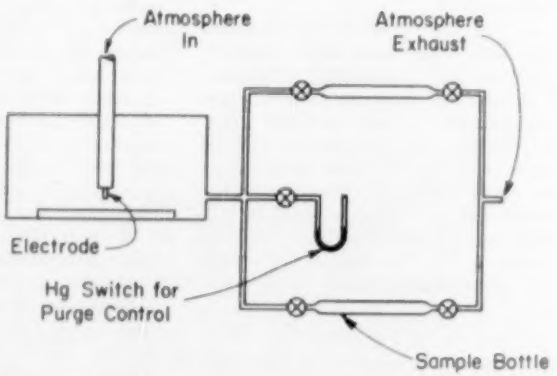

Fig. 5 Schematic of gas sampling system for welding chamber

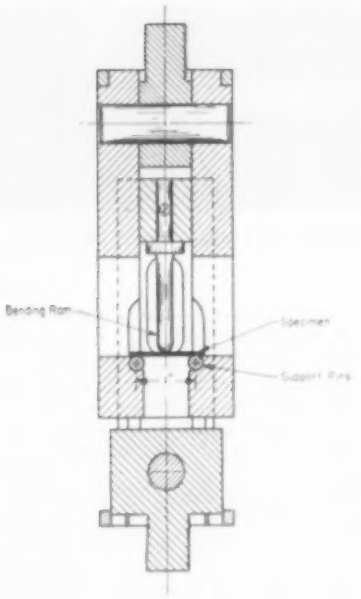

Fig. 6 Bend test fixture

spark for arc initiation. A $^{3}/_{32}$-in. diam tungsten electrode was used at an arc length of $^{3}/_{32}$ of an inch. The welding plate was moved relative to the electrode by means of a screw drive so that a constant arc-travel speed was maintained without manual manipulation during welding. The arc-travel speed was held at 5.9 to 6.2 ipm and was constant for any given weld. The weld specimen consisted of a fused bead on a solid plate with no filler metal added. Figs. 1 and 2.

Guided-bend tests were used to determine the ductility of the weld metal. A special bend-test fixture (Fig. 6) was used in a constant strain rate machine for all testing in these investigations. This test device required a sample 0.060 x 0.250 x 1.125 in. The specimen is placed in the test fixture with the weld bead in the position of maximum fiber stress. The rate of advance of the bending ram provided a strain rate on the outer fiber of the specimen of 0.0183 ipm. This strain rate was computed for elastic strain and the true strain rate will change beyond the elastic limit. The data from bend tests are given in inches of deflection. The deflection of the sample has been correlated with the angle of bending so that these data can be compared with the work of other investigators (Fig. 7).

Testing at temperatures above ambient was accomplished by means of a conventional type tube furnace controlled to ±5° F and having a maximum temperature gradient of ±5° F over the test zone. Testing below ambient temperatures was accomplished with the special low-temperature chamber. The temperature of the specimen is controlled in both cases by means of a thermocouple placed in the center of the bending ram at its point of contact. In the low-temperature chamber the thermocouple controls a solenoid valve which allows liquid nitrogen to pass into a double-walled inner cylinder. The nitrogen may be liquid or gaseous depending upon the flow rate required to maintain the desired temperature. This device is a modification of a similar unit described by Wessel and Olleman.[5]

In the low-temperature chamber and in the tube furnace the sample is always surrounded with a gaseous medium except when liquid nitrogen temperatures are required. This eliminates the possible errors which may result when tests are made in a medium which wets the sample, as shown by Benedicks.[3]

Vacuum-sintered molybdenum was used to determine the effectiveness of different deoxidizers on the welding properties of molybdenum. This material was obtained in small laboratory lots. The deoxidizers used were Ti, C, Al, Ta and Nb. Detailed discussion of these materials will be given as each deoxidizer is discussed.

The work on the effects of oxygen contamination of the welding atmosphere was done with arc-cast carbon-deoxidized molybdenum since this material, as was shown in Fig. 2, can be welded in commercially pure argon without forming gross cracks or porosity. The material used came from a single ingot. The material was reduced to 0.060-in. sheet according to the grain size control program developed by Bechtold.[4] The sheet had a uniform fine fibered structure in the as-worked condition. By check analysis the arc-cast molybdenum contained 0.0018% oxygen, 0.003% nitrogen and 0.06% carbon. The final rolled cross-section dimensions of the sheet were 0.060 x 7 in. Weld test plates were cut from the strip in pieces 2 x 7 in. perpendicular to the length of the sheet so that the weld test beads could be made perpendicular to the final direction of rolling.

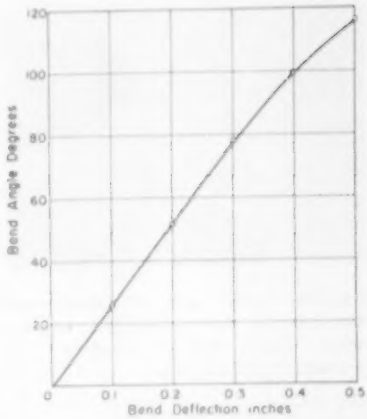

Fig. 7 Relationship between bend deflection and angle of bend

Oxygen in the Base Metal

Titanium-deoxidized vacuum-sintered molybdenum was obtained to determine the range of titanium additions which gave a material with the best welding properties. The vacuum sintered material used for these welding studies was prepared in laboratory lots and these sintered molybdenum heats were welded in the chamber (Fig. 3) using welding-grade argon as an atmosphere. Photographs of two typical welds (Figs. 8 and 9) give visual evidence of the beneficial effect of titanium as a deoxidizer for vacuum-sintered molybdenum. Gross cracking occurred in the control sample, vacuum sintered without a deoxidizer addition (Fig. 8). This sample also showed evidence of porosity. The welds in material deoxidized with titanium were sound and free of gross porosity. The control sample, made without deoxidizer additions, shows grain boundary cracking and porosity (Fig. 10). A typical weld sample deoxidized with 0.2% Ti is shown in Fig. 11. There is no evidence of porosity at the edge of the weld zone. The center of the weld was also free of cracks and porosity. The irregularity in the grain boundaries is most probably due to the existence of very fine precipitates which impede the local movement of the grain boundaries. The grain size in the

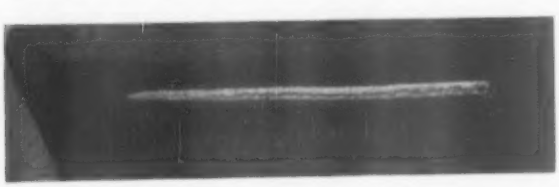

Fig. 8 Weld in vacuum-sintered molybdenum, not deoxidized, made under argon

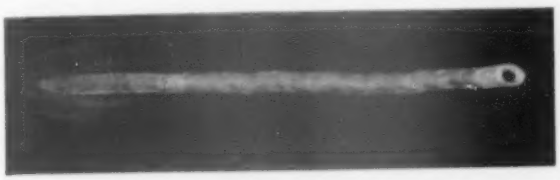

Fig. 9 Weld in vacuum-sintered molybdenum, deoxidized with 0.2% titanium, welded under argon

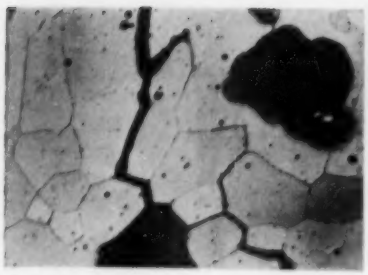

Fig. 10 Weld zone vacuum-sintered molybdenum, not deoxidized, welded under argon, X 100. (Reduced by $^1/_2$ upon reproduction)

(a) Edge of weld, X 100

(b) Center of weld, X 100

Fig. 11 Weld in vacuum-sintered molybdenum, deoxidized with 0.2% titanium, welded under argon. (Reduced by $^1/_2$ upon reproduction)

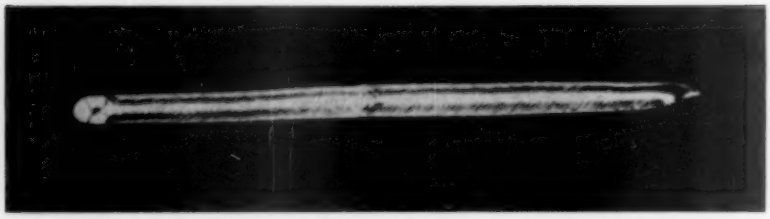

Fig. 14 Weld in vacuum-sintered molybdenum, deoxidized with 0.1% carbon, welded under argon

welded area is relatively fine compared to arc-cast material discussed later. Similar results were found in a weld in 0.5% titanium-deoxidized vacuum-sintered molybdenum.

The welds made in titanium-deoxidized sintered molybdenum were cut into bend test specimens and tested over a range of temperatures. The results of these tests are given in Figs. 12 and 13. These data show that titanium as a deoxidizer for sintered molybdenum is best in the range 0.2 to 0.5%. Welds in this material did not become completely brittle until tested at −130 to −160° F and were ductile, that is, withstood a 118-deg bend or 0.5-in. deflection, at 320° F. These results are comparable to some of the welds in arc-cast carbon-deoxidized molybdenum discussed later. The welds in molybdenum sintered in vacuum and deoxidized with 1.88% Ti showed completely brittle behavior at 0° F and did not become fully ductile at temperatures below 400° F.

The relationship existing between the stress in the outer fiber at the proportional limit and the test temperature is shown in Fig. 13. If the curves in Fig. 13 are compared with curves for the welds obtained from arc-cast carbon deoxidized molybdenum (Fig. 29), it will be seen that the rise in the proportional limit occurs at a lower temperature in the sintered molybdenum than in the arc-cast material. There is an exception to this in the case of the sintered molybdenum deoxidized with carbon only. The stress at the proportional limit in this case is almost identical over the range of test temperatures examined as was found for the arc-cast carbon-deoxidized material. This condition suggests an effect due to the type of deoxidizer used rather than the degree of deoxidization. The proportional limit of the weld in titanium-deoxidized material did not achieve as high a value prior to completely brittle fracture as did the weld in carbon-deoxidized material. However, the lower temperature for the rise in the proportional limit permits the material to show better bend properties at lower temperatures than the carbon-deoxidized molybdenum. It is possible that the maximum stress at the proportional limit could be increased by changes in the deoxidizing technique. Examination of Fig. 12 shows that the welds in material deoxidized with 0.2 and 0.46% titanium show the best bend ductility. The samples deoxidized with 1.88% titanium were not completely ductile at temperatures below 400° F. From these data it appears that vacuum-sintered molybdenum deoxidized with 0.2 to 0.5% titanium shows weld properties comparable to the welds obtained in arc-cast carbon-deoxidized material. However, part of the improved properties of the sintered material may be due to the type of deoxidizer used.

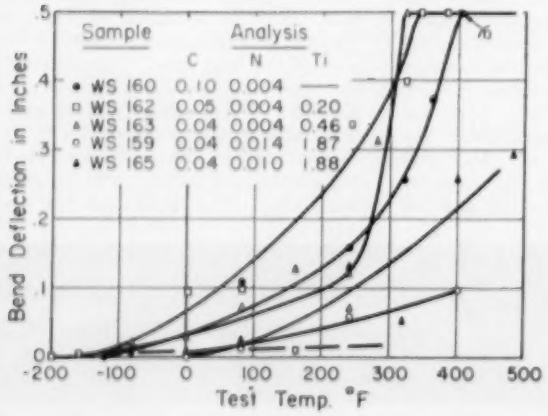

Fig. 12 Bend deflection vs. temperature relationships for vacuum-sintered deoxidized molybdenum

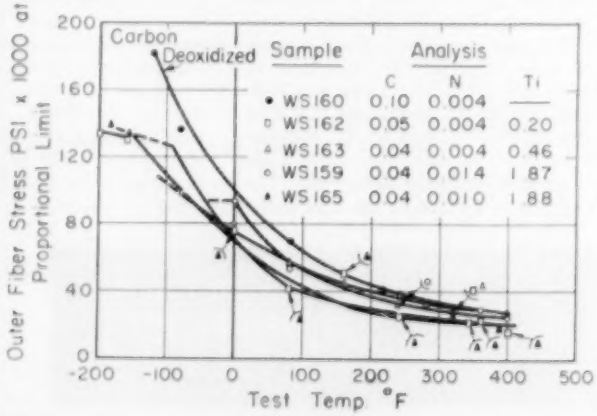
Outer Fiber Stress PSI x 1000 at Proportional Limit
Test Temp °F
Carbon Deoxidized
Sample
Analysis
C N Ti
• WS160 0.10 0.004 —
□ WS162 0.05 0.004 0.20
▲ WS163 0.04 0.004 0.46
○ WS159 0.04 0.014 1.87
▲ WS165 0.04 0.010 1.88

Fig. 13 Stress at proportional limit test temperature relationship for vacuum-sintered deoxidized molybdenum

Table 1—Welding Data Carbon-Deoxidized Vacuum-Sintered Molybdenum

Sample	Composition aim	Atmosphere	Current, amp	Welding voltage	Speed, ipm	Comments
WS160	0.1% C, bal. Mo	99.9% A 0.1% N_2	180	14	6	Clean, bright, with crater crack
WS160A	0.1% C, bal. Mo, annealed 1 hr. 1200° C	99.9% A 0.1% N_2	180	13	6	Bright, clean, medium width bead. No cracks
WS173	0.05% C	<0.05 Impurity	208	14	6.2	Trouble starting arc. Gas evolution in bead. No crack. Edge porosity
WS176	0.1% C	<0.05 Impurity	205	13.3	6.2	Clean, bright, rough bead, no cracks. Edge porosity

Carbon deoxidization was first thought to be a good method for vacuum-sintered molybdenum because the products of deoxidization are volatile and would be expected to be removed during the vacuum-sintering process. Exploratory investigations indicated that carbon-deoxidized vacuum-sintered molybdenum showed some promise as a weldable material. Several heats of carbon-deoxidized molybdenum were obtained covering a range of carbon contents to quantitatively determine the usefulness of carbon as a deoxidizer. Carbon was added over the range 0.01 to 0.1%. Carbon at 0.01% was found in material to which no carbon additions had been made. This material was used as a control for data collected on vacuum-sintered molybdenum. Some difficulty was experienced in obtaining vacuum-sintered carbon-deoxidized heats which were sufficiently sound to roll. Three heats were rolled into sheet suitable for welding from five original sintered compacts.

Weld beads were made in the carbon-deoxidized heats in the welding chamber using an atmosphere of welding-grade argon. Welding data are presented in Table 1. Two samples were made on heat WS160, one in the as-rolled condition and one after the material had been annealed one hour at 1200° C. A photograph of one of these welds is shown in Fig. 14. The radiographs show no evidence of porosity. A crater crack was found in the unannealed sample, however, this type of crack has been found to occur in a random fashion when the weld is terminated on the plate. Crater cracks are probably due to the stresses in the plate resulting from the type of bead on plate specimen used. Mark[12] has shown that stresses exist in the direction of the weld bead in this type specimen. The reduced section at the weld crater and the residual stresses would account for the crater cracking. It will be shown later that oxygen in the welding atmosphere over 0.02% will also cause crater cracking.

The improvement due to deoxidization is evident if the weld shown in Fig. 14 is compared with a weld made in a sample which was not deoxidized (Fig. 8). A gross center-bead crack occurs when deoxidization is not accomplished. A photomicrograph of the weld area is shown in Fig. 15 and should be compared with the control sample (Fig. 10) where grain boundary cracking occurred. Gross porosity also occurred in the sample without deoxidizer additions. Center-bead cracks are absent in the carbon-deoxidized sample but there is some evidence of fine porosity. The bend ductility of sample WS160, 0.1% C, was shown earlier in Figs. 12 and 13. This material was ductile in the bend test, that is, it withstood 118-deg bend

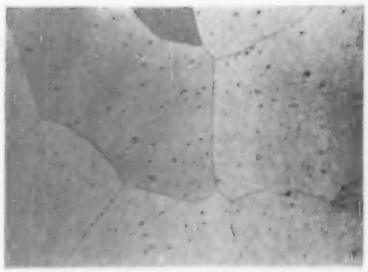

Fig. 15 Weld in 0.1% C deoxidized molybdenum, X300. (Reduced by 1/2 upon reproduction)

at 400° F and did not become completely brittle until −130° F. The properties, however, were not as good as those obtained with Ti-deoxidized molybdenum. The carbon-deoxidized material also shows the rise in the elastic limit with decreasing temperature. This increase occurs at higher temperatures than in the Ti-deoxidized material.

The welding results obtained with the first lot of carbon-deoxidized vacuum-sintered molybdenum could not be duplicated. Two later heats were tried, one with 0.05% C and one with 0.1% C. The welds showed no cracks after cooling. Both welds showed gross porosity at the edge of the weld bead. This porosity is shown in the photomicrographs of the weld area (Fig. 16).

Removal of the products of deoxidization by formation of a volatile de-

(a) Center of weld, X100

(b) Edge of weld, X100

Fig. 16 Weld in carbon-deoxidized sintered molybdenum. (Reduced by 1/2 upon reproduction)

Table 2—Welding Data for Vacuum-Sintered Aluminum-Deoxidized Molybdenum

Sample	Deoxidizer	Atmosphere	Current, amp	Welding, voltage	Speed, ipm	Comments
WS189	0.05% Al	N_2 0.02% O_2 0.02%	175	12.5	6	Very porous, center bead crack
WS188	0.1% Al	N_2 0.02% O_2 0.02%	180	13	6	Very porous, crack down center
WS177	0.2% Al	N_2 0.02% O_2 0.05%	203	13.5	6	Rough bead surface, center-bead crack. Edge porosity
WS193	0.2% Al	N_2 0.06% O_2 0.02%	175	13.5	6	Oxides on bead, rough bead, very porous
WS194	None	N_2 0.06% O_2 0.02%	180	13	6	Center-bead crack

oxidization product was mentioned as being one of the advantages in using carbon. Unfortunately, this characteristic does not operate where welding applications are involved. Deoxidization does not appear to be completed during the sintering process. Completion of the deoxidizing action during welding and the production of gaseous products of deoxidization produce porosity in the weld bead. Porosity at the edge of the weld bead indicates the occurrence of deoxidization during welding and the absence of hot center-bead cracking shows that deoxidization was reasonably complete after welding. The data collected in these investigations indicate that carbon is not successful as a deoxidizer in vacuum-sintered molybdenum if the material is to be used in welding applications.

Aluminum-deoxidized molybdenum used in exploratory investigations indicated that aluminum could be used as a deoxidizer. The product of the deoxidization reactions should be reasonably stable at elevated temperatures and should not cause difficulty in welded applications. Unfortunately, one very important factor was overlooked in the selection of aluminum for deoxidization reactions in sintered molybdenum for welding. Aluminum boils at 2450° C which is well below the melting point of molybdenum and above the sintering temperature used. The welding data shown in this report demonstrate the effect of deoxidizers which boil at or below the melting point of the metal deoxidized.

Six heats of aluminum-deoxidized vacuum-sintered molybdenum were obtained in the range of 0 to 0.2% Al.

Weld beads were made on aluminum-deoxidized molybdenum samples in the welding chamber using a welding-grade argon atmosphere. The welding data are given in Table 2. All of these welds showed porosity and all but one showed center-bead cracking. The boiling action of the aluminum is evident and it appears that some form of grain boundary eutectic may exist after the molybdenum has solidified so that boundary cracking occurs during cooling. However, this type of failure could have been caused by incomplete deoxidization and the residual molybdenum oxides could cause cracking and porosity during welding. Either one of these reactions would produce material not suitable for welding applications.

From these data it is obvious that aluminum is not successful as a deoxidizer for vacuum-sintered molybdenum which is to be used in welding applications. It is also apparent that deoxidizing materials which boil below the melting point of molybdenum will be unsuccessful unless all of the deoxidizer is removed during sintering and the deoxidization is also completed during that time. Materials which form low-melting point oxides or oxide eutectics or themselves form eutectics will also be unsatisfactory.

Tantalum and niobium are both strong oxide-forming materials and the possibility was considered that they might be successful as deoxidizers. Both of these materials have high-boiling temperatures and melting points near that of molybdenum. Tantalum melts at

Table 3—Welding Data for Tantalum- and Niobium-Deoxidized Molybdenum

Sample	*Composition aim*	*Impurity content*	*Current amp*	*Welding voltage*	*Speed, ipm*	*Comments*
WS174	0.2% Ta	$O_2 < 0.05$	203	13	6	Porous; crack down bead center; crater crack
WS175	0.2% Nb	$O_2 < 0.05$	203	14	6	Crater crack; center-bead crack; gas evolution from bead; general porosity

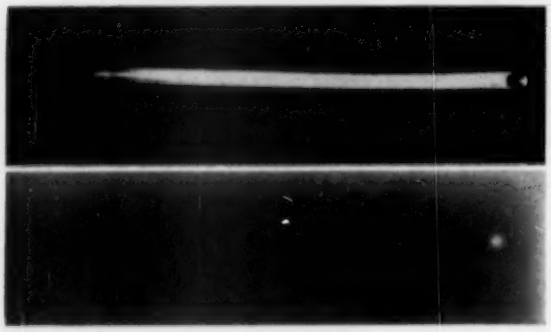

Fig. 17 (*a*) Sample G14—Atmosphere: argon 99.97%, oxygen nil, nitrogen or CO 0.03%

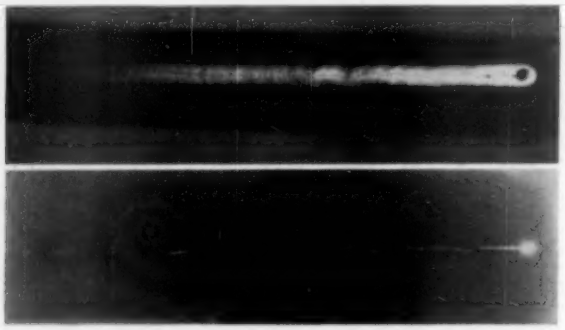

Fig. 17(*b*) Sample G8—Atmosphere: argon 99.7%, oxygen0.2%, nitrogen or CO 0.1%

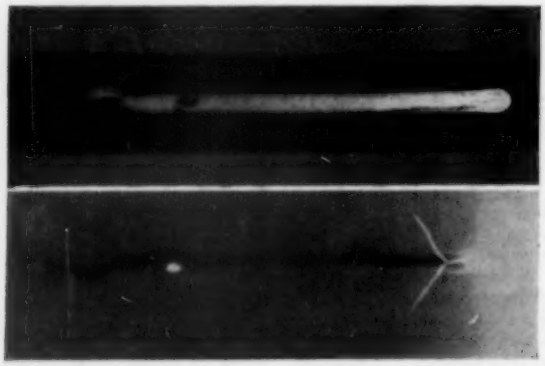

Fig. 17(*c*) Sample G7—Atmosphere: argon 99.6%, oxygen 0.3%, nitrogen or CO 0.1%

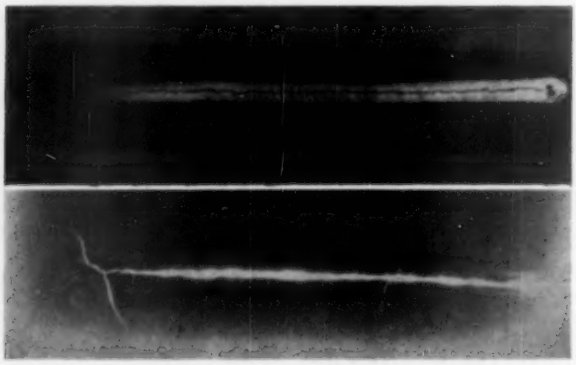

Fig. 17(*d*) Sample G6—Atmosphere: argon 99.4%, oxygen 0.4%, nitrogen or CO 0.2%

3027° C and niobium melts at 1950° C as compared to molybdenum which melts at 2620° C. These materials should not be subject to the difficulties encountered with aluminum deoxidized molybdenum.

Two heats of vacuum-sintered molybdenum were obtained, one deoxidized with 0.2% Nb and the other with 0.2% Ta. Weld beads were made on these samples in the welding chamber under an atmosphere of argon. Welding data appear in Table 3. The welding data indicated that neither Ta nor Nb shows much promise as a deoxidizer for vacuum-sintered molybdenum for welding applications. The gross cracking and porosity encountered with these materials suggest that the oxides may have decomposed during welding or sintering and the oxygen is then free to form molybdenum oxides which are known to contribute to hot cracking and porosity. The oxide of Ta decomposes at 1470° C.[13] This decomposition could explain the difficulty encountered with this material. The oxides of Nb both melt below 1780° C and could form eutectics with Mo or wet the grain boundaries. A low-melting point grain boundary film would account for centerbead cracking. However, incomplete deoxidization is more probably the cause of cracking and porosity in this material.

Summary of Work on Sintered Molybdenum

The work on vacuum-sintered molybdenum has shown that if this material is properly deoxidized it can be welded. Welds made in suitably deoxidized molybdenum will be sound and have a degree of ductility. However, there are many restrictions upon the deoxidization practices used for molybdenum.

If weldable molybdenum is to be obtained the deoxidizer must form nonvolatile products which do not wet the grain boundaries or remain as molten films below the freezing point of the molybdenum. The deoxidizer must not become volatile at the temperatures of molten molybdenum. The only material found which meets these requirements is titanium. This deoxidizer forms a nonvolatile product which melts at the temperatures of molten molybdenum but does not form boundary films. Some of the oxides formed when titanium is used are floated off on the surface of the weld bead while the remaining oxides appear as spheres in the bead.

Table 4—Welding Data Argon-Oxygen Test Welds

Sample	Atmosphere A%	Atmosphere O_2%	Atmosphere N_2%	Welding current, amp	Welding voltage	Travel, rpm	Comments
G-1	99.95	...	...	160	13	...	Insufficient melting
G-1a	99.95	...	...	180	13	6.2	Repeat bead on top of G1. Distortion. Sample rejected
G-2	Sample bottle leaked. Input gas welding grade argon			175	13	6.9	Weld bead bright. Sample clean and free from oxide
G-3	99.95	0.05	Nil	178	13.5	6.9	Welding voltage on before stabilizer. Weld bright and clean
G-4	Sample bottle leaked air			180	13	6.5	Weld bright, clean. No oxide on sample or bead
G-5	99.95	0.05	Nil	185	13	7.1	Sample bright and clean, no oxide
G-6	99.4	0.4	0.2	170	15	6.9	Sample cracked down center of bead
G-7	99.6	0.3	0.1	180	14	7.1	Weld cracked at ends of bead
G-8	99.7	0.2	0.1	175	13.5	6.2	Weld cracked down center of bead
G-9	99.7	0.2	0.1	175	14	6.9	Small crack at start of bead
G-10	...	...	...	...	...	...	Speed too high, insufficient melting. Sample rejected
AG-11*	99.9	Nil	0.1	185	12	5.6	Sample clean, bright, free from cracks. Sample annealed before welding 1200° C one hr
G-12	99.85	0.02	0.13	180	12.7	5.12	Arc flare at start of weld. Weld not cracked
G-13	99.9	0.05	0.05	180	13	5.05	Crack across crater occurred after sample had been removed and was cold
G-14	99.97	Nil	0.03	180	13	5.57	Weld not cracked
G-15	Welded in air. Conventional torch and shielding			180	...	5.41	Argon flow 5 l/min, 10.6 cu ft/hr
G-16	99.76	0.18	0.06	170	14	5.73	Weld cracked
G-17	99.75	0.20	0.05	175	13.5	5.88	Weld cracked
G-27	Analysis error			180	12.75	5.45	Narrow bead with faint brown oxide deposit, small bead and crater crack
G-28	Analysis error			185	12.5	6.4	Faint brown oxide deposit, crack at crater and start of bead
AG-30a*	99.88	0.02	0.1	185	13	6.20	Clean, bright, no cracks, 90% penetration
AG-30b	99.88	0.02	0.1	180	13	6.2	Bright, clean, 90% penetration, no cracks
AG-30c	99.88	0.02	0.1	180	12	6.2	Narrow bead, no cracks, bright, clean
AG-30d	99.88	0.02	0.1	180	12	6.2	Clean, bright, 95–100% penetration, no cracks
AG-31b	99.88	0.02	0.1	175	13	6.2	Same as AG-31a
AG-32a*	99.9	0.05	0.05	175	13	6.2	Arc had trouble starting. Crack near crater. 90–100% penetration
AG-32b	99.9	0.05	0.05	170	13.5	6.2	Oxides around bead. Crack near crater and at one end
AG-31a	99.9	0.08	0.02	175	13.5	6.2	Oxides around bead, 90–100% penetration, crater crack
AG-33a	99.8	0.1	0.1	170–175	13	6.02	Crack down center of first quarter of bead. Crater crack, 100% penetration
AG-33b	99.8	0.1	0.1	170	14	6.02	Difficulty starting arc. Crater crack and cross-bead crack

* All samples with prefix "A" were annealed 1 hour at 1200° C prior to welding.

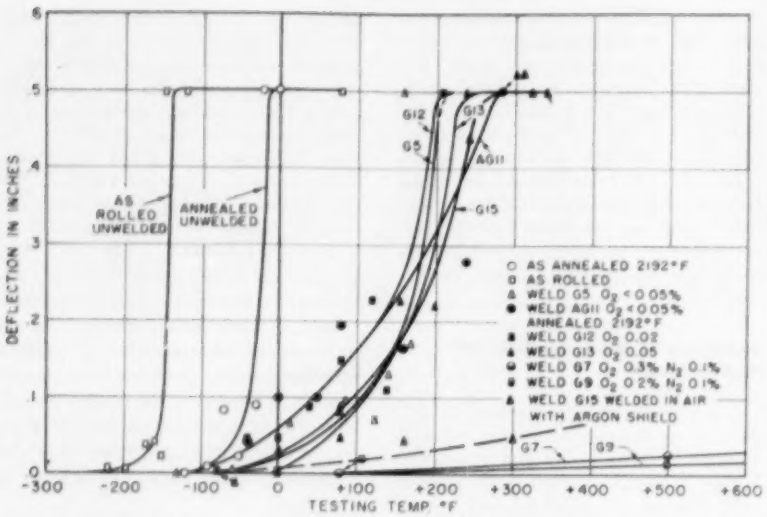

Fig. 18 Deflection vs. test temperature for molybdenum welds made in argon with oxygen added

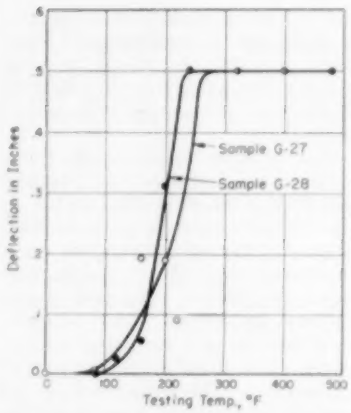

Fig. 19 Relation between bend deflection and test temperature for welds made in atmospheres containing 0.1% O_2, balance argon (arc-cast molybdenum)

Deoxidizing agents tried in these investigations which failed to meet all of the above requirements for deoxidizers failed to produce weldable sintered molybdenum. Tantalum, niobium, aluminum, and carbon were all found to be unsatisfactory as deoxidizers for sintered molybdenum for welding applications.

Oxygen in the Welding Atmosphere

The effects of oxygen upon weld quality and ductility were established by making additions of a 1% oxygen-argon mixture to welding grade argon (99.95%) so that atmospheres were obtained over the range from 0.02 to 0.4% oxygen. The upper limit of 0.4% was established by the formation of hot center-bead weld cracks. The lower limit was the best purity obtained from commercial welding grade argon without purification.

Typical welds (Fig. 17), demonstrate the effects of oxygen in the welding atmosphere upon the formation of hot cracks. These welds were made in as-rolled plate and also in plate annealed for one hour at 1200° C. The welding data and results for welds made in argon-oxygen atmospheres are given in Table 4. Center-bead cracking was observed in welds made in atmospheres containing 0.2 to 0.4% oxygen (Fig. 17*b*, *c*, *d*). The effect of oxygen upon weld beads made in annealed sheet was also examined (Table 4). Fourteen weld beads were made using arc-cast carbon-deoxidized molybdenum which had been annealed for one hour at 1200° C. The first four of these welds, AG30a-d, were made with less than 0.02% oxygen in the welding atmosphere as a control. Other welds were made using 0.05, 0.08 and 0.1% oxygen in the argon atmosphere.

It was observed from both surface appearance and the radiographs of the welds described in Table 4 that all types of weld cracking increase grossly with oxygen contents above 0.05%. When oxygen was 0.02% or less in the welding atmosphere, no cracking was observed. These results are similar for annealed or as-worked sheet so that annealing prior to welding does not appear to be beneficial. Two types of hot cracks appear in these samples. Center-bead cracks which occur along the longitudinal axis of the weld bead are found in welds made with more than 0.1% oxygen in the welding atmosphere. This type of cracking is possible between 0.1% and 0.2% oxygen, probable between 0.2% and 0.4%, and will always occur with more than 0.4% oxygen in the atmosphere. These data apply when the nitrogen content of the welding atmosphere is 0.1% or less. (The effect of nitrogen on weld cracking and ductility will be discussed in a later paper.) Between 0.02 and 0.1% oxygen in the welding atmosphere, crater cracking occurs. Between 0.02 and 0.05% crater cracking is intermittent, but above 0.05% crater cracking is probable in welds where the weld crater occurs in an area surrounded by the plate.

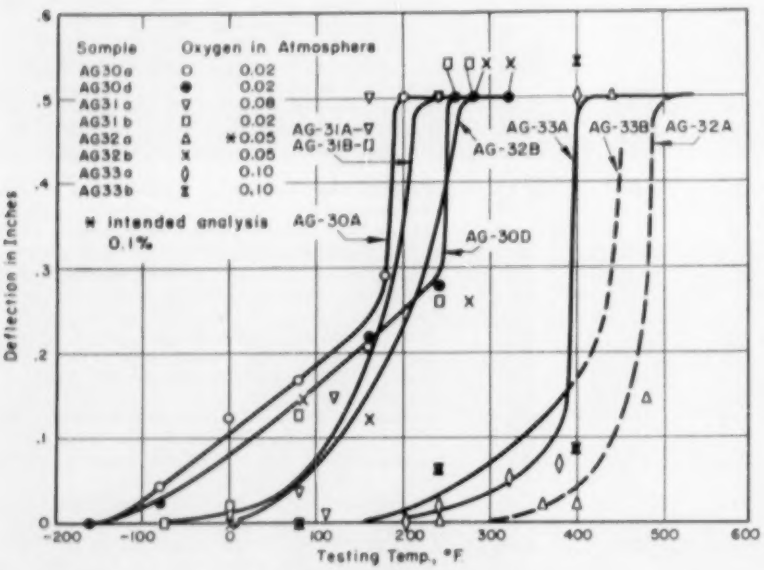

Fig. 20 Relations between obtained deflection and test temperature for welds made in atmosphere containing oxygen. (Material annealed 1 hr at 1200° C prior to welding)

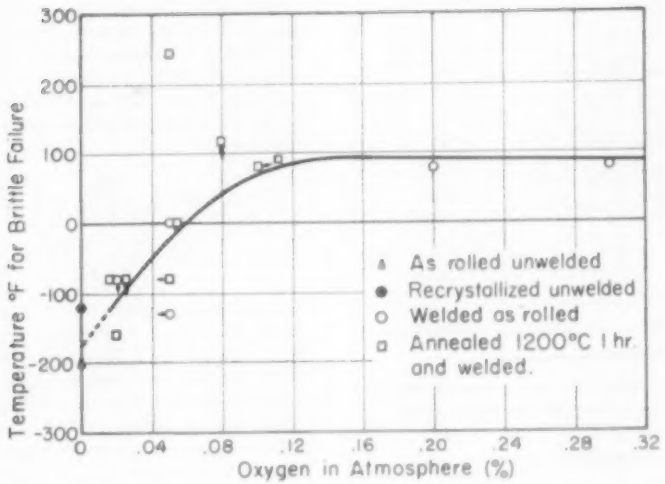

Fig. 21 Temperature for brittle failure related to oxygen in welding atmosphere

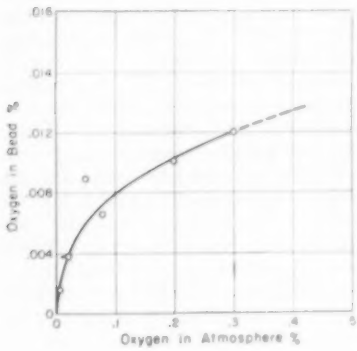

Fig. 22 Oxygen acquired during welding as a function of oxygen in the welding atmosphere

Welds made in carbon-deoxidized arc-cast molybdenum under argon-oxygen atmospheres were tested in bending using the test equipment discussed earlier. Specimens from each weld bead were tested over a range of temperatures to determine the effect of test temperature upon the bend ductility (Figs. 18-21). The curves demonstrate the effects of oxygen acquired during welding on the ability of molybdenum weld metal to sustain plastic deformation. The most obvious effect is the shift in the temperature for 0.5-in. deflection or 118-deg angle of bend. Additions of 0.1% O_2 increase the temperature for 0.5-in. bend deflection to 400° F or more. Oxygen additions to the atmosphere of 0.2 to 0.3% increased the 0.5-in. deflection temperature to above 600° F which was the upper limit of the test fixture.

A second effect occurs as a result of oxygen additions to the welding atmosphere. The temperature of completely brittle failure, fracture without measurable plastic deformation, increases with increased oxygen additions. This effect is shown in Fig. 21. It can be seen that as the oxygen in the welding atmosphere is increased, the temperature for completely brittle fracture increases up to 0.1% oxygen. Beyond 0.1% oxygen there is little change in the temperature for brittle failure. Hot center-bead cracking frequently occurs when the oxygen in the welding atmosphere is in excess of 0.1% so that studies of the fracture characteristics in this range become impractical.

The relationship is known between the oxygen in the welding atmosphere and the oxygen acquired by the weld metal during welding (Fig. 22). From these data, it has been possible to show by means of a cross plot the relationship between the percent oxygen in the weld bead and the temperature of completely brittle behavior in the bend test (Fig. 23). These curves show the relationship between the amount of oxygen in the weld metal and two criteria for weld ductility in the bend test. The dotted curve suggests the possible effect of grain size on the temperature for 0.5-in. deflection. It is apparent from these data that the ductility of the weld metal is closely related to the amount of oxygen acquired by the weld metal during welding. The location of the points for the unwelded recrystallized material (Fig. 23) suggests that an increase in the weld grain size increases the temperature required to obtain a bend deflection of 0.5 in.

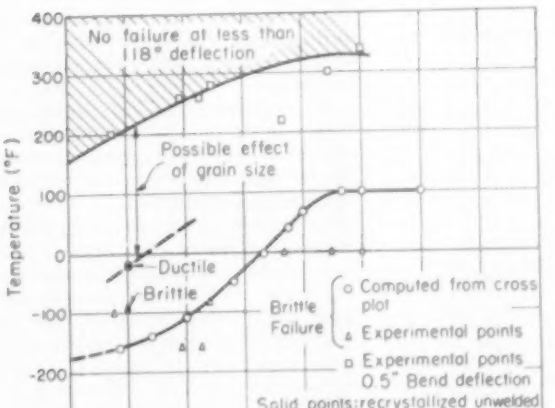

Fig. 23 Relationship between oxygen in the weld bead, brittle-failure temperature and the temperature for 0.5-in. bend deflections

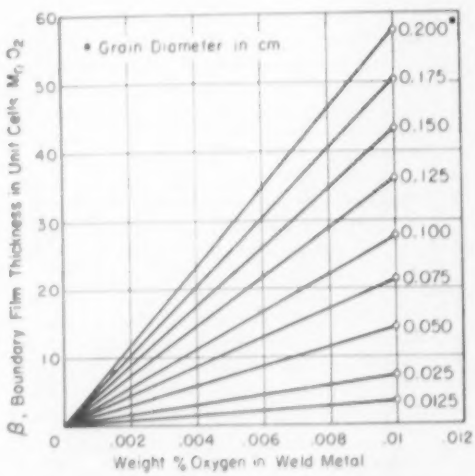

Fig. 24 Relationship between oxygen in the weld and boundary calculated film thickness

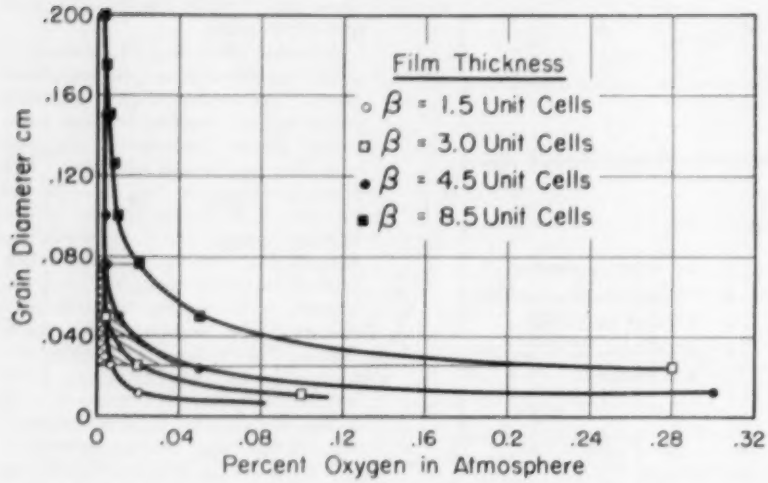

Fig. 25 Oxygen in weld bead and grain size for several MoO_2 film thicknesses

The decrease in the temperature required for brittle failure (Fig. 23) with decreasing oxygen in the weld metal may be explained by grain boundary films. The existence of such films has been established by Johnston and Wulff of Massachusetts Institute of Technology and by Battelle investigators. The effectiveness of these films in changing the temperature of brittle failure can be closely related to the size of the grains in the weld bead. The curve for brittle fracture in Fig. 23 shows that there is a decrease in the temperature of brittleness with decreasing oxygen in the weld metal. At oxygen contents of 0.0085%, the temperature of brittle fracture is 100° F while welds with oxygen contents of 0.0015% do not become completely brittle above −160° F. An explanation of the change in the temperature of brittleness is found by considering the combined effect of grain size and oxide film thickness. If cylindrical grains are assumed in the weld area and the axes of these grains are assumed to have an angle of 45 deg with the plane of the sheet and with the axis of the weld bead the maximum length will be $t\sqrt{3}$, where t is the sheet thickness. The diameter, d, of a grain which will be covered with an oxide film β unit cells thick is given by eq. (1).

$$d = \frac{4\delta\beta C\, t\sqrt{3}}{\Delta t\sqrt{3}\,(4\,W_o) - 2\delta\beta C} \qquad (1)$$

where

d = the diameter of a grain in cm,
δ = the density of the oxide, gm/cm³, 6.47 for MoO_2,
β = the number of unit cells of oxide,
C = the dimension of unit cell which is monoclinic for MoO_2 and equals 5.526A,
t = sheet thickness in cm, 0.152 cm for sheet used,
Δ = the density of metal, gm/cm³, 10.2 for Mo,
W_o = wt. % O_2 in molybdenum.

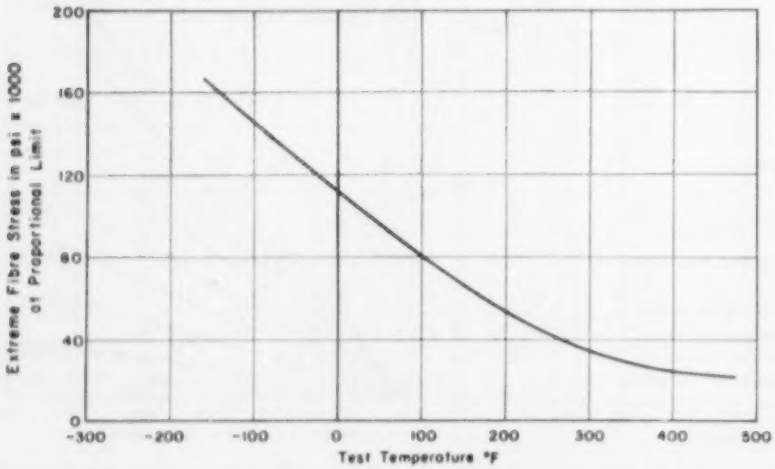

Fig. 26 Curve showing relation of calculated fiber stress at proportional limit as related to test temperature for welds made in oxygen-bearing atmospheres

This equation can be simplified by dropping the $2\,\delta\beta C$ term from the denominator. The value of this term is small and can be neglected. Equation (1) may be further simplified by substitution of the constants as in eqs. (2) and (3).

$$d = \frac{37.6\beta}{10.7 \times 10^6\, W_o} \qquad (2)$$

$$\beta = \frac{10.7 \times 10^6\, W_o d}{37.6} \qquad (3)$$

For a given value of d, β is a linear function of W_o. A series of diameters from 0.0125 to 0.200 cm, 0.0049 to 0.079 in., was used and the relationship between W_o and β is shown (Fig. 24). These curves demonstrate the grain size effect as related to oxide films. The diameter of grains found on the weld bead surface was taken as d and falls in the range 0.01 to 0.03 in. or 0.0254 to 0.0762 cm.[11] Using the curve for brittle failure in Fig. 23, two oxygen contents were arbitrarily selected at 0.002 and 0.004%. The 0.002 value is near the oxygen content of the original molybdenum sheet, and the 0.004% value is one that is obtainable with commercial welding grade argon. In Fig. 24, the 0.002% oxygen content intersects the 0.025 and 0.075-cm diameter curve at β equals 1.5 and 4.5, and the 0.004% oxygen line intersects these curves at β equals 3.0 and 8.5. Thus at oxygen contents of 0.004% and with a grain diameter of 0.075 cm, the grain boundary film would be 47×10^{-8} cm thick, assuming that all the oxide is in the grain boundary and that the film is continuous. A film of this thickness would not be resolved at ×2000 where the resolving power is 5×10^{-6} cm. However, the effectiveness of these films diminishes below 0.002% oxygen. It is believed that if the limit of the oxygen in the weld metal can be held below 0.002% the temperature for brittle failure will approach that of the unwelded plate in the recrystallized material.

It is possible to predict the requirements of the welding atmosphere with respect to oxygen from the grain size of the material in the weld and the molybdenum oxide film thickness which will cause the material to behave in a brittle manner. If the value of 0.002% oxygen is used with a grain size of 0.025 cm. the condition for brittle behavior shifts with grain size as shown in Fig. 25. This relationship shows that the oxygen in the welding atmosphere must be below 0.003% to avoid brittle behavior in the larger grains. However, if the larger grains are the controlling factor in the fracture behavior as they would seem to be, since the oxygen tolerance is smaller with increased grain size for a given film thickness, then the curve derived from the value of β equals 4.5 should be

used. The oxygen tolerance for grains 0.075 cm in diameter is then 0.004% and the upper limit is 0.04% for grains 0.025 cm in diameter. It is most important to note that if in some manner the grain size of the weld zone could be decreased the tolerance for oxygen could be increased.

Most body-centered cubic metals show an increase in the stress at the proportional limit with decreasing temperature. Molybdenum welds follow this general pattern (Fig. 26). The data used were computed from the bending equation and apply to the outer fiber of the bend test specimens. This curve has been replotted in Fig. 27 and the points for brittle rupture are shown for a number of samples welded in atmospheres containing various amounts of oxygen. As the oxygen in the welding atmosphere is increased the stress at brittle rupture decreased along the stress at the proportional limit curve. There are a few exceptions to this relationship but these exceptions may be explained by the drop in the stress required for rupture with decreasing temperature after the temperature for brittle rupture has been reached. However, it is apparent from these data that, as the oxygen in the welding atmosphere increases, the temperature for completely brittle failure increases according to the function given in the relation of stress at the proportional limit to the test temperature. When the oxygen in the weld bead is related to the stress for brittle failure the stress decreases with the oxygen content according to the relationship shown in Fig. 28. The upper point on this curve is for unwelded recrystallized material and this point follows the data for the weld metal.

Examination of the stress at the proportional limit data for welds with known oxygen contents brought out the fact that the oxygen in the weld causes a premature rise in the stress at proportional limit-temperature relationship. An examination of Fig. 29 shows that the proportional limit starts to rise at a lower temperature when the oxygen in the weld metal is at a minimum. Thus far the lowest oxygen content found in a weld bead was 0.0015% (Fig. 29). However, the slope of the stress at proportional limit-temperature curve is apparently a function of some other variable.

The data shown on the effect of oxygen on the stress at the proportional limit and the stress at brittle rupture indicate that as the oxygen in the weld metal is increased the stress required for brittle rupture decreases. The data also show that the temperature at which such failure occurs increases according to the stress at proportional limit relationship. The temperature at which

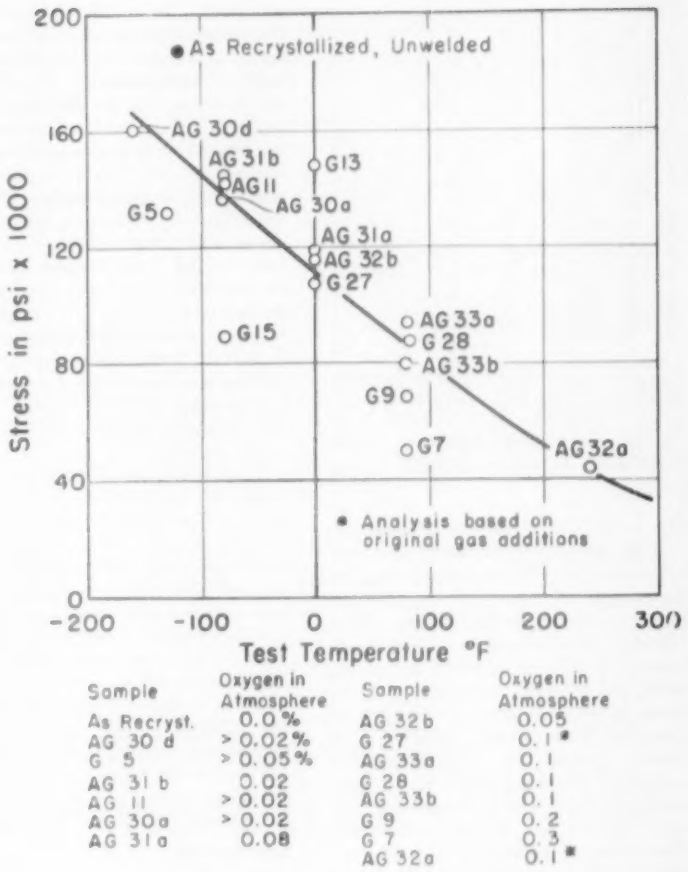

Sample	Oxygen in Atmosphere	Sample	Oxygen in Atmosphere
As Recryst.	0.0 %	AG 32 b	0.05
AG 30 d	> 0.02%	G 27	0.1 *
G 5	> 0.05%	AG 33a	0.1
AG 31 b	0.02	G 28	0.1
AG 11	> 0.02	AG 33b	0.1
AG 30a	> 0.02	G 9	0.2
AG 31a	0.08	G 7	0.3
		AG 32a	0.1 *

Fig. 27 Relation between fiber stress at brittle failure and test temperature for welds in oxygen-bearing atmospheres

the stress at the proportional limit begins to rise depends on the oxygen content of the weld metal and the effectiveness of the oxygen depends on the grain size of the material. The effect of grain size is indicated by the dotted portion of the curve for recrystallized material (Fig. 29). This dotted section is justified by the fact that the point at 0° F attained a maximum deflection in bending and other data indicate that while this condition exists the stress at the proportional limit remains reasonably constant. The grain size of the recrystallized material was much smaller than the as-welded samples. Thus the temperature of brittle behavior is related to the oxygen content of the weld metal and the grain size through the stress at the proportional limit relationship.

The fractured surfaces of the bend-test specimens made in atmospheres bearing oxygen in the range 0.02 to 0.3% were studied to determine the nature and origin of fracture. The examination showed that the origin of fracture was predominately intergranular. From a total of 62 specimens examined, 57 had their fracture origin in the grain boundaries, one was in the grain and four were of doubtful origin. However, after the fracture has started the path of the fracture may be either transcrystalline or intercrystalline. Only the samples welded in relatively high oxygen-containing atmospheres were completely intergranular. In general, the specimens examined were more than 50% transgranular in spite of the intergranular origin of fracture. In a few cases the only intergranular surface in the fracture was found to be the origin of fracture. After the fracture has started the amount of transgranular fracture surfaces in the specimens increases with the temperature of testing. In general, the fracture study confirmed the other data which indicated that the fracture strength was a function of the grain boundary strength. It appears that the grain boundaries are the weakest point in the material and as the temperature of testing is decreased and the stress at the proportional limit is increased, the grain boundary having the most nearly complete or the thickest

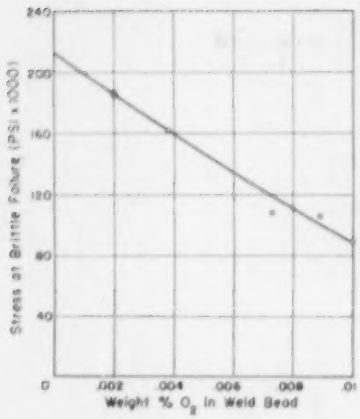

Fig. 28 Relationship between oxygen in the weld and stress at brittle failure

film of oxide will be the first to fail.

It has definitely been established that oxygen in the weld metal will reduce the ductility of the material. The mechanism involved is dependent on grain boundary film formation. Thus it appears that in order to reduce the effects of oxygen on weld ductility to a minimum, it is necessary to eliminate or minimize these boundary films. Two factors control the effectiveness of oxygen in the weld metal, the oxygen concentration in the weld metal and the size of the grains in the weld metal. The oxygen in the weld metal may be reduced to a minimum by careful atmosphere control as indicated in Fig. 25. However, the control of the grain size in the weld metal will require the addition of some material which will restrict the grain size. It is believed that a material such as titanium which forms nonvolatile oxides at welding temperatures and does not wet the grain boundaries could be used. The oxide of titanium has been found to form spherical particles which could restrict the growth of the grains during solidification. The use of molybdenum which has been deoxidized with titanium is strongly suggested.

Summary

The work on both sintered and arc-cast molybdenum has indicated that if certain welding and material conditions are carefully controlled, it will be possible to make joints having appreciable ductility. Molybdenum made in usable quantities requires a deoxidizing agent regardless of its means of fabrication, sintered or arc cast. The nature and requirements of the deoxidizer have been established by work reported here. The deoxidizer must not only remove oxygen from the molybdenum but it must be nonvolatile at welding temperatures; it must not form grain boundary films nor be molten in the grain boundaries after the molybdenum has solidified. The products of deoxidization must either be removed during sintering or arc casting or be nonvolatile at welding temperatures. If the deoxidization products are not removed during fabrication, they must not be molten in the grain boundaries after the grains solidify nor can they form precipitates which interfere excessively with plastic deformation. With one exception the deoxidizing agents tried—C, Al, Ta, Nb and Ti—have failed to meet one or more of these requirements. Titanium appears to meet all the requirements. It forms a nonvolatile oxide which is floated off during welding or remains as spheres and inhibits grain growth without complete boundary films. It does not volatilize during welding and its oxide is stable.

The welding atmosphere used to form joints in molybdenum must be very carefully controlled with respect to oxygen. Oxygen causes hot center-bead cracking when present in the gaseous atmosphere in excess of 0.1% and crater cracks when in excess of 0.02%. Oxygen must be minimized in the weld by some means since it reduces the ductility when present in the weld metal in excess of 0.004% as compared to 0.0018% in the unwelded plate. Oxygen can be eliminated by prior purification of the atmosphere and careful selections of the material with regard to surface and sheet lamination.

Conclusions

The following conclusions have developed from the work with deoxidized vacuum-sintered and arc-cast molybdenum:

1. Oxygen in the base metal will cause hot cracking and porosity.

2. The harmful effects of oxygen in sintered molybdenum can be greatly reduced by the use of deoxidizers during vacuum sintering.

3. Carbon, tantalum, niobium and aluminum have not been found to be satisfactory for deoxidization of vacuum-sintered molybdenum.

4. The ductility and soundness of weld beads in vacuum-sintered titanium-deoxidized molybdenum are comparable to the properties of welds in arc-cast material.

5. Titanium-deoxidized vacuum-sintered molybdenum shows better bend ductility than the carbon-deoxidized vacuum-sintered material.

The work with welding atmospheres led to a number of conclusions with regard to atmosphere requirements with respect to oxygen:

1. Oxygen concentrations in the welding atmosphere of 0.2% produce hot center-bead cracking and cross cracks.

2. Oxygen in the welding atmosphere between 0.1 and 0.2% will probably produce both center-bead and crater cracking.

3. Oxygen above 0.02% and below 0.05% will cause crater cracks in bead on plate welds.

4. As oxygen in the welding atmosphere is increased from 0.02 to 0.2%, the temperature for brittle failure increases.

5. The brittle-failure strength decreases with increases in oxygen in the welding atmosphere.

6. The brittle-failure strength vs. temperature curve for different oxygen contents in the atmosphere falls along the proportional limit vs. temperature curve for molybdenum.

7. Oxygen in the weld metal increases the temperature of brittle behavior from −150 to 0° F between 0.004 and 0.007% oxygen in the weld bead.

8. The temperature at which maxi-

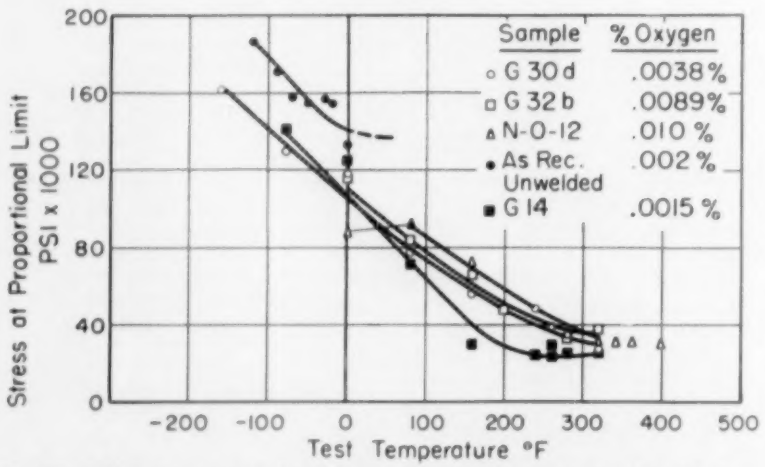

Fig. 29 Effect of oxygen in the weld metal on the stress at proportional limit vs. temperature curves

mum bend ductility, 118 deg bend angle, is obtained is moderately increased by oxygen below 0.1% but is drastically increased above this value.

Acknowledgments

The work reported was done under USAF Contract No. AF 18(600)-114 administered under the direction of the Materials Laboratory, Directorate of Research, Wright Air Development Center, with Lt. T. Hikido acting as project engineer.

The assistance of many portions of the Westinghouse Research Laboratories was required in these investigations. Special sintered heats of molybdenum as well as the arc-cast Climax molybdenum material were fabricated by D. D. Lawthers. Chemical analyses were made under the supervision of F. P. Byrne, assisted by E. W. Beiter, J. F. Reed, R. Meyer, F. Hickman, J. Warneck and M. Mistrik. Photography was done by D. Glasser and K. Molk. X-ray photographs were made by G. Gilpin and G. Ondo. Metallographic work was done by R. L. Anderson; mechanical testing was done by W. H. Pryle, E. T. Wessel and R. Olleman. The original design of the welding chamber was furnished by H. C. Ludwig. The weld test plates were made by H. W. Parks, Jr.

The author wishes to thank J. H. Bechtold, H. Scott and J. Heuschkel for their advice during the course of this study.

Bibliography

1. Johnston, J. H., and Wulff, J., "Molybdenum Welding." WADC TR 53-260.
2. Heuschkel, J., "The Welding of Molybdenum," *Iron Age*, 162, 87, (Dec. 16, 1948).
3. Nippes, E. F., and Chang, W. H., "The Flash Welding of Commercial Molybdenum, Parts I and II." THE WELDING JOURNAL, 34, Research Suppl., 132-s to 140-s, 251-s to 264-s (1955).
4. Bechtold, J. H., "Recrystallization Data Applied to Control of the Mechanical Properties of Molybdenum," *Trans., ASM*, 46, 1449.
5. Perry, T. C., Spaeil, R. S., and Wulff, J., "Effective Heat Treatment of Molybdenum," *Metal Progress* (February 1954).
6. Fisher, R. B., and Jackson, J. H., "Ductility of Cast Molybdenum," *Trans. AIMME*, 188, 1149-1153 (1950).
7. Rengstorff, C. W. P., and Fisher, R. B., "Cast Molybdenum of High Purity," *Trans. AIMME*, 194, 157-160 (1952).
8. Wessel, E. T., and Olleman, R. D., "Apparatus for Tensile Testing at Subatmospheric Temperatures," *ASTM Bulletin* (January 1953).
9. Benedicks, C., "Influence of Nonaggressive Liquids on the Resistance to Fracture of Solid Bodies," *Revue de Metallurgie* (January-February, 1948).
10. Battelle Memorial Institute, First Quarterly Report, A Metallurgical Study of Molybdenum. Contract No. N9onr82100. Task N9onr82101.
11. Platte, W. N., "Joining of Molybdenum." WADC TR 54-17.
12. Mark, M., "A Qualitative Study of Residual Stresses in Welds by Photoelasticity," THE WELDING JOURNAL, 32 (8), Research Suppl. 374-s to 377-s (1953).
13. Mellor, J. W., "A Comprehensive Treatise on Inorganic & Theoretical Chemistry, Vol. VII," Longmans, Green & Co.

EFFECT OF NOTCH ORIENTATION ON WELD-METAL IMPACT PROPERTIES

Technical note discusses results of V-notch Charpy-impact tests on weld metal deposited with E9015 electrodes

BY DANIEL J. SNYDER

A review of the literature dealing with Charpy-impact tests on specimens of multiple-pass weld metal shows that some data have been obtained for specimens with the root of the notch parallel to the weld axis,[1-3] whereas other data have been obtained for specimens with the root of the notch perpendicular to the weld axis.[4-6] The ASME Boiler and Pressure-Vessel Code requires keyhole-notch Charpy-impact tests on weld metal, but the Code does not specify whether the root of the notch shall be perpendicular to or parallel to the weld axis.

In tests on weld metal deposited with E12015 electrodes (Ni-Mo-V),* Pellini and Eschbacher used specimens with the notch root parallel to the weld axis and obtained ductility-transition temperatures considerably lower than did Doty,[4] who used specimens with the notch root perpendicular to the weld axis. The E12015 electrodes used in both investigations were obtained from the same manufacturer. A summary of

Daniel J. Snyder is Senior Research Technologist, Welding, United States Steel Corp., Monroeville, Pa.

* Designated as E12016 by Pellini and Eschbacher.[1] However, the author has been advised by Pellini that this was in error and that an E12015 electrode was used.

Table 1—Charpy-Impact Properties of Weld Metal Deposited with E12015 Electrodes

Type of notch	*Orientation of notch*	*Ductility-transition temperature,° F** *Value*	*Difference*	*Source*
Keyhole	Perpendicular	− 78	82	†
Keyhole	Parallel	−160		†
V	Perpendicular	− 40	80	†
V	Parallel	−120		†

* Selected at the middle of the scatter band for keyhole-notched specimens and at an energy level of 10 ft-lb for V-notched specimens.

† From unpublished data at the Applied Research Laboratory, United States Steel Corp.

Table 2—Composition of Weld Metal Deposited with E9015 Electrodes, %

C	*Mn*	*P*	*S*	*Si*	*Ni*	*Cr*	*Mo*	*V*	*Cu*	*Ti*
0.07	1.72	0.016	0.018	0.30	0.06	0.04	0.32	0.010	0.06	0.016

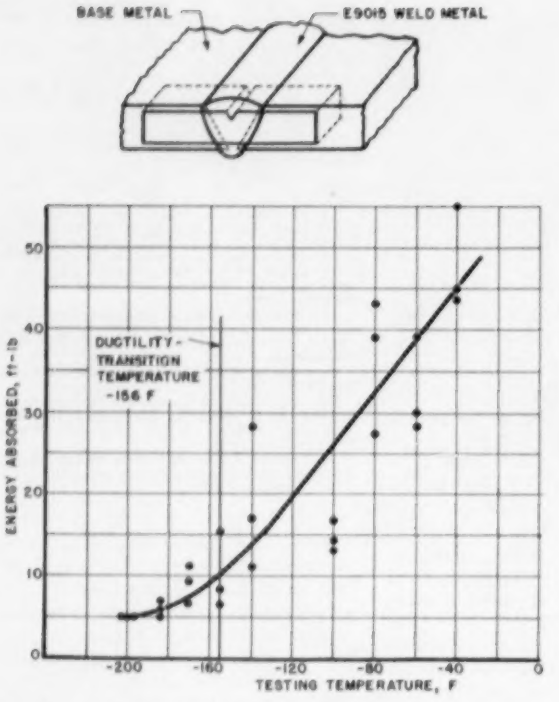

Fig. 1 Charpy-impact data for specimens with V-notches parallel to weld axis

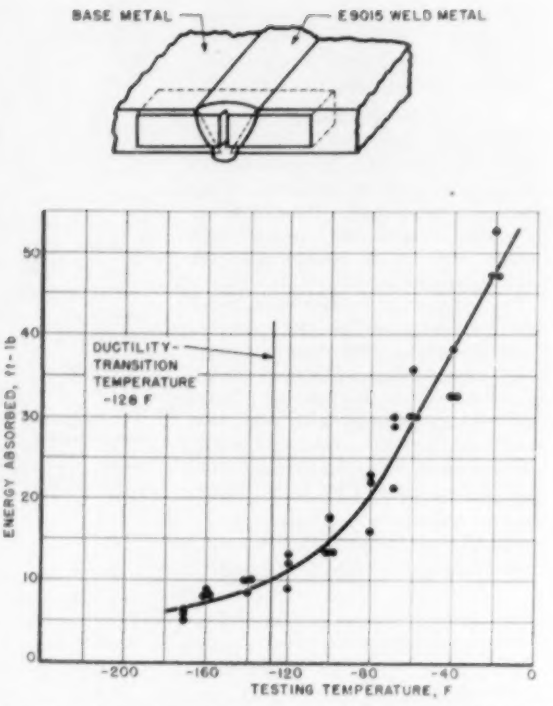

Fig. 2 Charpy-impact data for specimens with V-notches perpendicular to weld axis

the published Charpy data, together with some additional data recently obtained by the author, is presented in Table 1. It will be noted that the keyhole-notch ductility-transition temperatures differ by 82° F and that the V-notch ductility-transition temperatures differ by 80° F. Also, the difference in the V-notch ductility-transition temperatures selected at the 20 ft-lb level was the same as that shown in Table 1 for ductility-transition temperatures selected at the 10 ft-lb level.

These differences are believed to be largely due to the difference in the orientation of the notch in the weld metal. A notch parallel to the weld axis will have its root located either in dendritic or in recrystallized weld metal, depending on the location of the notch root with respect to the layers of weld metal in the joint. (To the author's knowledge, the various investigators have not deliberately tried to locate the root of parallel notches either in dendritic or in recrystallized weld metal.) A notch perpendicular to the weld axis will have its root pass through many layers of weld metal, both dendritic and recrystallized.

To further evaluate the effect of notch orientation on weld-metal impact properties, the Applied Research Laboratory of the United States Steel Corp. recently conducted Charpy-impact tests on weld metal deposited with E9015 electrodes (Mn-Mo), Table 2. The tests were made on V-notched specimens with the root of the notch parallel to and perpendicular to the weld axis. The specimens were obtained from a welded joint in a $^1/_2$-in.-thick plate of T-1 constructional alloy steel. For the specimens with notches parallel to the weld axis, no attempt was made to locate the root of the notch in a specific weld-metal structure.

The Charpy data for the tests on the E9015 weld-metal specimens with the root of the notch parallel to the weld axis are presented in Fig. 1, and those on specimens with the root of the notch perpendicular to the weld axis are presented in Fig. 2. When the ductility-transition temperature is selected at the 10 ft-lb energy level, the transition temperature obtained when notches are parallel with the weld axis is 28° F lower than that obtained when the notches are perpendicular. An even greater difference exists if the ductility-transition temperature is selected at the 20 ft-lb energy level. Also, considerably more scatter is observed in the plot of energy absorbed versus temperature for the specimens with notches parallel to the weld axis than in that for the specimens with perpendicular notches. This suggests that in some of the specimens with notches parallel to the weld axis, the root of the notch was located in dendritic weld metal, and that in others, it was located in recrystallized weld metal. If this is correct and if the root of the notch had been located in recrystallized weld metal in all the specimens, the transition temperature for E9015 weld metal would probably have been lower than −156° F. The difference between the ductility-transition temperatures of the specimens with the root of the notch parallel to and perpendicular to the weld axis would then have been even greater than the observed 28° F.

These results are presented to encourage other investigators to conduct similar evaluations of multiple-pass weld-metal Charpy specimens having differently oriented notches so that more information may become available for many types of weld metals.

References

1. Pellini, W. S., and Eschbacher, E. W., "Ductility Transition of Weld Metal," The Welding Journal, **33** (1), Research Suppl., 16-s to 20-s (1954).
2. Smith, D. C., and Rinehart, W. G., "Heat-Treating Properties of Low-Hydrogen Electrode Weld Metals," *Ibid.*, **31** (4), 296–305 (1952).
3. Armstrong, T. N., and Warner, W. L., "Effect of Welding on Transition Temperature of Nickel Steel Plate," *Ibid.*, **34** (5), Research Suppl., 209-s to 215-s (1955).
4. Doty, W. D., "Properties and Characteristics of a Quenched and Tempered Steel for Pressure Vessels," *Ibid.*, **34** (9), Research Suppl., 425-s to 441-s (1955).
5. Swan, D. A., Lythe, A. R., and McKinsey, C. R., "Stress Relieving and Fracture Strength," *Ibid.*, **30** (3), Research Suppl., 135-s to 145-s (1951).
6. Mathias, D. L., and Bunk, A. P., "Development and Applications of Lime-Ferritic Electrodes," *Ibid.*, **26** (3), 209–217 (1947).

EMBRITTLEMENT OF A SHIP STEEL IN A NITRATE SALT BATH

Nitrogen pickup found responsible for the severe embrittlement of a 1025 semikilled ship steel after subcritical heat treatment in nitrate salt

BY D. J. GARIBOTTI, C. A. BEISER AND E. B. EVANS

ABSTRACT. An investigation was made to determine the cause of the severe embrittlement of a 1025 semikilled ship steel (C steel) after subcritical heat treatment for long times in a nitrate salt bath. The ductility was evaluated by means of Charpy V-notch transition temperatures. Metallographic studies, X-rays and chemical analyses showed that the embrittling agent was nitrogen introduced by a scaling reaction of the steel with the nitrate salt. The embrittlement due to nitrogen pickup was superimposed on any embrittlement resulting from subcritical heat treatment carried out in air.

Introduction

In the first stages of an investigation on the effect of subcritical heat treatment on the transition temperature of a 1025 semikilled ship steel (C steel*), both air and a nitrate salt bath were used as the heating media. It was observed that test specimens heated in the salt had the same or higher transition temperatures and hardnesses as specimens comparably heated in air. This irregular behavior led to the supposition that the salt was introducing an embrittling agent whose effect was superimposed on any embrittlement arising from the normal quench-aging behavior of this steel.[1]

In the present investigation this phenomenon was studied more closely by determining the impact properties of C steel after various subcritical heat treatments in a nitrate salt bath, employing various cooling rates. Metallographic studies and X-ray and chemical analyses were made to establish the existence of an embrittling agent. These results are compared with those previously obtained after similar heat treatments in air.

D. J. Garibotti is Research Metallurgist, Rem-Cru Titanium Corp., Midland, Pa.; C. A. Beiser and E. B. Evans are Research Assistant and Research Associate, respectively, Department of Metallurgical Engineering, Case Institute of Technology, Cleveland, Ohio.

The work was conducted at the Department of Metallurgical Engineering, Case Institute of Technology, Cleveland, Ohio, under the sponsorship of the Committee on Ship Steel of the National Research Council, Bureau of Ships, Contract NOBS-45490.

* The designation "C" refers to Steel C in the Ship Structure Committee "Project" Steels.

Material and Procedure

The C steel used in the present work was from the same heat used in the earlier work at this laboratory. It was a semikilled 1025 steel in the form of $^3/_4$-in. hot-rolled plate. The properties reported for this steel[2] are given in Table 1.

Table 1—Properties of C Steel

Chemical analysis, %			
C	0.24	Cu	0.03
Mn	0.48	Cr	0.03
P	0.012	Mo	0.005
S	0.026	Sn	0.003
Si	0.05	N	0.009
Al	0.016	V	0.02
Ni	0.02	As	0.01

Mechanical Properties	
Yield point, psi	39,000
Tensile strength, psi	67,400
Elongation (8-in. gage length), %	25.5

Charpys-pecimen blanks were taken from the mid-thickness of the plate so that the long axis was perpendicular to the rolling direction. The blanks were rough machined 0.020 in. oversize, subcritically heat treated, machined to size and the notch cut perpendicular to the plane of the plate.

The subcritical heat treatments consisted of heating series of specimen blanks at a temperature within the 700–1100° F. range for various times up to one week in an immersed electrode type of salt bath. The salt was a mixture of potassium nitrate and sodium nitrate. Three different cooling rates—air cool, furnace cool,* water quench—were employed. All series were tested one month after heat treating. Both the energy absorbed in fracture and the percent fibrous fracture values were used in establishing impact transition curves.

* Furnace cool consisted of an average cooling rate of 1.8° F per minute down to 500° F, followed by an air cool to room temperature.

Results

The individual transition curves are shown in Fig. 1 (*a–q*). The transition temperature and hardness results are summarized in Table 2. In the following sections, the 15 ft-lb transition temperature (temperature at which 15-ft-lb are absorbed in fracture) is used to evaluate the degree of embrittlement arising from the various subcritical heat treatments.

Air Cooled Properties

The individual transition curves after an air cool, Fig. 1 (*a–m*), show that not only is the transition range shifted to higher testing temperatures with both increasing subcritical temperature and time, but the upper energy level is lowered as well. This is in contrast to air-heated specimens which show that the transition range is relatively unaffected and that the upper energy level increases with both increasing subcritical temperature and time.[1]

The embrittling effect is more evident in Fig. 2, wherein the transition temperature is plotted as a function of time at temperature for treatments in salt and in air.

Furnace-Cooled Properties

One series of impact specimens was tested in the furnace-cooled condition after heating at 1100° F for 112 hr. The transition curve for this treatment, Fig. 1*q*, indicates the same embrittling effect of the same magnitude as that obtained with the same heat treatment employing an air cool, Fig. 1*m*.

Water Quenched and Aged Properties

The transition curve obtained after water quenching and aging one month at room temperature shifts to higher testing temperatures and the upper energy level is lowered as well with increasing time at 1100° F, Fig. 1 (*n–p*).

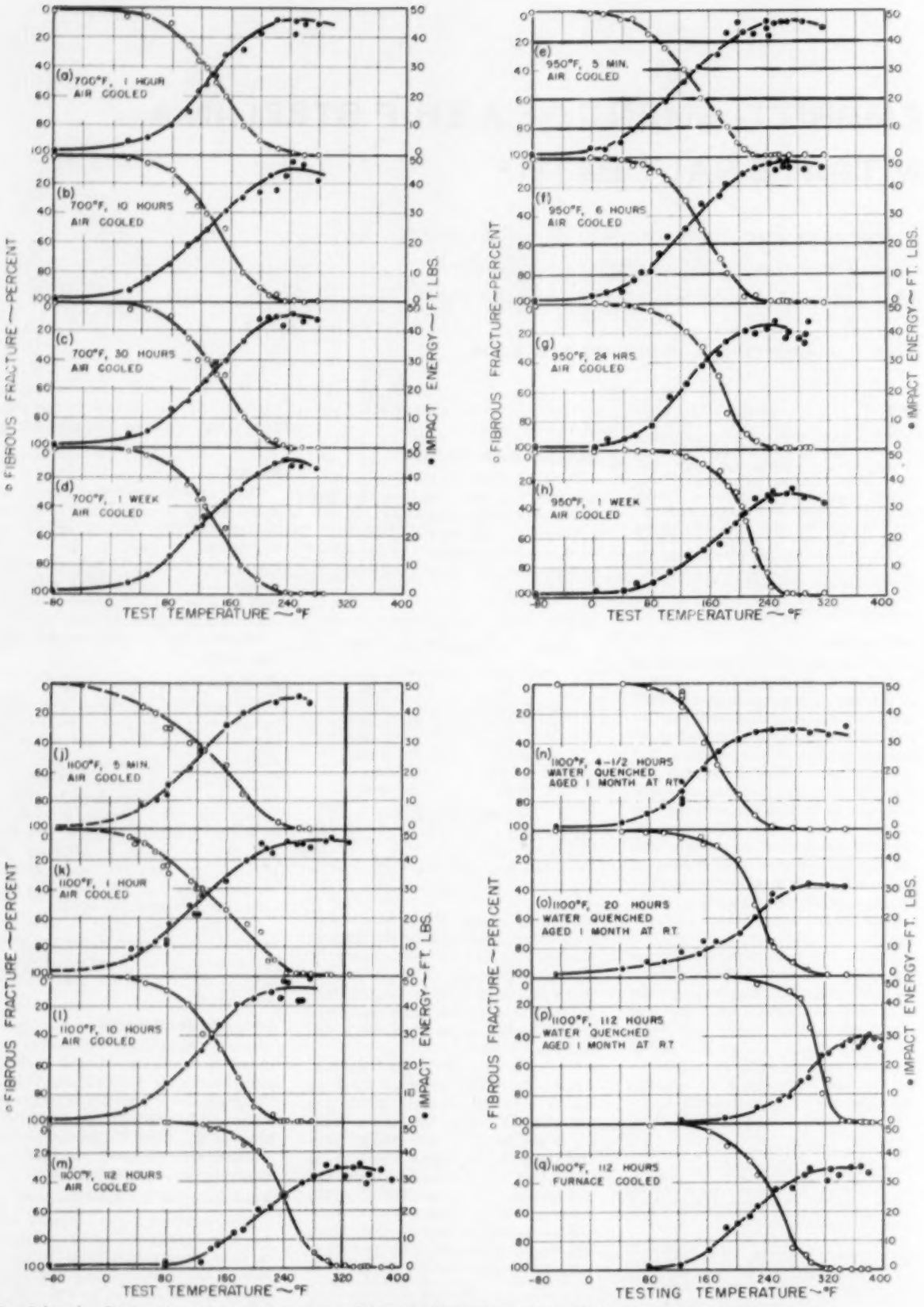
(a) 700°F, 1 HOUR AIR COOLED
(b) 700°F, 10 HOURS AIR COOLED
(c) 700°F, 30 HOURS AIR COOLED
(d) 700°F, 1 WEEK AIR COOLED
(e) 950°F, 5 MIN. AIR COOLED
(f) 950°F, 6 HOURS AIR COOLED
(g) 950°F, 24 HRS. AIR COOLED
(h) 950°F, 1 WEEK AIR COOLED
(j) 1100°F, 5 MIN. AIR COOLED
(k) 1100°F, 1 HOUR AIR COOLED
(l) 1100°F, 10 HOURS AIR COOLED
(m) 1100°F, 112 HOURS AIR COOLED
(n) 1100°F, 4-1/2 HOURS WATER QUENCHED AGED 1 MONTH AT RT
(o) 1100°F, 20 HOURS WATER QUENCHED AGED 1 MONTH AT RT
(p) 1100°F, 112 HOURS WATER QUENCHED AGED 1 MONTH AT RT
(q) 1100°F, 112 HOURS FURNACE COOLED
o FIBROUS FRACTURE—PERCENT
• IMPACT ENERGY—FT. LBS.
TEST TEMPERATURE—°F
TESTING TEMPERATURE—°F

Fig. 1 (a–q) Charpy V-notch transition curves of C steel after various subcritical heat treatments in nitrate salt

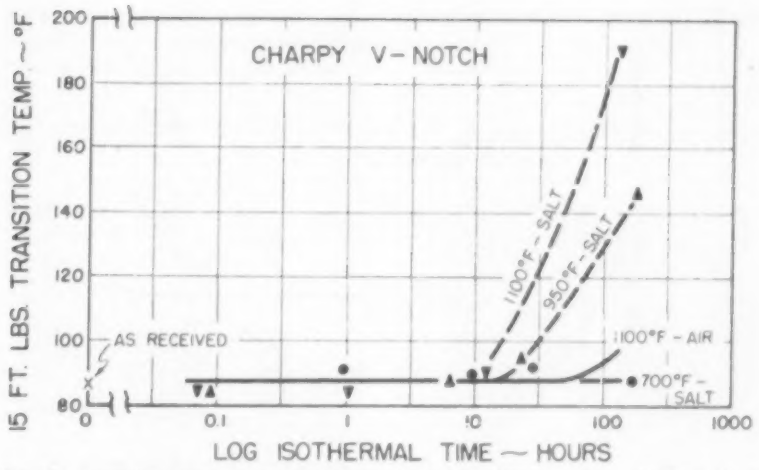

Fig. 2 Transition temperatures of C steel resulting from various subcritical heat treatments in nitrate salt bath and in air, employing an air cool

A comparison of the transition temperatures for comparable treatments in salt and in air, Fig. 3, clearly shows that the nitrate salt has introduced some embrittling agent whose effect is noticeable after about four hours at 1100° F.

From a summary of the test results of the air-cooled and the water-quenched series, using both salt and air as the heating media, Figs. 4 and 5, it is apparent that the degree of embrittlement is a function of the heating medium, time at temperature and cooling rate. For both the air-cooled and water-quenched series, there is an incubation period before the embrittling effect of the nitrate salt is noticeable.

Table 2—Transition Temperature and Hardness of Charpy V-Notch Specimens after Subcritical Heat Treatment in Air and in Nitrate Salt Bath

Time at temp, hr	15 ft-lb transition temperature, ° F — Air heated*	15 ft-lb transition temperature, ° F — Salt heated	Rockwell B surface hardness — Air heated	Rockwell B surface hardness — Salt heated
As-received	87		74	
		700° F, air cool		
1	..	92	73	73
10	..	90	73	73
30	..	92	73	73
168	..	88	73	73
		950° F, air cool		
0.1	..	85	73	73
6	..	88	73	73
24	..	95	72	83
168	..	147	70	85 (80, core)
		1100° F, air cool		
0.1	..	85	..	73
0.2	85	..	74	..
1	85	85	73	73
10	..	90	..	73
20	88	..	71	..
40	85	..	69	..
72	92	..	68	..
112	98	192	67	86 (81, core)
120	95	..	67	..
		1100° F, furnace cooled		
0.2	85	..	74	..
112	..	192	..	86 (80, core)
120	102	..	66	..
		1100° F, water quench, aged 1 month at room temperature		
0.2	110	..	85	..
1	116	..	86	..
4.5	..	130	..	94 (86, as-quenched)
14	116	..	86	..
20	..	200	..	99 (89, core)
112	122	292	82	101 (94, as-quenched)
168	118	..	81	..

* These results previously reported.[1]

Metallographic Study

In order to detect any structural differences which could account for the embrittling action of the nitrate salt, air-heated and salt-heated specimens were examined at a high magnification.

The only difference between air-cooled and water-quenched microstructures after heat treatment in salt, Fig. 6 (*b* and *c*), is the more mottled appearance of the ferrite after water quenching. A comparison of these structures with that of the as-received plate, Fig. 6*a*, indicates that slight spheroidization has occurred during subcritical heat treatment.

With a critical cooling rate (furnace cool), an unusual microstructure was evident after treatment in the nitrate salt. Figure 6*d* taken at the center of a Charpy bar shows short platelets of a precipitate arranged in a Widmänstatten pattern. At the edge of the bar, Fig. 6*e*, a mixed precipitate of short plates and long needle-like plates apparently nucleated at the grain boundaries is evident. Electron micrographs of these latter two structures show somewhat more detail. Figure 7*a* taken at the center of the bar shows, in addition to the Widmänstatten pattern, a fine precipitate distributed throughout the grains. At the surface of the bar, Fig. 7*b*, a fine precipitate is distributed throughout the grains in heavier concentration than that in the core. In addition, it is apparent that the long needles at the surface need not be initiated at grain boundaries and that many of these needles are fringed with a precipitate.

The two different forms of the precipitate suggest a concentration gradient from the edge of a specimen to the core, and their form and distribution suggest nitride needles. This structure is not evident with furnace-cooled specimens after the same heat treatment in air, Fig. 6*f*, although C steel has the highest original nitrogen content of the project steels. It would seem that the nitrate salt served to introduce nitrogen during subcritical heat treatment.

Nitrogen Analyses

To confirm that the specimens heated in salt were enriched with nitrogen, nitrogen analyses were made by both the wet method for combined nitrogen and the vacuum-fusion method for total nitrogen. The results are tabulated in Table 3; each value is the

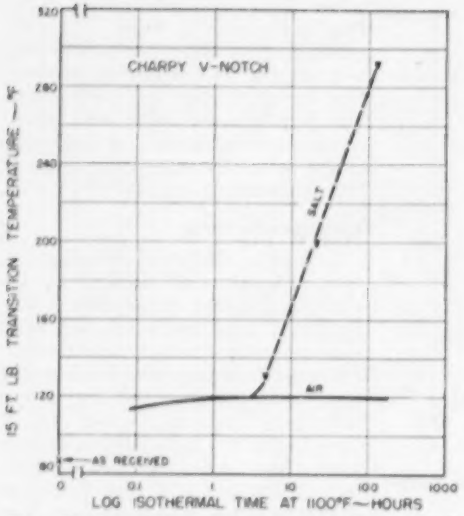

Fig. 3 Transition temperatures of C steel resulting from heating at 1100° F for various times in nitrate salt bath and in air, employing a water quench. Aged one month at room temperature

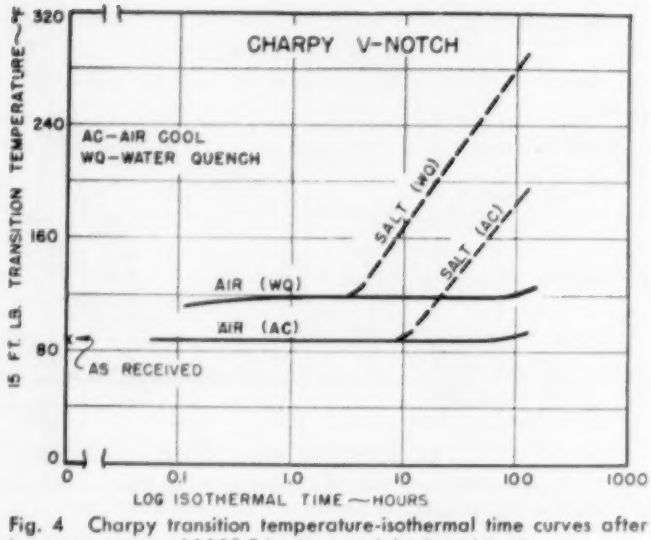

Fig. 4 Charpy transition temperature-isothermal time curves after heat treatment at 1100° F in nitrate salt bath and in air

average nitrogen content of the cross section of a broken Charpy specimen.

Table 3—Nitrogen Analyses of C Steel

Condition	Nitrogen content, wt. %: Combined* nitrogen	Total† nitrogen
As-received	0.017	0.0098
Heated at 1100° F for 112 hr:		
In air; air cool	0.015	0.0104
In salt; furnace cool	0.126	
In salt; water quench	0.106	0.1120

* Wet method.
† Vacuum fusion method.

Both methods of analysis show that subcritical treatment in salt resulted in a high nitrogen pickup, whereas the comparable treatment in air did not. For the heat treatments in the nitrate salt, the combined nitrogen content (wet method) of the furnace-cooled series is greater than that of the water-quenched series, indicating that an appreciable amount of nitrogen is retained in solution by water quenching.

It should be noted that, for both the as-received and air-heated conditions, the combined nitrogen value is greater than the total nitrogen value. This is hardly possible and, undoubtedly, the wet method for combined nitrogen is in error. Therefore, all values obtained by this method have no numerical significance other than to show the relative nitrogen content.

X-ray Study

In order to identify the nitrogen phases, X-ray diffraction patterns were obtained of specimens which had been heated in the salt at 1100° F for 112 hr and furnace cooled. Samples about 0.020 in. square and $^1/_2$ in. long were cut from the edge and core of a broken impact specimen and Debye patterns made from both positions, using monochromatic CoKα radiation. Exposure times of 40 hr or more at 45 kv and 7 ma were required to show up the nitrogen compounds.

The core X-rayed as Fe_4N and iron; the edge X-rayed as Fe_2N, Fe_4N and iron. The short plates in the microstructure (see Figs. 6*d* and 7*a*) can now be labeled the Fe_4N phase and the long plates (see Figs. 6*e* and 7*b*), the Fe_2N phase.

Although X-ray patterns of specimens heated in salt and either air cooled or water quenched failed to disclose the presence of a nitride phase, the mottled appearance of the ferrite (see Fig. 6 (*b* and *c*)) indicated that a second phase was present, but in amounts too small to be detected by X-rays.

Source of Nitrogen

The increase in nitrogen after treatment in the nitrate salt could arise as follows: (*a*) preferential oxidation of the iron, thus decreasing the amount of metal without the loss of any nitrogen,* or (*b*) scaling reaction of the specimens with the nitrate salt, allowing nitrogen to diffuse into the metal.

The first reason was considered possible since specimens heated in the salt

* It has been shown[3, 4] that the preferential oxidation of the iron in iron nails results in an increase in the relative nitrogen content of the remaining metal. When the extent of oxidation is great (50% decrease of metal volume), nitride needles are visible in the microstructure after slow cooling.

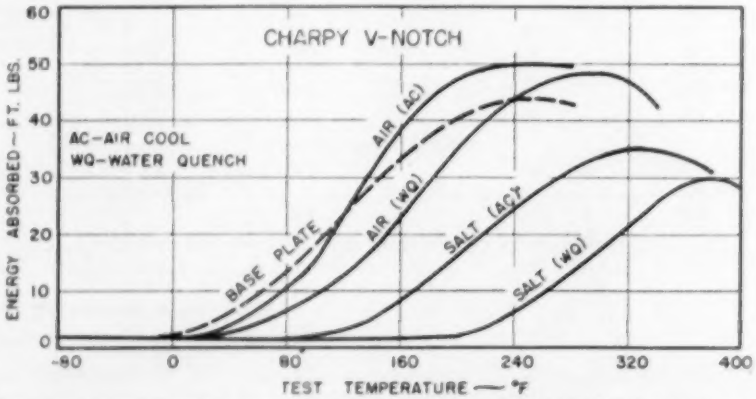

Fig. 5 Charpy transition curves after heat treatment at 1100° F for 112 hr in nitrate salt bath and in air

medium were coated with a thick multilayered scale. The extent of metal loss was determined for impact specimen blanks heated in salt and in air at 1100° F for 112 hr by breaking off the scale, wire brushing and determining the decrease in cross-sectional area of the metal. The loss of metal was $\frac{1}{2}\%$ in air and 6% in salt. The metal loss in salt corresponds to an increase in nitrogen content of from 0.0098% to 0.0104% if the nitrogen does not diffuse out, whereas the actual nitrogen content is about ten times greater than this value, see Table 3.

Although this difference would seem to preclude the first reason, attempts were made to duplicate the structure

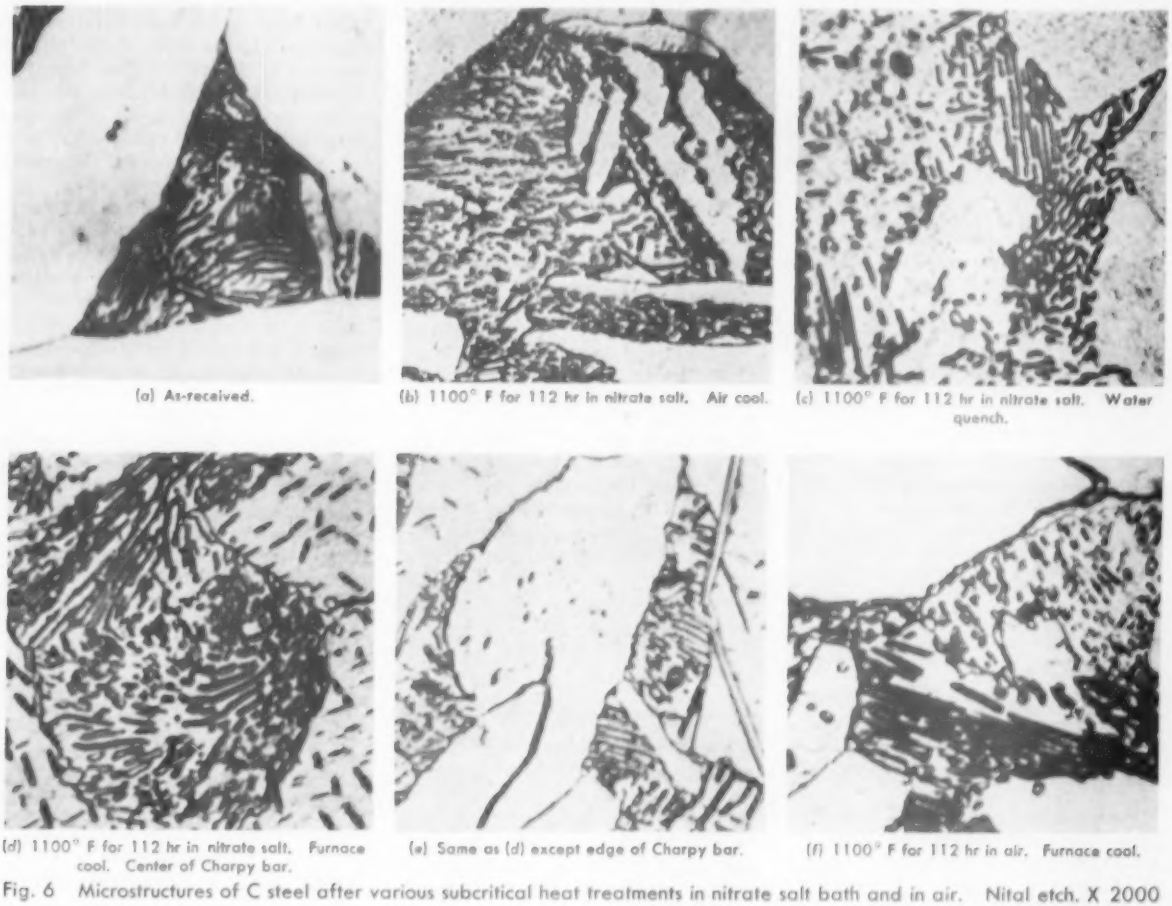

(a) As-received. (b) 1100° F for 112 hr in nitrate salt. Air cool. (c) 1100° F for 112 hr in nitrate salt. Water quench.

(d) 1100° F for 112 hr in nitrate salt. Furnace cool. Center of Charpy bar. (e) Same as (d) except edge of Charpy bar. (f) 1100° F for 112 hr in air. Furnace cool.

Fig. 6 Microstructures of C steel after various subcritical heat treatments in nitrate salt bath and in air. Nital etch. X 2000

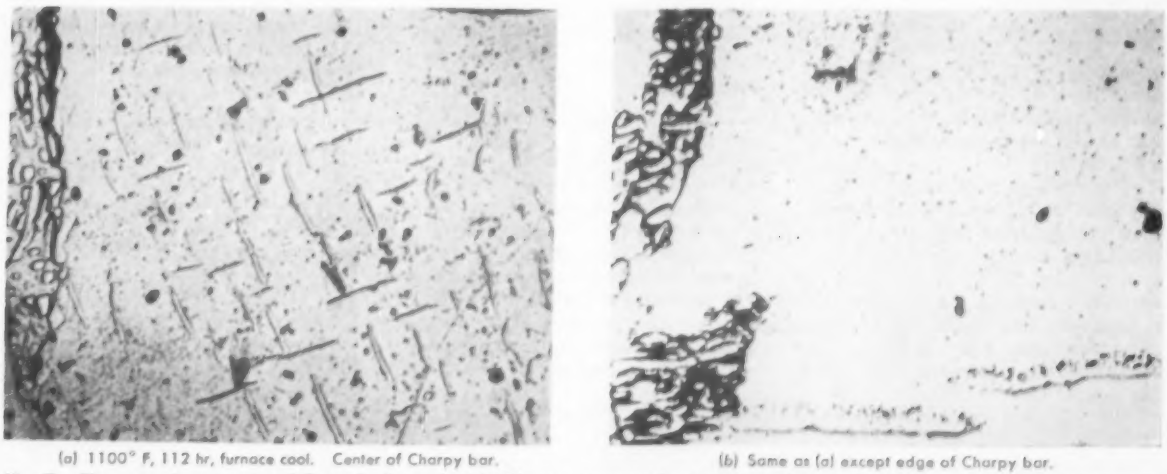

(a) 1100° F, 112 hr, furnace cool. Center of Charpy bar. (b) Same as (a) except edge of Charpy bar.

Fig. 7 Electron micrographs of C steel after subcritical heat treatment in nitrate salt bath. Samples prepared by mechanical polishing and etching with nital. X 6000. (Reduced by 20% upon reproduction)

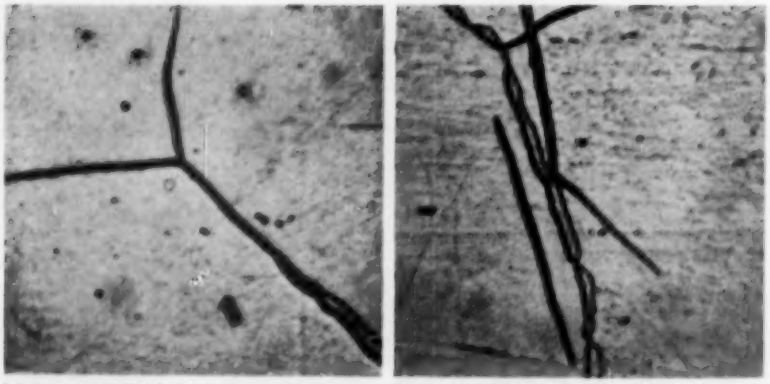

(a) Heated at 2200° F for two days in vacuum, followed by subcritical heat treatment at 1100° F for 112 hr in air, and furnace cooled.

(b) Same as (a) except subcritical heat treatment was carried out in nitrate salt.

Fig. 8 Microstructures of C steel vacuum annealed before subcritical heat treatment. Nital etch. X 2000

showing nitride needles by conducting various heat treatments in pure oxygen, see Table 4.

Table 4—Heat Treatment of C Steel in Oxygen

Temp, ° F	*Time, hr*	*Cooling rate*	*Metal loss, %*
1830	21	Furnace cool	18½
1830	21	Air cool	18

Although the metal loss from these two scaling treatments was greater than that from any treatment in salt, microscopic examination failed to reveal the presence of a nitride phase.

Both specimens were then wrapped in copper foil and heated in air at 1100° F for 112 hr and furnace cooled. Again, the microscopic evidence was negative.

A still further check was made by removing nitrogen from impact blanks by vacuum heating at 2200° F for two days. Subsequent heat treatment at 1100° F for 112 hr in nitrate salt and in air, employing a furnace cool, definitely showed the presence of the nitride in the salt-heated specimen, Fig. 8*b*, but not in the air-heated specimen, Fig. 8*a*.

As a check on contamination of the salt bath and also on the possibility that the electrical circuit was contributing a catalytic effect, as-received samples were placed in two different crucibles containing old and new salt, respectively, and heated in a heavy-duty furnace at 1100° F for 112 hr. The resulting microstructures after furnace cooling showed the presence of nitride needles in the specimen heated in the old salt but not in the specimen heated in the new salt. The specimen in the new salt was then reheated at 1100° F for 96 hr more and furnace cooled. The microstructure now revealed the presence of nitrides. Apparently the nitrate salt had decomposed and reacted with the steel thus introducing nitrogen. The extent of decomposition is indicated by the chemical analyses of the new and the old salt, Table 5.

Table 5—Chemical Analyses of Nitrate Salt, Wt. %

	New salt	*Old salt*
Nitrite	0.2	2.8
Nitrate	68.7	62.3
Potassium	13.6	16.9
Sodium	17.6	15.6

NOTE: The analysis of new salt is equivalent to a nitrate mixture of 65% $NaNO_3$ and 35% KNO_3.

Discussion

Two factors may account for the embrittlement of C steel after subcritical heat treatment in the nitrate salt; namely, an "alloying" effect and a combined solid solution and aging effect, both due to nitrogen pickup.

The first effect is manifested by an increase in hardness and loss in ductility with increasing nitrogen content due to a simple alloying reaction of nitrogen with iron, employing approximately equilibrium cooling conditions as with the air-cooled and furnace-cooled specimens.*

The second effect—the combined solid solution and aging phenomenon—is commonly referred to as "quench-aging." In the present case, it consists of (*a*) the formation of a supersaturated solid solution of nitrogen in ferrite obtained by water quenching from elevated temperatures, and (*b*) the precipitation of some form of iron nitride (see mottled ferrite in Fig. 6*c*) from the supersaturated solid solution at room temperature. (The aging effect was indicated by the fact that the hardness of as-quenched specimens increased with time at room temperature.)

Since both carbon and nitrogen are believed to embrittle steel by the quench-aging mechanism, the contribution of each to the over-all embrittlement cannot be readily separated. It is to be expected, however, that the maximum embrittlement due to nitrogen only would occur after water quenching from about 1090° F, the lower critical temperature of the Fe-N equilibrium diagram. Fast cooling from this temperature gives maximum supersaturation; consequently, more nitrogen is available for the subsequent aging reaction. Similarly, the maximum embrittlement due to carbon only would occur after treatment at 1330° F, the lower critical temperature (A_1) for Fe-C alloys.

Conclusions

Nitrogen pickup was responsible for the severe embrittlement of C steel after subcritical heat treatment in nitrate salt. The embrittlement due to nitrogen was superimposed on any embrittlement arising from the normal quench-aging behavior of this steel.

Acknowledgments

The authors are indebted to the Ship Structure Committee for permission to publish this information; Dr. W. M. Baldwin, Jr., for directing the work; the Republic Steel Corp. for the vacuum fusion analyses; and Dr. Althea Revere, Stevens Institute of Technology, for the electron micrographs.

Bibliography

1. Evans, E. B., and Klinger, L. J., "Heat-Treatment Effects on Transition Temperature of a Ship Steel," THE WELDING JOURNAL, Research Suppl., **32**, 417-s to 431-s (1953).
2. Technical Progress Report of the Ship Structure Committee, *Ibid.*, Research Suppl., **27**, 377-s to 384-s (1948).
3. Enzian, G. H., Beeghly, H. F., and Tarasov, P. P., "Nails from Ruins of St. Pierre," *Metals Progress*, **41** (2), 208–211 (1942).
4. Enzian, G. H., Beeghly, H. F., and Tarasov, P. P., "Auto-Nitrification of Steel as It Scales," *Ibid.*, **41** (4), 522–526 (1942).

* Hardness checks showed no change with time at room temperature, indicating that aging effects were absent.

STRESS-CORROSION CRACKING OF TYPE 304 AUSTENITIC STAINLESS STEEL

PVRC-sponsored project aimed at determining the mechanism of stress-corrosion cracking; accelerated test procedure is developed

BY H. L. LOGAN and R. J. SHERMAN, JR.

ABSTRACT. In a study of the mechanism of stress-corrosion cracking approximately 40 solutions were investigated as possible corrodents to be used in stress-corrosion tests of types 304 and 304L stainless steels. A boiling 3½% NaCl-1% commercial NH_4NO_3 solution, pH 7.0, produced stress corrosion cracking in a few hours in the 304 steel stressed to 80% or more, and in the 304L steel stressed to 100% or more of their room temperature yield strengths. Cracking was produced in 0.2-in. gage lengths strained 0.5% or more. There was, however, no correlation between macroscopic strain and tendency to develop stress-corrosion cracks. Pitting was generally produced by solutions having pH's less than 4.0. Studies of the developments of cracks, made both by interrupting tests and by photographing specimens *in situ* indicated that stress-corrosion cracks can develop with little, or possibly no, previous pitting. Gas, believed to be hydrogen, was shown escaping from cracks. Corrosion products contain metal ions in approximately the same proportion as the parent metal. Limited data indicate that stress-corrosion cracking is not limited to any particular crystallographic plane or set of planes.

Introduction

Stress-corrosion cracking in austenitic stainless steels has been known for at least twenty years. Some of the earlier papers reported specific instances of stress-corrosion failures while others gave methods of testing the susceptibility of stainless steels to stress-corrosion cracking together with the results of tests on specific materials. The discussion following Heger's[1] paper on the stress-corrosion of stainless steel indicated that the phenomenon was widely known. Nathorst[2] lists specific cases reported in the literature of stress-corrosion cracking in many media.

There have been no catastrophic failures of stainless steel equipment reported to date that can be attributed directly to stress-corrosion cracking. However, during the last few years metallurgists and management in the chemical industry have become increasingly cognizant of the fact that many of the thousands of leaks that develop in stainless steel equipment are due to stress-corrosion cracking. These leaks represent a very considerable loss to industry not only in capital replacements but also in downtime and lost products. As a result of this increased recognition of the problem, the Pressure Vessel Research Committee has supported an investigation of the mechanism of stress-corrosion cracking in austenitic stainless steels at the National Bureau of Standards. This paper presents some of the results that have been obtained to date in this investigation.

H. L. Logan is Metallurgist, National Bureau of Standards, Washington, D. C.; R. L. Sherman, Jr., is associated with the Naval Research Laboratory, Washington, D. C.

Presented at 1956 AWS Spring Meeting in Buffalo, N. Y., May 7–11.

Materials and Methods

In order to reduce the number of variables, the investigation was limited initially to two types of stainless steel, namely, types 304 and 304L. Sheet material of both grades, 0.0625 in. thick, was supplied by the United States Steel Corp. and $^9/_{16}$- and $^5/_{16}$-in. diam rods, of the 304L grade, by the Baltimore Works of the Armco Steel Corp. The chemical compositions and the tensile properties of these materials, as determined at the National Bureau of Standards, are given in Table 1.

Most of the austenitic stainless steel specimens used in stress-corrosion tests reported in the literature were formed by bending the material around a mandril and clamping or bolting it into a U-shape so that the specimen contained both elastic and plastic strains. While the magnitude of the applied stresses are not known this type of specimen was convenient to use in the boiling 42% magnesium chloride solution that has generally been used as a corrodent in this country.[3] Stress-corrosion cracking has been obtained in this laboratory on specimens stressed to only 40% of their yield strength in this solution. Copson[4] reported cases of stress-corrosion cracking in a hydro-

Table 1—Steels Used in This Investigation

(*a*) Chemical composition, percent by weight

Type	*Form*	*C*	*Mn*	*P*	*S*	*Si*	*Ni*	*Cr*	*Mo*
		%							
304	Sheet	0.049	1.14	0.026	0.010	0.74	9.9	18.5	0.26
304L	Sheet	0.029	1.23	0.010	0.016	0.84	10.2	18.7	0.014
304L	Rod, $^9/_{16}$ in. diam	0.023	0.77*	0.023	0.019	0.51	9.4	18.4	0.29*

(*b*) Tensile properties of material annealed at the National Bureau of Standards

Type	*Form*	*Yield strength,† lb/in.²*	*Ultimate tensile strength, lb/in.²*	*Elongation in 2 in., %*	*Reduction in area, %*
304	Sheet	36,900	87,500	70	
304L	Sheet	33,200	84,100	74	
304L	Rod, $^9/_{16}$ in. diam	24,900	79,900		81

* Mill analysis.

† 0.2% offset from modulus line.

fluoric, fluosilicic acid mixture from residual stresses from stencil marks on test specimens. Franks, Binder and Brown[5] reported that stress-corrosion cracking was also produced in boiling concentrated solutions of lithium chloride, ammonium chloride and zinc chloride. Nathorst[6] used a 36% calcium chloride solution maintained at 100° C as his test solution; Edeleanu[6] obtained stress-corrosion cracking in a boiling $3^1/_2$% sodium chloride solution containing various oxidizing additives.

In stress-corrosion investigations, in this laboratory,[7] specimens have been dead loaded by means of lever systems and immersed in suitable corrodents. For most phases of the current investigation, $^1/_2$-in. reduced section sheet tensile specimens (standard except that the grip ends were 1 in. wide) were machined from the sheet material with their long axes transverse to the direction of rolling. The edges of these specimens were broken with metallographic polishing paper; the specimens were then annealed for 15 min at 1950° F to remove residual stresses due to machining and were quenched into water at room temperature.

Prior to testing, all specimens were either pickled in a 12% HNO_3, 2% HF, 1% HCl solution[8] maintained at 80° C or electropolished using a proprietary solution until the scale from the heat treatment had been removed. After thorough rinsing in distilled water, the pickled or polished specimens were placed in a test cell containing the corrodent without being permitted to dry. The pyrex glass cells were closed at the top and bottom with slotted rubber stoppers and were surrounded by insulated heating coils. A specimen, cell, and the gripping arrangements are shown in Fig. 1. Evaporation of the corrodent was prevented by means of an air condenser attached to the top of the cell. To prevent vapor phase attack, most specimens were protected with plastic tape to approximately $^1/_2$ in. below the liquid line.

Results

Service failures of austenitic stainless steels have generally been reported in solutions containing less than 1500 ppm of chloride. Hence, it was decided to investigate the possibility of using a dilute solution as a corrodent rather than one of the concentrated chloride solutions. In all, some 40 solutions were investigated. These, together with the results obtained, are given in Tables 2 and 3. The most satisfactory solution contained $3^1/_2$% sodium chloride and 1% ammonium nitrite* and had a pH of approximately 7.

Fig. 2 Specimen stressed to 90% of yield strength for 48 hr in boiling $3^1/_2$% NaCl + 1% NH_4NO_2 solution. Note grid lines for determining strain and distortion associated with cracking

Fig. 1 Stress corrosion cell

Specimen is supported between crossed flexure plates and is loaded by means of a lever system. The solution is heated by the surrounding heating coil. The air condenser connection, shown at upper left, maintains the level of the liquid in the cell.

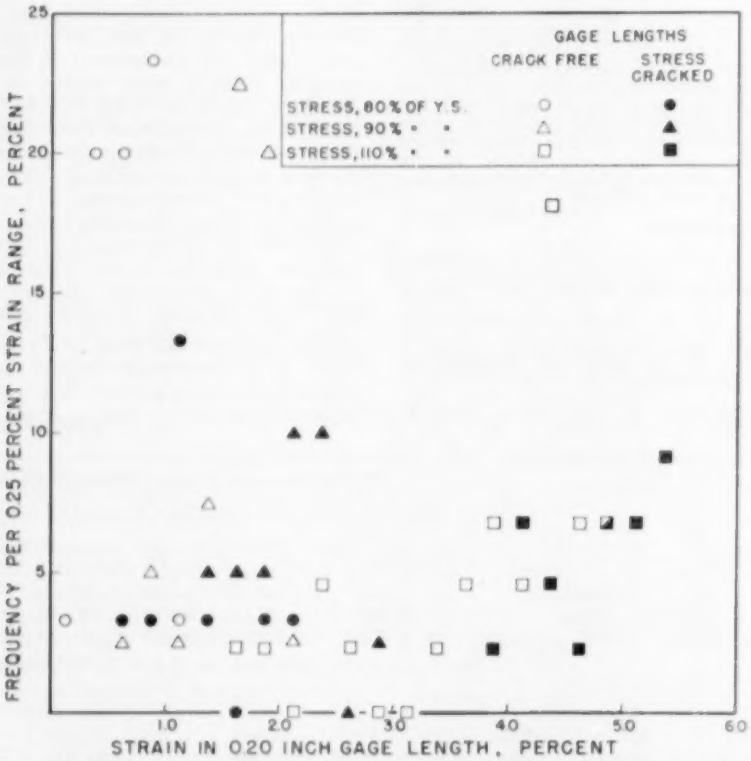

Fig. 3 Distribution of strains in 0.2-in. gage lengths of Type 304 stainless steel specimens stressed to 80, 90 and 110% of their yield strengths

Each plotted point gives percent of all gage lengths, subjected to a given stress level, that fall within a 0.25% strain range.

Stress-corrosion cracking was produced in Type 304 specimens stressed to 80% of their yield strength† in the boiling sodium chloride-ammonium nitrite solution. Specimens of the same chemical composition, stressed to 90% of the yield strength, generally developed stress-corrosion cracks in 2 hr. In order to produce stress-corrosion cracking in Type 304L specimens it was necessary to stress them to 100% of the yield strength.

An analysis of the strain associated with stress-corrosion cracking was made by ruling successive 0.20-in. gage lengths on the reduced sections of type 304 specimens. Specimens stressed to 80, 90 and 110% of their room temperature yield strengths were exposed for 48 hr in the boiling chloride-nitrite solution. A typical specimen, after its removal from the solution, is shown in Fig. 2. The strain along the central line and along each edge of one face of the specimen was determined for each gage length. The frequency of occurrence of strain values in each 0.25% strain interval is plotted in Fig. 3. It was noted that the smallest strain in any gage length containing a crack was 0.52%. In each stress range the average strain in gage lengths free from cracks was generally less than in those containing cracks. However, the fact that at the higher stress levels many gage lengths free from cracks were strained an equal or greater amount than the gage lengths containing most of the stress cracks produced at lower stress levels indicates that there is little or no correlation between strain and the development of stress-corrosion cracks. It seems obvious that other factors in addition to strain are necessary for the development of stress-corrosion cracks in the Type 304 alloy. The width of the

* 1% by weight of the commercial liquid ammonium nitrite. The composition of NH_4NO_2 used to obtain data in Table 2 was not determined. Composition of present stock as determined at NBS is NH_4, 0.0267 g/ml; Na, 0.0082 g/ml; K, 0.046 g/ml; NO_2, 0.122 g/ml and Cl, 0.0026 g/ml; specific gravity 1.107 at 27° C.

† The yield strength was taken as the stress at 0.2% offset from the modulus line and was determined at room temperature.

Table 2—Results of Stress-Corrosion Tests on Type 304 Stainless Steel (in Boiling Media Which Have Produced Cracking)*

Corroding medium	No. of specimens	pH Beginning of test	pH End of test	Stress, % of yield strength	Phase of corroding medium†	Number of cracks
$MgCl_2$, 42%	3	...	...	90	L	3 fractured
	1	...	...	40	L	1 fractured
	1	...	...	60	L	1 fractured
$MgCl_2$, 30%	1	5.2	5.6	105	L	1
$MgCl_2$, 5%	3	...	...	90	L	1
NaCl, 3½% + NH_4NO_2, 1%	4	7.0	6.4–8.4	70	L	0
	8	7.0	6.2–7.5	80	L	5‡
	8	7.0	6.2–7.8	90	L	32
	2	6.6–7.0	6.3–5.1	100	L	5
	1	6.6	6.4	110	L	2
	4	7.0	6.4–7.2	80	V + L	29
	5	7.0	6.6–7.7	90	V + L	23 + 1 fracture
	6	7.0	6.6–8.0	100	V + L	42
	1	6.8	8.0	110	V + L	1 fractured
	1	4.6	6.8	90	L	Pitted
	1	4.6	5.6	100	L	1
	1	4.6	5.2	110	L	Pitted
	1	4.6	6.9	90	V + L	1
	1	4.6	7.1	100	V + L	0
	1	4.6	7.1	110	V + L	3
NaCl, 1% + NH_4NO_2, 1%	1	6.8	7.5	90	L	1
	1	6.8	6.2	100	L	1
	1	6.8	6.2	110	L	1
	1	6.8	7.3	90	V + L	2
	1	6.8	6.6	100	V + L	0
	1	6.8	...	110	V + L	1 fractured
	1	5.0	6.9	90	V + L	1
	1	5.0	7.1	100	V + L	1
	1	5.0	7.3	110	V + L	0
NaCl, 50 ppm §	2	4.5–5.5	6.5–7.5	110 → 165	V + L	2 fractured
NaCl, 3.5% + $NaNO_2$, 1%	1	3.0	7.4	110	L	3
	1	4.4	7.7	110	L	1
	1	5.1	8.0	110	L	1
	2	5–6	7–8	110	L	2 + 1 fracture
	1	3.0	7.8	100	L	4
	1	4.4	8.0	100	L	0
	1	5.1	7.9	100	L	0
	1	6.4	7.9	100	L	1
	1	5.8	8.0	105	V + L	1 fractured
	1	5.1	8.0	105	V + L	0
	1	4.3	7.8	105	V + L	1
	1	5.8	7.4	100	V + L	0
	1	5.1	8.1	100	V + L	0
	1	4.3	8.0	100	V + L	1
NaCl, 3% + $NaNO_2$, 1%	1	...	...	95	L	4

* Specimens were immersed for 10 days under stresses indicated. Fracture indicates complete failure of specimens; number of cracks is total obtained in all specimens tested.

† L, liquid phase; V, vapor phase.

‡ All cracks were found in two specimens.

§ Stress periodically increased until fracture occurred.

Table 3—Results of Stress-Corrosion Tests on Type 304 Stainless Steel (in Boiling Media Which Did Not Produce Cracking)[a]

Corroding medium[b]	pH range: Start of test	pH range: End of test	Stress, % of yield strength
NaCl, 3.5% + $NaNO_2$, 2%	7.0	8.0	95, 105
NaCl, 3.5% + $NaNO_2$, 1% + NaOH[c]	8.4	8.2	105
NaCl, 3.5% + K_2CrO_4, 2%	...	...	105
NaCl, 3.5% + Na_2SO_4, 2%	6.6	5.3	105
NaCl, 3.5% + $(NH_4)_2C_2O_4$, 1%	6.4	6.5	105
NaCl, 3.5% + $KMnO_4$, 0.2%	...	...	105[d]
NaCl, 3.5% + $FeCl_3$[e]	3.4	7.0	105
NaCl, 3.5% + $NaNO_2$, 2% + $FeCl_3$,[e]	2.4	6.0	105
NaCl, 3.5% + Na_2SO_4, 2%	6.7	6.6	105
NaCl, 3.5% + Na_2SO_4, 1%	8.8	7.8	105
NaCl, 3.5% + Na_2SO_4, 0.5%	8.8	7.5	105
NaCl, 3.5% + NaOH[f]	11.1	9.0	105
NaCl, 3.5% + K_2CrO_4, 2% + NaOH[c]	10.7	8.0	105
NaCl, 3% + $NaNO_2$, 1%	6.9	6.6	95
NaCl, 2% + $NaNO_2$, 1/2%	6.7	8.3	95, 105
NaCl, 500 ppm	...	...	75, 85, 95
NaCl, 50 ppm	4.9-5.7	8.0-8.4	95, 105[f]
NaCl, 50 ppm + $NaNO_2$, 1/2%	6.9	6.6	105
NaCl, 50 ppm + KI, 100 ppm	...	...	95[d]
NaCl, + $NaNO_2$, 1%	...	...	95, 105
$CaCl_2$, 40%	5.7	3.9	105[d]
$CaCl_2$, 30%	...	...	105[d]
NH_4Cl, 30%	...	4.5	105[d]
KCl, 50%	...	...	105
NH_4NO_3, 20%	...	3.5	105
$ZnCl_2$, 5%	...	5.4	105
$FeCl_3$, 5%	...	...	105[d, g]
$FeCl_3$, 0.1%	2.3	4.0	95
H_3PO_4, 17% + NaF, 0.5%	0.8	...	105[h]
$MgCl_2$, 20%	...	...	60, 90
$MgCl_2$, 5% + $FeCl_3$[e]	2.8	6.7	105

[a] Specimens were immersed for 10 days at stresses indicated.
[b] All specimens tested in liquid phase only unless otherwise indicated.
[c] NaOH added to desired pH.
[d] Specimen pitted.
[e] $FeCl_3$ added to desired pH.
[f] Tested in both liquid and vapor phases.
[g] Fractured as result of pitting.
[h] Specimen tested at room temperature.

cracks themselves does not appreciably affect the measured strain. By suitably orienting a specimen, the distortion associated with the cracks could be seen with the unaided eye. This distortion coupled with the fact that in any stress group the strain, both in gage lengths containing cracks and in adjacent gage lengths free from cracks, is greater than that of the average for the crack-free group suggests that the increased strain in the cracked specimens may be the result, not the cause, of the cracking. Microscopic examinations of the edges of specimens that had been electropolished prior to testing showed an abundance of slip markings associated with both fine cracks and elsewhere as shown in Fig. 4. There was no marked evidence of distortion associated with these microscopic cracks. This fact is further evidence that the macroscopic cracks were the cause rather than the result of the distortion discussed above. There was no consistent relationship between the crack paths and slip markings.

The presence of corrosion products immediately adjacent to the stress-corrosion cracks is also evident in Fig. 4. These products and those actually removed from the cracks are dark in color. X-ray diffraction patterns indicate that they were both probably Fe_3O_4. The specific gravity of this oxide is 5.7, hence, its volume is approximately 1.4 times that of the steel from which it was formed. Any oxide of this type formed in the stress-corrosion crack could thus exert a tensile force tending to open the crack further.

Reddish brown rust deposits were found outside of, but associated with, stress-corrosion cracks. The X-ray diffraction patterns of this material indicate that it is primarily $Fe_2O_3 \cdot nH_2O$ mixed with sodium chloride and ferric chloride. The presence of the sodium chloride is of particular interest because this salt was recently reported mixed with the rust in service failures.[9]

Spectrochemical analysis of the rust products indicated that the metal ions were present in approximately the same proportions as in the parent metal. This would indicate that no specific constituent or constituents were particularly subject to attack along the path of the stress-corrosion crack.

It is seen in Fig. 4 and also in Fig. 5 that the stress-corrosion cracks produced in the sodium chloride-ammonium nitrite solution were transcrystalline. This is characteristic of stress-corrosion cracks found in service failures in austenitic stainless steels.

Area effects have been reported in stress-corrosion studies of certain materials, particularly magnesium[10] and aluminum[11] alloys. In order to determine whether the stress-corrosion cracking of stainless steels was area-dependent, specimens were masked with plastic tape, leaving areas from 1/4 to 2 sq in. exposed to the corrodent. As the exposed areas decreased in size, the probability of stress corrosion cracking also decreased. No cracks were obtained in the smallest areas exposed, even with these areas electrically connected to much larger unstressed areas of the same material exposed in the same cell.

As was indicated earlier, the sodium chloride-ammonium nitrite solution was used at a pH of approximately 7. Increasing the pH of this solution to 8.5 slightly increased the susceptibility of the 304L alloy to stress-corrosion cracking without, however, affecting that of the Type 304 specimens. Solutions with a pH as low as 4.0 produced stress-corrosion cracking in the latter steel. Solutions with a pH less than 4.0 generally produced pitting only and no stress-corrosion cracks. Determinations of pH were made at the conclusion of many tests in which the neutral NaCl + NH_4NO_2 solution had been used. Changes in pH were usually less than 1.0 and were not consistent in either amount or direction.

The problem of whether or not pitting must precede stress-corrosion cracking has not as yet been completely resolved in this investigation. Stress-corrosion cracks obtained by subjecting a specimen previously pitted in an NaCl solution to stress in the corroding medium produced cracks that were not associated with any of the larger pits that had been formed previously. When specimens were periodically removed from the corroding solution for photographing they had to be reactivated before their return to the solution. Hence, each time the test was interrupted it was, in effect, started at the beginning again. Taking into account these limitations, the data, never-

Fig. 4 Stress-corrosion crack in Type 304 stainless steel specimen electropolished and exposed stressed to 90% of the yield strength in a boiling 3½% NaCl + 1% NH_4NO_2 solution for 4 hr

Note the pit, corrosion products indicated by arrows, and the slip markings. Unetched. X 400

Fig. 5 Stress-corrosion cracks in Type 304 stainless steel

Cracks are transcrystalline. Etched electrolytically in 10% chromic acid. X 200.

theless, indicate that stress-corrosion cracking may develop with little or no previous pitting.

In order to avoid interrupting the test to follow the progress of corrosion, a cell was designed which contained an optically flat window through which the specimens could be photographed. A sheet tensile specimen with a gage length of 1 in. and a width of 0.125 in. is used in this cell which permits photographing of the top surface of the entire gage length of the specimen. The cell as set up to be used with a still camera is shown in Fig. 6; it is currently being used with a 16-mm motion picture camera in time lapse studies of the progress of stress-corrosion cracking.

Figures 7 and 8 are from a series of still photographs showing evidences of the development of two stress-corrosion cracks and one pit. Gas bubbles were seen coming from both the cracks and the pit. Bubbles were noticed evolving from the first crack in about 1¼ hr after the specimen was first stressed. The second crack developed after approximately 2½ hr and the pit after 2 hr.

Samples of the gas evolved from specimens under test were analyzed by the Mass Spectrograph Section of the National Bureau of Standards. Hydrogen was present in all samples and as the test progressed increasing amounts of nitrogen were also found. No oxides of nitfogen have been found. This is interpreted to mean that the ammonium nitrite is breaking down with time[12] according to the equation $NH_4NO_2 \rightarrow 2H_2O + N_2$ and most probably explains why very few complete failures of

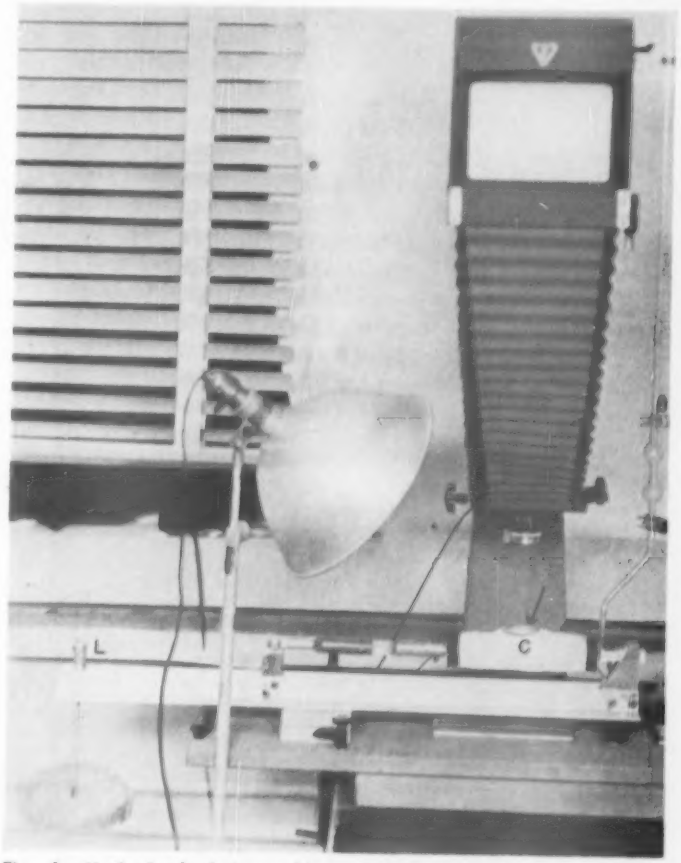

Fig. 6 Method of photographing specimen without interrupting the test

Specimen is incased in cell C and is photographed through optical flat at the bottom of the well indicated by arrow. Cell is heated by surrounding resistance coil. Evaporation is prevented by air condenser B at right. Specimen is stressed by means of lever system L.

specimens were obtained even after 10 days' exposure in the corroding medium.

Large-grained specimens of the 304L alloy having both rectangular and square cross sections and of the 304 alloy having rectangular cross sections were exposed in the boiling NaCl + NH_4NO_3 solution stressed so as to produce plastic deformation, until stress-corrosion cracks developed. The edges of such specimens are stress raisers. Hence, it is assumed that a stress-corrosion crack extending continuously from the first to the second of two adjacent surfaces of a large grained specimen had its origin at the common edge of the two surfaces. It is then easily possible from back reflection X-ray patterns of the two crystal surfaces to determine the crystallographic plane on which the stress-corrosion crack had its origin.[13] This investigation is in progress. Determinations of the crystallographic planes on which stress-corrosion cracks developed have now been made for 4 crystals in the large grained specimens. The distribution of the normals to these crystallographic planes is shown in Fig. 9.

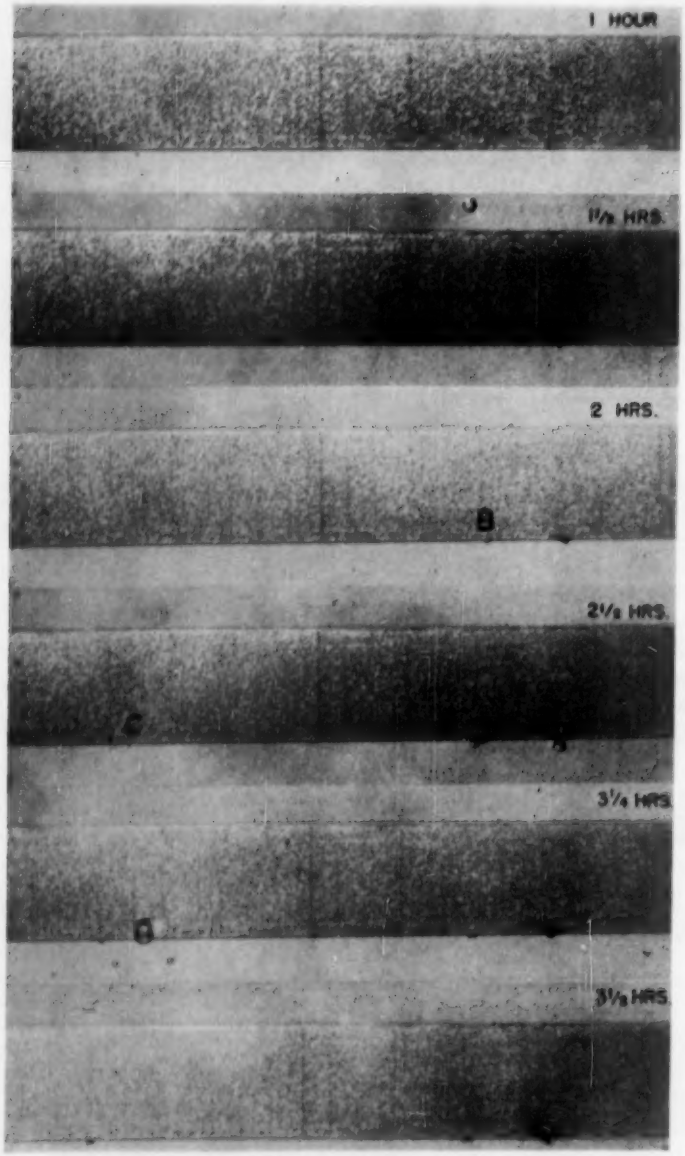

Fig. 7 Photographs, taken by method of Fig. 6, showing face of Type 304 stainless-steel specimen after exposure for periods indicated at a stress of 90% of the yield strength in a boiling 3½% NaCl + 1% NH_4NO_3 solution

Gas bubbles escaping indicate beginning of cracks at A and C and of a pit at B, all on lower edge of specimen. X 6. (Reduced by 9% upon reproduction.)

Discussion

Stress-corrosion cracking in metals and alloys is generally considered to be electrochemical.[10] In a suitable corrodent, surface areas extremely narrow with respect to their length and with their long axes approximately normal to the applied tensile stress are believed to be anodic to the material as a whole. An electric current will then flow through the corroding solution from this anodic area to surrounding cathodic areas; the circuit is of course completed through the metal itself. If the anodic area is extremely narrow the current density becomes relatively high and the metal goes into solution rapidly at that area.

The passivity of stainless steel depends upon the availability of oxygen at its surface,[14] that is, on the formation and retention of a protective film. In a chloride solution the electrochemical solution potential of unstressed stainless steel, which is in effect an indication of the homogeneity and continuity of this protective film, is constantly changing. It has been shown that the application of stress can rupture this film[15] and that the film-free material may then be as much as 0.5 v anodic to the passive surface in a chloride solution. "Oxygen concentration cells" may also be set up in a chloride solution where a foreign material, even as inert as glass, is in contact with the steel so that the supply of oxygen at the contact is limited. Pitting then results.

It is suggested that during application of tensile forces microscopic slip in a favorably oriented crystal may rupture the protective film on the metal under such conditions of oxygen supply that this film cannot be immediately repaired. Corrosion occurs in a very narrow area normal to the applied stress and the corrosion product formed at the site tends to form an oxygen concentration cell. As the corrosion continues, the crack becomes deeper and the corrosion product formed, because of its increased volume, adds considerably to the driving stress, thus providing a vicious cycle of continuity.

The idea that a stress-produced martensite transformation[5, 16] provides the anodes for the electrolytic stress corrosion of stainless steel has never had wide acceptance in this country. In the studies of martensite transformations in many materials "habit" crystallographic planes[17] have been determined. No data have come to the authors' attention for such transformations in the austenitic stainless steels. In low-carbon, low-alloy steels the habit plane is reported to be the (225) plane of the austenitic phase. The normals to planes

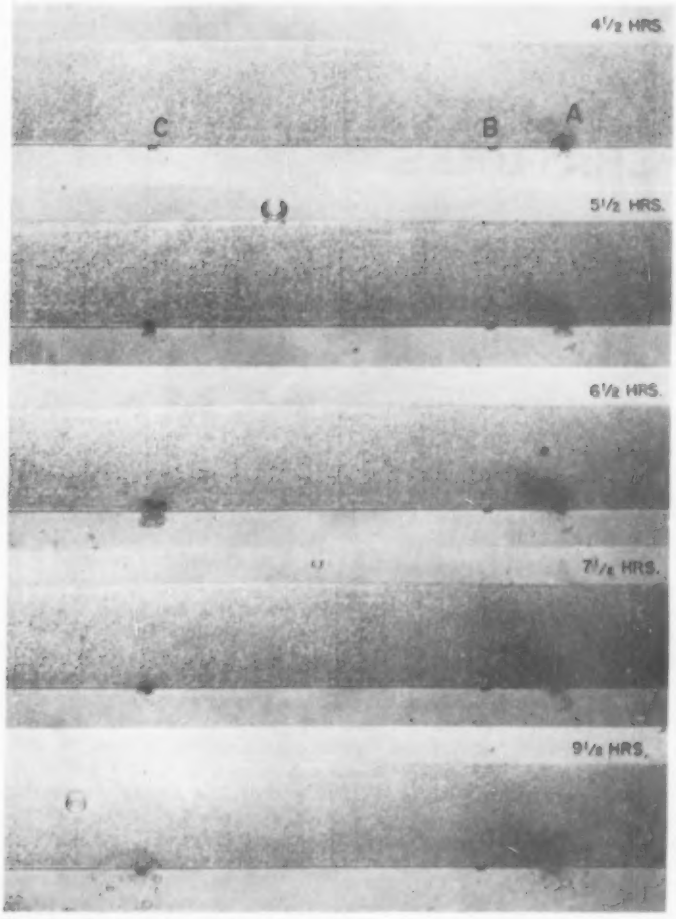

Fig. 8 Continuation of test shown in Fig. 7

Between $3^1/_2$- and $4^1/_2$-hr photographs the solution was cooled to room temperature and stress removed overnight (but specimen not removed from solution). Periods reported are for exposure at temperature and under stress. X 6. (Reduced by 20% upon reproduction.)

Fig. 9 Stereographic triangle showing pole of (225) crystallographic plane and normals (○) to planes on which stress-corrosion cracks originated in large grained types 304 and 304L stainless steels

on which the stress-corrosion cracks were initiated, shown in Fig. 9, do not lie near the pole of the (225) plane. The limited data indicate that there is no plane or family of planes that is particularly susceptible to stress-corrosion cracking.

Summary

1. Approximately 40 solutions were investigated as possible test corrodents for the stress-corrosion cracking of types 304 and 304L stainless steels.

2. A boiling $3^1/_2$% NaCl-1% NH_4NO_2 solution, pH approximately 7.0, produced stress-corrosion cracking in a few hours in the Type 304 steel stressed in tension to 80% or more of its room temperature yield strength. It was necessary to stress the Type 304L alloy to 100% of its yield strength to produce stress-corrosion cracking in this corrodent.

3. A stress-corrosion crack was found in a 0.20-in. gage length of a specimen that had been strained as little as 0.52%. There was no correlation, however, between the amount of strain in a given gage length and the presence of cracks.

4. Pitting was the general type of corrosive attack in solutions having a pH of less than 4.0. Stress-corrosion cracking could be obtained at a higher pH. Increasing the pH of the NaCl + NH_4NO_2 solution from 7.0 to 8.5 increased the susceptibility of the 304L stainless steel to stress corrosion cracking but had little effect on the Type 304 material.

5. The development of stress corrosion cracks was followed both by interrupting the test and by photographing the specimen *in situ*. In some instances at least, stress-corrosion cracks developed with little or, possibly, no previous pitting.

6. Hydrogen was given off during the corrosion process and also, as boiling of the solution continued, increasing amounts of nitrogen. The latter fact indicated that the NH_4NO_2 was being broken down into N_2 and H_2O.

7. It is postulated that stress-corrosion cracking of the 304 stainless steel results from rupturing of the passive film by the application of stress under conditions favorable to the formation of oxygen concentration cells.

References

1. ASM Educational Lecture Series on Stress Corrosion, Cleveland Meeting, 1949 (unpublished).

2. Nathorst, Helmer, "Stress-Corrosion Cracking of Stainless Steels," Welding Research Council Bulletin No. 6 (October 1950).

3. Scheil, M. A., Zmeskal, O., Weber, J., and Stockhausen, F., "First Report on Stress Corrosion Cracking of Stainless Steel in Chloride Solutions," The Welding Journal, **22** (10), Research Suppl., 493-s (1943).

4. Comeon, H. R., "The Influence of Corrosion on the Cracking of Pressure Vessels," *Ibid.*, **32** (2), Research Suppl., 75-s to 91-s (1953).

5. Franks, Russell, Binder, W. O., and Brown, Charles M., "The Susceptibility of Austenitic Stainless Steels to Stress-Corrosion Cracking," Symposium on Stress Corrosion Cracking of Metals, ASTM-AIME, 411 (1944).

6. Edeleanu, C., "Transgranular Stress Corrosion in Chromium-Nickel Stainless Steels," *Jnl. Iron Steel Inst.*, **173**, 140 (February 1953).

7. Logan, Hugh L., and Hessing, Harold, "Stress-Corrosion Tests on High-Strength Aluminum Alloy Sheet," *Jnl. Research Natl. Bur. Standards*, **41**, 69 (July 1948).

8. Mahla, E. M., and Nielsen, N. A., "A Study of Films Isolated from Passive Stainless Steels," *Trans. Electrochemical Soc.*, **93**, 1 (1948).

9. Monack, M. L., private communication.

10. Mears, R. B., Brown, R. H., and Dix, E. H., Jr., "A Generalized Theory of Stress Corrosion of Alloys," Symposium on Stress Corrosion Cracking of Metals, ASTM-AIME, 334 (1944).

11. Colner, William H., and Francis, Howard T., "Influence of Exposed Area on Stress-Corrosion Cracking of 248 Aluminum Alloy," NACA Tech. Note 3292 (November 1954).

12. Ray, P. C., "The Decomposition and Sublimation of Ammonium Nitrite," *Jnl. Chem. Soc. (London)*, **95**, 349 (1909).

13. Barrett, Charles S., *Structure of Metals*, 2nd ed., p. 40, McGraw-Hill (1952).

14. Uhlig, H. H., Editor, *Corrosion Handbook*, John Wiley & Son, Inc., New York, p. 23 (1948).

15. Logan, Hugh L., "Film-Rupture Mechanism of Stress Corrosion," *Jnl. Research NBS*, **48**, 99, RP2291 (February 1952).

16. Rocha, H. J., "Die Spannungskorrosion Austenitischer Stähle," *Stahl u. Eisen*, **62**, 1091-1094 (1942).

17. Barrett, Charles S., *Structure of Metals*, 2nd ed., p. 564.

18. Hoar, T. P., and Hines, J. G., "Stress-Corrosion Cracking of Austenitic Stainless Steels," *J. Iron and Steel Inst.*, **182**, 124 (1956).

19. Williams, W. L., and Eckel, J. F., "Stress Corrosion of Austenitic Stainless Steels in High Temperature Waters," *J. Am. Soc. Naval Eng.* (February 1956).

ARC-WELDING TEMPERATURES

Experimental and analytical studies of quasistationary temperature distribution in thick and thin arc-welded stainless-steel plates found to be in excellent agreement

BY R. J. GROSH AND E. A. TRABANT

ABSTRACT. This paper compares the results of two recent measurements of the quasistationary temperature distribution in thick and thin arc-welded stainless steel plates with an analytical study previously reported. The analytical results were obtained for one, two, and three-dimensional heat conduction from a moving plane, line, and point energy source where the thermal properties of the solid are certain functions of temperature. The analytical results are outlined. Excellent agreement is noted between experiment and theory.

Introduction

Knowledge of the temperature distribution in welding enables estimates to be made of distortion, thermal stresses, and the mechanical properties of the weld. The theory relating to this distribution is of interest because it provides estimates for the temperature and can also be applied to analogous problems involving convection, diffusion and electricity.

A survey indicates that the temperature distribution has been measured and reported for steel, aluminum, copper, iron, magnesium and titanium plates which were arc welded, gas welded, resistance welded or welded with thermit. Techniques used to obtain these measurements have ranged from the use of crayons, wax pellets and cones with fixed melting points to thermocouples and automatic recording systems. This paper is concerned with the temperature distribution during arc welding.

R. J. Grosh is Assistant Professor, Mechanical Engineering, and E. A. Trabant is Associate Professor, Engineering Sciences, Purdue University, Lafayette, Ind.

Spraragen and Claussen[1] have reviewed the literature to 1937. Prior to this date, most investigators used different materials with results often reported for mild steels in the form of maximum temperature distribution curves or cooling curves. Since 1937, numerous papers have appeared on the thermal aspects of arc welding.

In 1943, Hess and co-workers[2] measured cooling rates in low-carbon steel plates 0.25, 0.50, 1.0, and 1.5 in. thick. The effects of electrode diameter and coating, a-c versus d-c welding current, chemical composition of the plates, and latent heat of metallurgical transformation were considered. In this same year, Doan and Stout[3] established a correspondence between hardness tests and cooling rates which was discussed by Mahla and co-workers[4] in 1941 and later by Rosenthal[5] in 1944. In 1943, Paschkis[6] established cooling curves of plates in the vicinity of the weld by means of an analog computer and postulated modes of heat transfer from the electrode and arc to the plate.

In 1946, Rosenthal extended previous results with a published theory of moving heat sources with some application to metal treatment.[7] Rosenthal and Schmerber[8] experimentally verified one of the theoretical results for the temperature distribution in welding. It is interesting to note, that certain results obtained independently by Rosenthal had been obtained earlier by Roberts,[9] in 1923, who was interested in certain diffusion problems and Wilson,[10] in 1904, who considered some cases of convection. Wells[11] used the theory of moving sources to predict the width of the melted zone in butt-welded steel plates. The results were in good agreement with the data of Jackson and Shrubsall[12] who measured the width of the melted zone and the energy distribution in electric welding.

Nippes and co-workers[13–15] have developed a method for obtaining the temperature distribution from a limited amount of experimental data. These data were used in conjunction with a device which developed a specimen which simulated the various regions of weld heat-affected zones and with which properties of the weld were studied.

The works cited and others have furnished means for understanding and estimating temperature transients during arc welding. It has been shown that

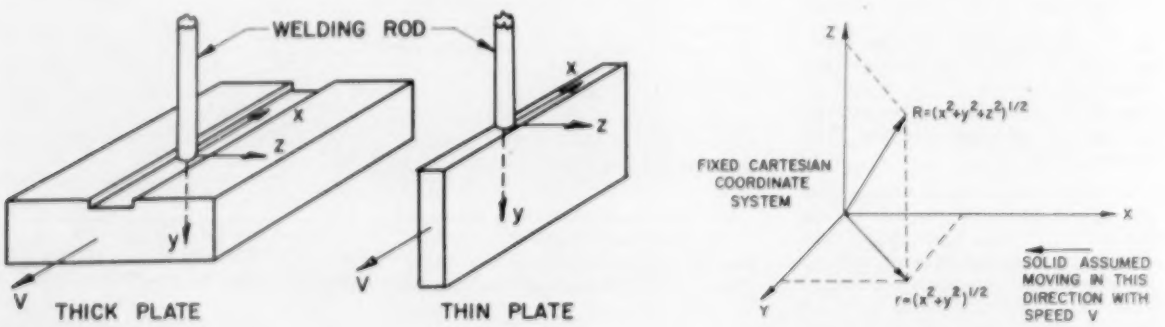

Fig. 1 Coordinate system

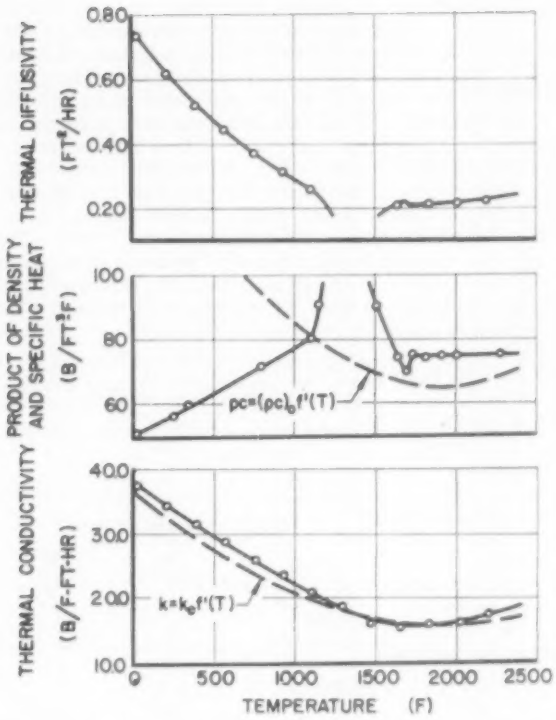

Fig. 2 Thermal conductivity, product of density and specific heat, and thermal diffusivity for a stainless steel[17]

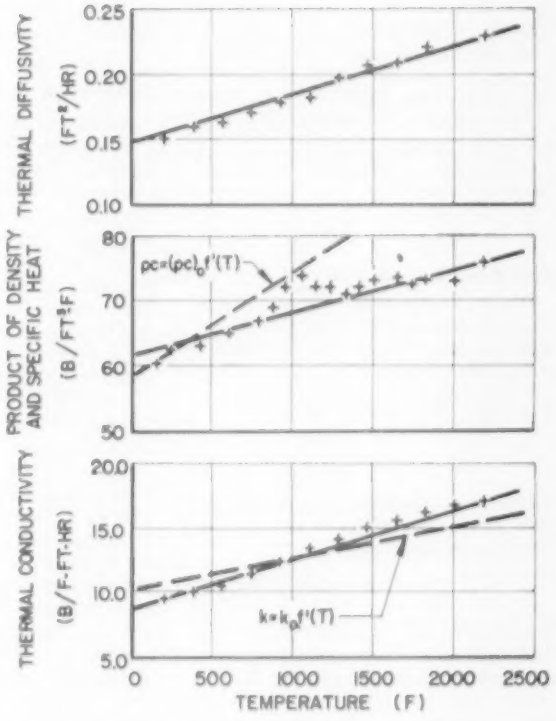

Fig. 3 Thermal conductivity, product of density and specific heat, and thermal diffusivity for a low-carbon steel[17]

geometry, thermal properties of the welded objects, arc current, voltage, efficiency, and speed are primary variables. Surface heat losses by radiation and convection, latent heat, finite electrode size and coating, and Joule heating are of secondary importance and can often be neglected in many cases.

This paper reports the effect of the variation in thermal properties with temperature on the temperature distribution in welding. Results of theory and experiment are compared. Excellent agreement is obtained. In the case of arc-welded mild-steel plates, previous investigations have shown that some discrepancy exists between measured temperatures and those obtained theoretically assuming constant thermal properties.[8]

The partial differential equation for quasistationary heat conduction in a solid moving with constant velocity, as shown in Fig. 1, is

$$\frac{\partial}{\partial x}\,k\,\frac{\partial T}{\partial x}+\frac{\partial}{\partial y}\,k\,\frac{\partial T}{\partial y}+\frac{\partial}{\partial z}\,k\,\frac{\partial T}{\partial z}=-\rho c v\,\frac{\partial T}{\partial x} \quad (1)$$

where the symbols, and the symbols used in subsequent equations correspond to those given in the Appendix. In general, the thermal properties of the solid are marked functions of temperature as shown in Figs. 2 and 3. Let

$$k = k_0 f'(T) \quad (2)$$

and

$$\rho c = (\rho c)_0 f'(T) \quad (3)$$

where $f'(T)$ is the temperature derivative of some function of temperature. The form of $f'(T)$ is chosen to best represent the data and avoid violation of the "second law of thermodynamics"; that is, avoid negative values of thermal conductivity and product of density and specific heat in the temperature ranges encountered. The efficacy of this representation for a stainless and low-carbon steel is shown in Figs. 2 and 3. Equation 1 neglects Joule heating by the arc current, and latent heat of metallurgical transformations; these effects are usually unimportant. Heat loss from the surfaces of the solid by convection and radiation are also neglected.

With these assumptions, the authors have developed a theory of moving sources for solids with variable thermal properties.[18] Analytical results have been obtained for a general $f'(T)$[13] but, for the purpose of this paper it is assumed that

$$f'(T) = 1 + mT \quad (4)$$

where m is a positive constant. No assumptions, other than those stated, have been used in deriving the following results.

Unidirectional Heat Flow

For unidirectional heat flow in the axial direction of an infinite rod, i.e., the x-direction, and energy supplied by a plane source moving with the velocity v in the x-direction, the temperature distribution is given by Reference 1*B*, for $x \geq 0$

$$T = \frac{1}{m}\left\{\left[\frac{2q_s m}{A(\rho c)_0 v}\,e^{-2\lambda v x} + (1+mT_i)^2\right]^{1/2} - 1\right\} \quad (5)$$

and for $x \leq 0$

$$T = \frac{1}{m}\left\{\left[\frac{2q_s m}{A(\rho c)_0 v} + (1+mT_i)^2\right]^{1/2} - 1\right\} \quad (6)$$

This can be contrasted with the case where thermal properties are considered invariants,[7] for $x \geq 0$

$$T = \frac{q_s}{A(\rho c)_0 v}\,e^{-2\lambda v x} + T_i \quad (7)$$

and for $x \leq 0$

$$T = \frac{q_s}{A(\rho c)_0 v} + T_i \quad (8)$$

Two-Dimensional Heat Flow

If heat flows in an infinite plate of small thickness, then temperature gradients may be neglected in the plate thickness. If heat is supplied by a line energy source in the thickness of the plate and moves with constant velocity in the x-direction, then the temperature distribution is given by[18]

$$T = \frac{1}{m}\left\{\left[\frac{q_L m}{\pi L k_0}\,e^{-\lambda v x}\,K_0(\lambda v r) + (1+mT_i)^2\right]^{1/2} - 1\right\} \quad (9)$$

where K_0 (λvr) is a modified Bessel function of the second kind and zero order with argument λvr. This solution is of interest because it approximates the temperature distribution in thin arc-welded plates. The coordinate system related to the plate is shown in Fig. 1.

If thermal properties are considered constant,[7] then

$$T = \frac{q_L}{2\pi k_s L} e^{-\lambda v x} K_0(\lambda v r) + T_i \quad (10)$$

Three-Dimensional Heat Flow

If heat flows in an infinite solid from a point source moving along the x axis with constant velocity, then the temperature distribution is[18]

$$T = \frac{1}{m} \int_0^t \left[\frac{q_e m}{2\pi k_s R} e^{-\lambda v x} e^{-\lambda v R} + (1 + mT_i)^2 \right] - 1 \Big|_0^t \quad (11)$$

This solution can be compared with the case where thermal properties are not functions of temperature[7]

$$T = \frac{q_e}{4\pi k_s R} e^{-\lambda v x} e^{-\lambda v R} + T_i \quad (12)$$

Equation 11 is of interest because it approximates the temperature distribution in thick arc-welded plates. The coordinate system related to the plate is shown in Fig. 1.

Comparison of Theory and Experiment

Grosh and Hawkins[19] have measured the quasistationary temperature field in thin, arc-welded, Type-304 stainless-steel plates.[15] The plates were $^1/_4$ in. thick, 30 in. wide and 47 in. long. The weld was deposited on the $^1/_4$-in. thick edge which was machined flat before welding. Six 0.035- or 0.046-in. diam holes were drilled halfway into the plate for thermocouples. The three largest holes were staggered along the edge between 0.095 and 0.206 in. from the weld for 28 B & S gage chromel-alumel thermocouples; the three remaining holes were also staggered and between 0.48 and 0.72 in. from the weld for 30 B & S gage iron constantan thermocouples. The wires were inserted in small two-hole ceramic insulators and the assembly soldered into the hole with a small mass of high-remelt temperature silver solder. The thermocouple output was recorded with an electronic automatic potentiometer or an oscillograph with amplifier.

Nippes, Wawrousek and Fleischmann[15] have measured the quasistationary temperature field in thick, arc-welded Type-347 stainless-steel plates. The plate was $1^1/_2$ in. thick and 12 in. square. The weld was deposited in a groove $^3/_8$ in. wide and $^1/_{16}$ in. deep machined in the surface of the plate. Eight thermocouples holes 0.052 in. in diam were placed fan-like between 0.2 and 1.25 in. from the centerline of the groove. The chromel-alumel thermocouples were percussion welded to the bottom of these holes. The output was recorded with a 14-channel oscillograph.

In each case, the welding was done with an automatic welder and electrical data recorded on chart-type recorders.

The pertinent data for the welds are shown in Table 1.

Table 1—Arc-Weld Runs*

	Thin plate[19]	*Thick Plate*[15]
Arc current, amp	81.0	130
Arc voltage, v	19.5	23.2
Arc speed, ipm	19.2	5.85
Electrode diameter, in.	3/32	5/32

* Data taken from References 15 and 19

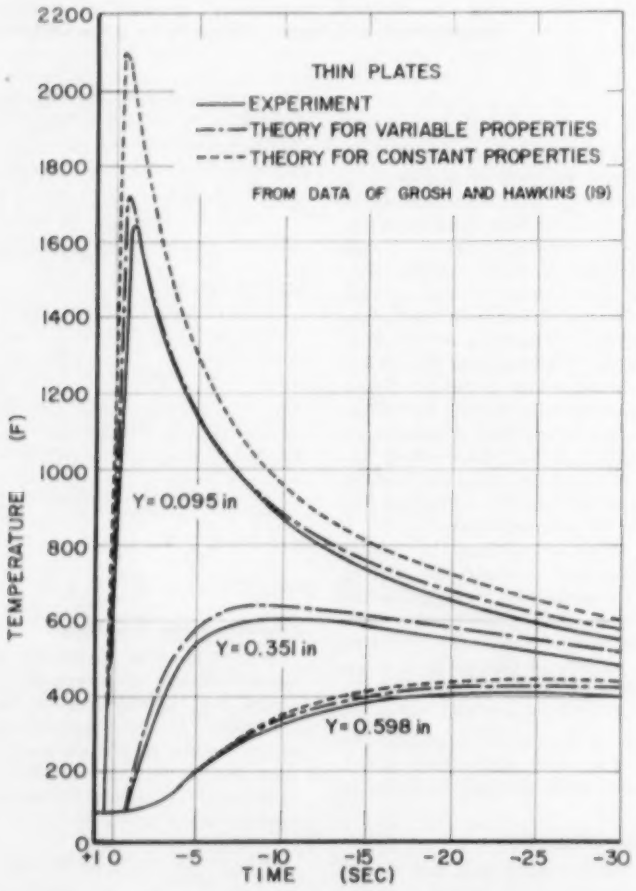

Fig. 4 Comparison of theory and experiment for thin plate

The theoretical result for two-dimensional heat conduction from a moving line source in a plate, eq. 9, where the thermal properties are linear functions of temperature was applied to the measurements of Grosh and Hawkins.[19] The comparison between theory and experiment is shown in Figs. 4 and 5. For purposes of comparison, the two-dimensional results where properties are considered constant, eq 10, are also shown in these figures. In the latter case, the properties used were taken as: thermal conductivity—10.0 B/hr ft °F, and thermal diffusivity—0.175 sq ft/hr. Both in eqs 9 and 10, the heat input was evaluated from the arc voltage and current assuming an arc efficiency of 74%. The representation for the variable properties will be discussed later.

The theoretical result for three-dimensional heat conduction from a moving point source, eq 11, for the thick plate where thermal properties are linear functions of temperature was applied to the measurements of Nippes, Wawrousek and Fleischmann.[15] The comparison between theory and experiment is shown in Fig. 6. Also, for purposes of comparison, the three-dimensional results where properties are considered constant, eq 12, is shown. In the latter case, the properties were taken as: thermal conductivity—13.0 B/hr ft ° F, product of density and specific heat—69.0 B/cu ft °F, and thermal diffusivity—0.188 sq ft/hr. Both in eqs

11 and 12, the heat input was evaluated from the arc voltage and current assuming an arc efficiency of 85%.

In the cases where thermal properties were considered linear functions of temperature, they were taken as

$$k = 10.0\left(1 + \frac{T}{3540}\right) \quad (13)$$

$$c = 57.4\left(1 + \frac{T}{3540}\right) \quad (14)$$

The compositions of Type-304, thin-plate, stainless steel and Type-347, thick-plate, stainless steel are shown in Table 2.

Table 2—Chemical Composition of Steels*

	Type 304	*Type 347*
C	0.08 max	0.08 max
Mn	2.00 max	2.00 max
Si	1.00 max	1.00 max
P	0.04 max	0.04 max
Sr	0.03 max	0.03 max
Cr	18.0/20.0	17.0/19.0
Ni	8.00/11.0	9.0/12.0
Cb	—	10x % C min

* Data taken from reference 16.

Since the composition of the two plates are similar, it is not unlikely that the thermal properties and their variations with temperature would be the same.[16]

The rate of heat input to the plates was determined from the arc current, voltage and efficiency. The arc efficiencies were assumed as 74 and 85% for the thin and thick plates, respectively. It is difficult to estimate the arc efficiency; however, the trend from the thin to thick plate is not unexpected.

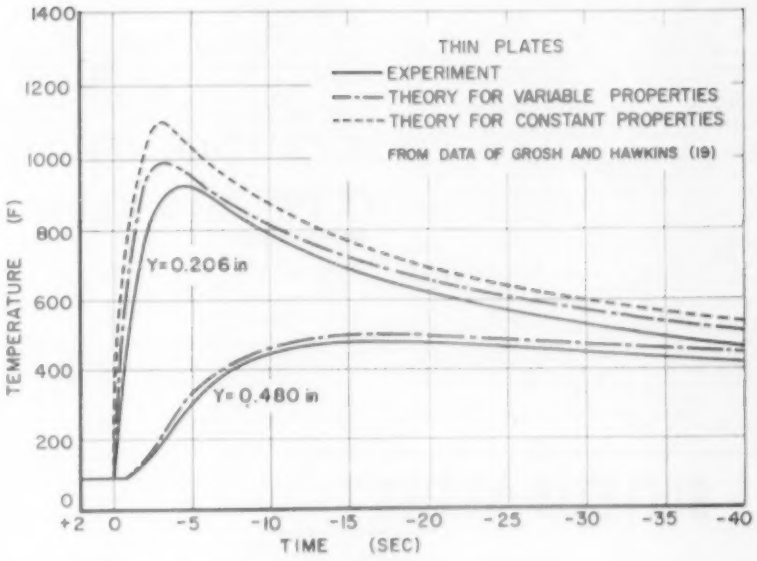

Fig. 5 Comparison of theory and experiment for thin plate

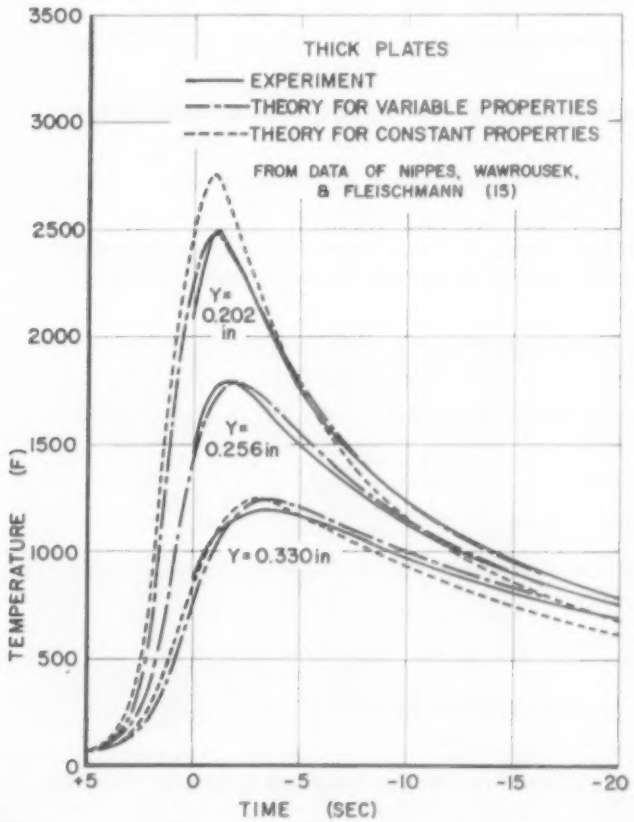

Fig. 6 Comparison of theory and experiment for thick plate

Conclusions

The main conclusions are as follows:

(*a*) A theory of moving sources has been developed to account for the variation of thermal properties with temperature.

(*b*) The fact that the type of variations considered requires the thermal diffusivity to be constant appears to be of secondary importance for the cases considered.

(*c*) The theory offers a useful and accurate means for obtaining the temperature distribution in thick and thin plates.

Acknowledgments

The writers wish to thank the Graver Tank and Manufacturing Co., East Chicago, Ind., for the assistance which has led to this work. Also appreciated is the assistance of Professor E. F. Nippes, Rensselaer Polytechnic Institute, Troy, N. Y., who furnished the writers with some of the original data from Reference 15.

References

1. Spraragen, W., and Claussen, G. E., "Temperature Distribution During Welding—A Review of the Literature to January, 1937," The Welding Journal, 16 (4) (1937).

2. Hess, W. F., Merrill, L. L., Nippes, E. F., and Bunk, A. P., "The Measurement of Cooling Rates Associated with Arc Welding and Their Application to the Selection of Optimum Welding Conditions," *Ibid.*, 22, 377 (1943).

3. Doan, G. E., and Stout, R. D., "A Tentative System for Preserving Ductility in Weldments—Parts I, II, and III," *Ibid.*, 22, 278 (1943).

4. Mahla, E. M., Rowland, M. C., Shook, C. A., and Doan, G. E., "Heat Flow in Arc Welding," *Ibid.*, 20, 459 (1941).

5. Rosenthal, D., "An Important Contribution to the Science of Welding," *Ibid.*, 23, 92 (1944).

6. Paschkis, V., "Establishment of Cooling Curves of Welds by Means of Electrical Analogy," *Ibid.*, **22**, 462 (1943).
7. Rosenthal, D., "The Theory of Moving Sources of Heat and Its Application to Metal Treatments," *Trans. ASME*, **68**, 829 (1946).
8. Rosenthal, D., and Schmerber, R., "Thermal Study of Arc Welding. Experimental Verification of Theoretical Formulas," THE WELDING JOURNAL, **17**, 2 (1938).
9. Roberts, O. F. T., "The Theoretical Scattering of Smoke in a Turbulent Atmosphere," *Proc. Roy. Soc.*, A, 104, 640 (1923).
10. Wilson, H. A., "On Convection of Heat," *Proc. Cambridge Phil. Soc.*, **12**, 406 (1904).
11. Wells, A. A., "Heat Flow in Welding," THE WELDING JOURNAL, **31**, 263 (1952).
12. Shrubsall, A. E., and Jackson, C. E., "Energy Distribution in Electric Welding," *Ibid.*, **29**, 231 (1950).
13. Nippes, E. F., Merrill, L. L., and Savage, W. F., "Cooling Rates in Arc Welds, in 1/2-in. Plates," *Ibid.*, **28**, 556 (1949).
14. Nippes, E. F., and Savage, W. F., "Development of Specimen Simulating Weld Heat-Affected Zones," *Ibid.*, **28**, 534 (1949).
15. Nippes, E. F., Wawrousek, H., W. F. Fleishmann, W. F., "Some Properties of the Heat-Affected Zone in Arc-Welded Type 347 Stainless Steel," *Ibid.*, **34**, 169 (1955).
16. ASME, "Metals Properties," McGraw-Hill Book Co., 1954.
17. Powell, R. W., "The Physical Properties of a Series of Steels—Part II," *J. Iron Steel Inst.*, **154**, 83 (1946).
18. Grosh, R. J., Trabant, E. A., and Hawkins, G. A., "Temperature Distribution in Solids of Variable Thermal Properties Heated by Moving Heat Sources," *Quart. Appl. Math.*, **13**, 161 (1955).
19. Grosh, R. J., and Hawkins, G. A., "Experimental Study of the Temperature Distribution in Plates During Arc Welding," *ASME Preprint*, No. 55-A-26 (November 1955).

APPENDIX

Nomenclature

Symbol	Description	Units
A	Area of plane source	ft²
c	Specific heat	B/lb ° F
k	Thermal conductivity	B/hr ft° F
L	Plate thickness	ft
q	Rate of heat flow from source	B/hr
r	$(x^2 + y^2)^{1/2}$	ft
R	$(x^2 + y^2 + z^2)^{1/2}$	ft
T	Temperature	° F
v	Speed of source	ft/hr
x,y,z	Cartesian coordinates	ft
α	Thermal diffusivity	ft²/hr
λ	$k/c\rho$	hr/ft³
ρ	Density	lb/ft³
Subscripts		
i	Initial condition	
L	Line source	
o	Evaluated at reference temperature	
p	Point source	
s	Plane source	

BULLETIN SERIES

Requests for single copies should be sent to the
AMERICAN WELDING SOCIETY, *29 W. 39th St., New York 18, N. Y.*

Requests for bulk lots ten or more, should be sent to the
WELDING RESEARCH COUNCIL, *29 W. 39th St., New York 18, N. Y.*

No. 1 **Steel Compositions and Specifications,** *by Charles M. Parker, March 1949. $0.50.*

No. 2 **The Nature of the Arc,** *by J. D. Cobine, April 1949. $0.50.*

No. 3 **Burn-Off Characteristics of Steel Welding Electrodes,** *by D. C. Martin, P. J. Rieppel and C. B. Voldrich, May 1949. $0.50.*

No. 4 **Testing Pressure Vessels,** *by F. G. Tatnall;* **Effect of Welding on Pressure Vessel Steels,** *by A. F. Scotchbrook, L. Erir, R. D. Stout and B. G. Johnston, February 1950. $0.50.*

No. 5 **How Plastic Deformation Influences Design and Forming of Metal Parts,** *by John R. Low, Jr.;* **Brittle Fracture in Mild Steel,** *by J. S. Hoggart, May 1950. $1.00.*

No. 6 **Stress Corrosion Cracking of Stainless Steels,** *by Helmer Nathorst; Part I*—**Practice Experiences;** *Part II*—**An Investigation of the Suitability of the U-bend Specimen,** *October 1950. $1.00.*

No. 7 **Instrumentation for the Evaluation of the Stability of the Welding Arc,** *by L. P. Winsor, L. McDonald Schetky and Robert A. Wyant, November 1950. $1.00.*

No. 8 **Tests of Columns under Combined Thrust and Moment,** *by Lynn S. Beedle, Joseph A. Ready and Bruce G. Johnston, December 1950. $1.00.*

No. 9 **Copper in Stainless Steels,** *by Helmut Thielsch, August 1951. $1.00.*

No. 10 **Thermal Fatigue and Thermal Shock,** *by Helmut Thielsch, April 1952. $1.00.*

No. 11 **Investigations of Effect of Fabrication Operations Upon Pressure Vessel Steels,** *by S. S. Tör and Robert D. Stout, May 1952. $1.00.*

No. 12 **An Analytical Study of Aluminum Welding,** *by C. O. Smith, E. R. Funk and H. Udin, June 1952. $1.00.*

No. 13 **A New High-Yield Strength Alloy Steel for Welded Structures,** *by L. C. Bibber, J. M. Hodge, R. C. Altman and W. D. Doty, July 1952. $1.00.*

No. 14 **Welding Processes and Procedures Employed in Joining Stainless Steels,** *by Helmut Thielsch, September 1952. $2.00.*

(continued on page 408-s)

WELDING THE CUPRO-NICKELS BY THE INERT-GAS-SHIELDED ARC PROCESSES

Detailed information provided includes recommendations for filler metal, joint design, welding currents, shielding gas, operational techniques and mechanical properties of the joint

BY L. H. HAWTHORNE AND R. F. BURTH

ABSTRACT. The purpose of this paper is to provide detailed information pertinent to the welding of the cupro-nickel alloys by both the inert-gas-shielded tungsten-arc and the inert-gas-shielded metal-arc processes.

Heretofore, the older 70-30 cupro-nickel alloy has been welded quite satisfactorily by the metal-arc process, but the new 90-10 cupro-nickel alloy which has been gaining in usage has presented some problem to fabricators because of the relatively higher thermal conductivity.

Proper use of the recently introduced 70-30 cupro-nickel filler metal designed for use with the inert-gas-shielded arc processes eliminates these difficulties as well as offering substantial savings in the cost of fabricating these alloys.

Recommendation for use of this filler metal for welding the cupro-nickels to themselves and to steel are outlined.

Complete details as to recommended joint design, welding currents, shielding gas, operational techniques and the mechanical properties of the joint are included herein.

Procedure details for a variety of commercial application are outlined in detail in this paper.

L. H. Hawthorne and **R. F. Burth** are associated with the Research Department, Revere Copper and Brass, Inc., Rome, N. Y.

Presented at the 1956 AWS National Spring Meeting in Buffalo, N. Y., May 7-11.

Table 1—Compilation of Chemical and Mechanical Requirements for the 70–30 and 90–10 Cupro-nickels as Given in ASTM B 171-55 and Mil-C-15726A (Ships) Specifications

Element	*ASTM-B 171-55*		*Mil-C-15726A (Ships)*	
	90–10	*70–30*	*90–10*	*70–30*
Copper	86.5 min	65.0 min	Balance	65.0 min
Nickel	11.0	29.0–33.0	9.0–11.0	29.0–32.0
Iron	0.5–2.0	0.7 max	1.00–1.75	0.40–0.70
Manganese	1.0 max	1.0 max	0.75 max	1.0 max
Zinc	1.0 max	1.0 max	1.0 max	1.0 max
Lead	0.05 max	0.05 max	0.05 max	0.05 max
Minimum tensile strength, psi	40,000	50,000	38,000	45,000

Introduction

The copper-nickel alloy of the 70 copper–30 nickel composition has long been recognized for its resistance to corrosion and erosion-corrosion.

More recently a 90 copper–10 nickel alloy has been developed that has corrosion resistance generally equal to and in some applications better than the 70–30 cupro-nickel alloy. Moreover, because of the lower nickel content the cost of this alloy is appreciably lower and availability is improved.

Until early in 1955 fabricators using either of these alloys were usually forced to employ the metal arc (coated electrode) method for all fusion welding operations.

This method of welding required careful slag removal, removal of spatter and was relatively slow for nearly all applications as compared to the inert-gas-shielded methods of welding which lend themselves well to automatic or semiautomatic operations.

In some instances fabricators were

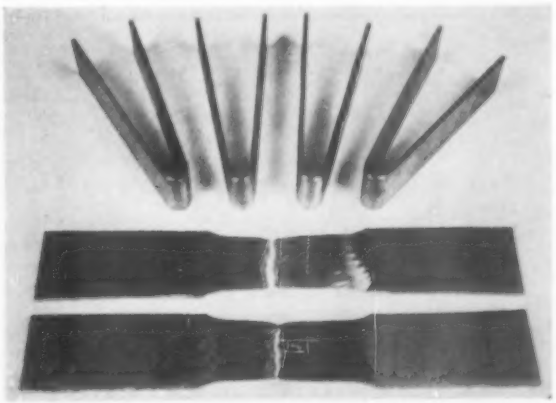

Fig. 1 Bend and tensile specimens of GSTA 104. Tensile specimens failed at 43,600 and 45,000 psi (see Table 5) with failure occurring in the weld. The base metal was 90–10 cupro-nickel

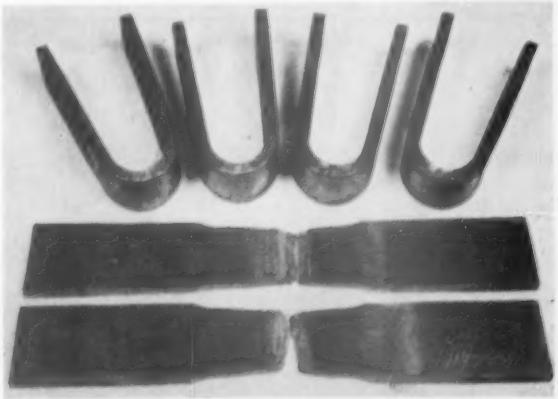

Fig. 2 Bend and tensile specimens of GSMA 87. Tensile specimens failed at 45,700 and 46,200 psi (see Table 5) with failure occurring at the edge of the weld in the base metal and in the base metal approximately $1/4$ in. from the weld. The base metal was 90–10 cupro-nickel

Table 2—Chemical Analysis of 70–30 Cupro-nickel Filler Metal Employed with the Inert-Gas-Shielded Arc Processes

Element	%
Copper	67.75
Nickel	Balance
Titanium	0.23
Silicon	0.12
Iron	0.59
Manganese	0.77
Aluminum	0.06

able to employ these methods of welding using a Monel filler metal.

The use of 70–30 cupro-nickel metal-arc coated electrodes presented few problems other than increased welding cost in the welding of the 70–30 alloy. However, because of the higher thermal conductivity of the 90–10 cupro-nickel, special techniques were necessary to produce consistently satisfactory joints in this alloy.

As a result, pressure was brought to bear on the producers of the cupro-nickel alloys and welding alloy suppliers to furnish a suitably modified rod and wire for use in welding the cupro-nickels by the inert-gas-shielded arc processes.

A wire of this type introduced early in 1955 was of a nominal 70 copper–30 nickel composition and was recommended for use in welding both the 70 copper–30 nickel and the 90 copper–10 nickel alloys.

This investigation was undertaken to determine whether or not a welding alloy of nominal 70 copper–30 nickel composition would consistently produce welds of code quality in these materials and in dissimilar joints between either of the cupro-nickel alloys and mild steel.

Procedure

Equipment

A d-c rectifier welder, three-phase, 60-cycle, with a welding current rating of 300–600 amp was used as a source of welding current for all experimental welding.

Recording volt and ampere meters were used to measure and record welding currents and arc voltages.

A consumable-electrode gun was used for all inert-gas-shielded metal-arc welding.

A 250-amp torch was used for all manual gas-shielded tungsten-arc welding.

Argon was used exclusively as the shielding gas with a standard argon flowmeter calibrated in cubic feet per hour.

All of the equipment employed was of commercial design and modified in no way for laboratory work.

Welding

At the start of this investigation it was decided to produce a series of test welds in 70–30 and 90–10 cupro-nickel including dissimilar joints between these alloys and between each of these alloys and mild steel to ascertain whether or not such welds could be qualified for ASME Boiler and Pressure Vessel Code applications.

The test welds made during the course of this investigation were in $^1/_8$- and $^3/_8$-in. thick 90–10 and 70–30 alloys employing both inert-gas-shielded metal and tungsten-arc processes.

Dissimilar welds were also made in $^3/_8$-in. material between 90–10 and 70–30 cupro-nickel, 90–10 cupro-nickel and mild steel and 70–30 cupro-nickel and mild steel.

Table 3—Summary of Joint Geometry Employed in the Production of Test Welds

Weld identification	*Base metal*	*Gage, in.*	*Joint design*	*Root face, in.*	*Root space, in.*	*Backing*
GSTA 103*	90–10 Cu-Ni	$^1/_8$	Square butt	$^1/_8$	None	Grooved copper
GSTA 104	90–10 Cu-Ni	$^3/_8$	60-deg included angle	None	$^1/_8$	Grooved copper
GSTA 102	70–30 Cu-Ni	$^1/_8$	Square butt	$^1/_8$	None	Grooved copper
GSTA 100	70–30 Cu-Ni	$^3/_8$	60-deg included angle	None	$^1/_8$	Grooved copper
GSMA 83†	90–10 Cu-Ni	$^1/_8$	Square butt	$^1/_8$	None	Grooved copper
GSMA 87	90–10 Cu-Ni	$^3/_8$	60-deg included angle	None	$^1/_8$	Grooved copper
GSMA 86	70–30 Cu-Ni	$^1/_8$	Square butt	$^1/_8$	None	Grooved copper
GSMA 89	70–30 Cu-Ni	$^3/_8$	60-deg included angle	None	$^1/_8$	Grooved copper
GSMA 82	90–10 Cu-Ni 70–30 Cu-Ni	$^3/_8$	60-deg included angle	None	$^1/_8$	Grooved copper
GSMA 84	90–10 Cu-Ni mild steel	$^3/_8$	60-deg included angle	None	$^1/_8$	Grooved copper
GSMA 83	70–30 Cu-Ni mild steel	$^3/_8$	60-deg included angle	None	$^1/_8$	Grooved copper

* The prefix GSTA indicates use of gas-shielded tungsten-arc process.
† The prefix GSMA indicates use of gas-shielded metal-arc process.

Table 4—Summary of Procedure Details Employed in the Production of Test Welds

Weld identification	*Base metal*	*Gage, in.*	*Welding current, amp*	*Arc voltage, v*	*Shielding gas, cfh*	*Filler metal, diam, in.*	*Tungsten electrode diam, in.*	*No. of passes*	*Average welding speed, ipm/pass*
GSTA 103*	90–10 Cu-Ni	$^1/_8$	300/310	25	Argon, 30	$^1/_8$	$^3/_{16}$	1	5
GSTA 104	90–10 Cu-Ni	$^3/_8$	300/310	25	Argon, 30	Pass No. 1, $^1/_8$; Passes 2, 3 and 4 $^3/_{16}$	$^3/_{16}$	4	6
GSTA 102	70–30 Cu-Ni	$^1/_8$	270/290	20	Argon, 30	$^1/_8$	$^3/_{16}$	1	5
GSTA 100	70–30 Cu-Ni	$^3/_8$	270/290	20	Argon, 30	$^5/_{32}$	$^3/_{16}$	4	6
GSMA 85†	90–10 Cu-Ni	$^1/_8$	280	27/28	Argon, 30	$^1/_{16}$		1	24
GSMA 87	90–10 Cu-Ni	$^3/_8$	280	27/28	Argon, 30	$^1/_{16}$		2	10–12
GSMA 86	70–30 Cu-Ni	$^1/_8$	280	27/28	Argon, 30	$^1/_{16}$		1	24
GSMA 89	70–30 Cu-Ni	$^3/_8$	280	27/28	Argon, 30	$^1/_{16}$		2	12
GSMA 82	90–10 Cu-Ni, 70–30 Cu-Ni	$^3/_8$	280	25/28	Argon, 30	$^1/_{16}$		4	18
GSMA 84	90–10 Cu-Ni to mild steel	$^3/_8$	280	27/30	Argon, 30	$^1/_{16}$		4	12
GSMA 83	70–30 Cu-Ni to mild steel	$^3/_8$	280	25/28	Argon, 30	$^1/_{16}$		4	12

* The prefix GSTA indicates use of gas-shielded tungsten-arc process. Direct-current straight polarity was used in all cases.
† The prefix GSMA indicates use of gas-shielded metal-arc process. Direct-current reverse polarity was used in all cases. All multi-pass welds were allowed to cool to below 212° F between passes.

Table 5—Summary of Test Results

Weld identification	Base metal	Gage, in.	Tensile strength, psi	Failure occurred in	Face bends 1	Face bends 2	Root bends 1	Root bends 2
GSTA 103*	90–10 Cu-Ni	1/8	43,600	Weld	OK	OK	OK	OK
			45,000	Weld				
GSTA 104	90–10 Cu-Ni	3/8	48,800	Base metal	OK	OK	OK	OK
			48,900	Base metal				
GSTA 102	70–30 Cu-Ni	1/8	48,800	Base metal	OK	Fracture occurred at edge of weld§	OK	OK
			50,800	Weld				
GSTA 100	70–30 Cu-Ni	3/8	50,700	Weld	OK	OK	OK	OK
			51,300	Weld				
GSMA 85†	90–10 Cu-Ni	1/8	43,900	Weld	OK	OK	OK	OK
			47,100	Weld				
GSMA 87	90–10 Cu-Ni	3/8	45,700	Base metal	OK	OK	OK	OK
			46,200	Base metal				
GSMA 86	70–30 Cu-Ni	1/8	48,300	Base metal	OK	OK	OK	OK
			50,600	Weld				
GSMA 89	70–30 Cu-Ni	3/8	52,000	Weld	OK	OK	OK	OK
			52,900	Weld				
GSMA 82‡	90–10 to 70–30 Cu-Ni	3/8	50,100	90–10 Cu-Ni	OK	OK	OK	OK
			50,500	90–10 Cu-Ni				
GSMA 84‡	90–10 Cu-Ni to mild steel	3/8	51,000	90–10 Cu-Ni	OK	OK	OK	OK
			51,800	90–10 Cu-Ni				
GSMA 83‡	70–30 Cu-Ni to mild steel	3/8	56,200	70–30 Cu-Ni	OK	OK	OK	OK
			56,300	70–30 Cu-Ni				

* The prefix GSTA indicates use of gas-shielded tungsten-arc process.
† The prefix GSMA indicates use of gas-shielded metal-arc process.
‡ Dissimilar joints were tested with longitudinal bends.
§ Face-bend failure in GSTA 102 obviously occurred as a result of faulty technique. This test plate was not remade.

The material used, of both the 70–30 and 90–10 alloys, conformed to the chemical and physical requirements given in ASTM B 171-55 and Mil-C-15726A (Ships) specifications.

Table 1 shows the chemical and mechanical requirements of these specifications.

All inert-gas-shielded metal-arc welds were made using 1/16-in. diam filler wire.

All inert-gas-shielded tungsten-arc welds were made using 1/8- and 3/32-in. diam filler metal in straight lengths.

Table 2 shows the analysis of the 70–30 cupro-nickel filler metal used in the experimental welding herein reported.

A total of 11 test plates was made and tested to compile the information included in this report. A summary of the information pertinent to joint geometry employed in the production of these test welds is shown in Table 3.

Table 4 is a summary of procedure details employed in the production of the test welds.

Inconsistencies noted in welding rod diameter used in the gas-shielded tungsten-arc welds were due to availability of material rather than optimum filler metal addition characteristics. Normally, welding rod diameters are selected so that filler metal added at the rate of 1 in. of rod per inch of weld or pass will produce the desired amount of reinforcement or depth of pass.

Mechanical Testing

All test plates were cut to provide two reduced-section-tensile, two face-bend, two root-bend specimens and one metallographic section for macroscopic examination.

The mechanical tests were conducted on a 100,000-lb capacity testing machine in conjunction with guided-bend testing jig.

The guided-bend tests were made on a mandrel or roll whose diameter was four times the thickness of the specimen being tested as prescribed by ASME procedure for weld qualification.

A summary of test results is shown in Table 5.

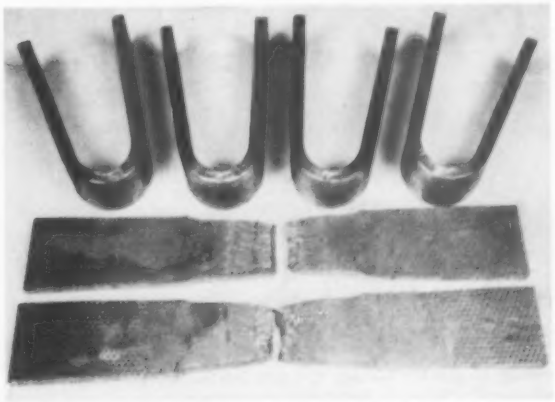

Fig. 3 Bend and tensile specimens of GSMA 89. Tensile specimens failed at 52,900 and 52,000 psi (see Table 5) with failure occurring in the weld metal. The base metal was 70–30 cupro-nickel

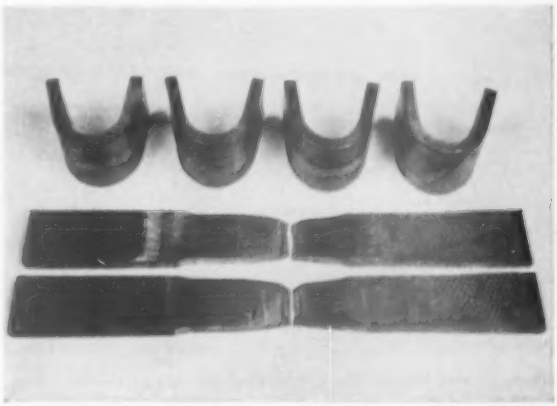

Fig. 4 Bend and tensile specimens of GSMA 84. Tensile specimens failed at 51,800 and 51,000 psi (see Table 5) with failure occurring in the 90–10 cupro-nickel. The base metals were 90–10 cupro-nickel and mild steel

It should be noted in Table 5 that all tensile specimens made in $^3/_8$-in. 90–10 cupro-nickel failed in the base metal, in some cases at considerable distance from the edges of the weld.

Tensile strengths in the welds made, employing 90–10 cupro-nickel as one of the base materials, averaged 47,900 psi or approximately 120% of the strength required for qualification.

Welds made employing 70–30 cupro-nickel as one of the base materials exhibited average tensile strengths of 51,570 psi or 104% of the strengths required for qualification.

Etchant: 1 part Precision No. 1, 1 part Etch No. 4, 1 part water. Magnification: X $7^1/_2$.

Fig. 5 A cross section of weld GSTA 103 made in $^1/_8$-in. 90–10 cupro-nickel using the gas-shielded tungsten-arc process. This weld was made without edge preparation and was completed in one pass

Etchant: 1 part Precision No. 1, 1 part Etch No. 4, 1 part water. Magnification: X $5^1/_2$.

Fig. 6 A cross section of weld GSTA 104 made in $^3/_8$-in. 90–10 cupro-nickel using the gas-shielded tungsten-arc process. This weld was made employing a 60-deg included angle and was completed in four passes. (Reduced by $^1/_2$ upon reproduction)

Etchant: 1 part Precision No. 1, 1 part Etch No. 4, 1 part water. Magnification: X $7^1/_2$.

Fig. 7 A cross section of weld GSTA 102 made in $^1/_8$-in. 70–30 cupro-nickel using the gas-shielded tungsten-arc process. This weld was made without edge preparation and was completed in one pass

Etchant: 1 part Precision No. 1, 1 part Etch No. 4, 1 part water. Magnification: X 5.

Fig. 8 A cross section of weld GSTA 100 made in $^3/_8$-in. 70–30 cupro-nickel using the gas-shielded tungsten-arc process. This weld was made employing a 60-deg included angle and was completed in four passes. (Reduced by $^1/_2$ upon reproduction)

Etchant: 1 part Precision No. 1, 1 part Etch No. 4, 1 part water. Magnification: X $7^1/_2$.

Fig. 9 Cross section of weld GSMA 85 made in $^1/_8$-in. 90–10 cupro-nickel using the gas-shielded metal-arc process. This weld was made without edge preparation and was completed in one pass

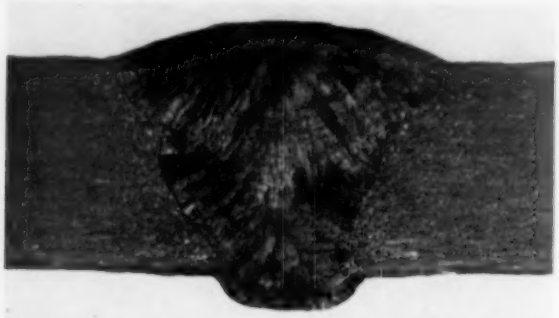

Etchant: 1 part Precision No. 1, 1 part Etch No. 4, 1 part water. Magnification: X 5.

Fig. 10 Cross section of weld GSMA 87 made in $^3/_8$-in. 90–10 cupro-nickel using the gas-shielded metal-arc process. This weld was made employing a 60-deg included angle and was completed in two passes

Etchant: 1 part Precision No. 1, 1 part Etch No. 4, 1 part water. Magnification: X 7 1/2.

Fig. 11 Cross section of weld GSMA 86 made in 1/8-in 70–30 cupro-nickel using the gas-shielded metal-arc process. This weld was made without edge preparation and was completed in one pass

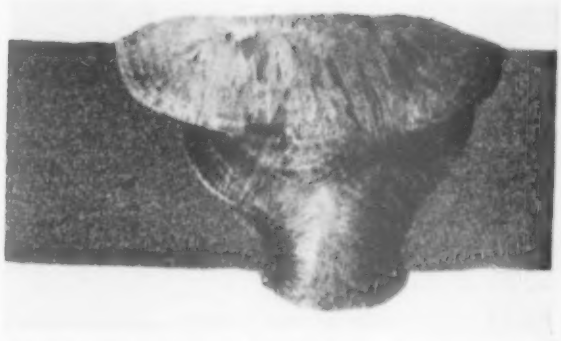

Etchant: 1 part Precision No. 1, 1 part Etch No. 4, 1 part water. Magnification: X 5.

Fig. 12 Cross section of weld GSMA 89 made in 3/8-in. 70–30 cupro-nickel using the gas-shielded metal-arc process. The weld was made employing a 60-deg included angle and was completed in two passes

Typical weld specimens made for this investigation are shown in Figs. 1, 2, 3 and 4, after mechanical tests were completed.

Metallographic

The metallographic sections taken from each test plate were submitted to the metallurgical section for examination. All sections showed complete absence of macroporosity.

Figures 5 through 15 are macrosections of the test weld as indicated in the captions.

The etchant which was used by the metallographic section for this investigation is composed of 1 part each of Precision No. 1, Etch No. 4 and distilled water. The composition of these etching solutions is as follows:

Precision No. 1
- 120 cc concentrated HNO_3
- 80 cc 36% CH_3COOH
- 5 cc concentrated NH_4OH
- 5 gm $CuNH_3Cl_2$

Etch No. 4
- 40 gm CrO_3
- 7.5 gm NH_4Cl
- 50 cc concentrated HNO_3
- 50 cc concentrated H_2SO_4
- H_2O to make 1 liter

Welding

In addition to the test welds described previously, restrained or "torture test" welds were made between 90–10 cupro-nickel and steel and 70–30 cupro-nickel and steel. This consisted of a 1 1/2- x 14- x 14-in. steel plate cut and beveled to size so that a 7-in. diam cupro-nickel plate could be welded into it. One of these completed welds is shown in Fig. 16.

These welds were made using these procedure details:

Welding current, 270/280 amp
Arc voltage, 25–27
Shielding gas, argon, 30 cfh
Welding speed—Pass No. 1, 16 ipm; Pass No. 2, 10–12 ipm; Passes No. 3 and No. 4, 20 ipm per pass.

These welds were completed without difficulty. No longitudinal or transverse cracking occurred during the execution of the root pass.

A cross section of this weld prior to the application of a reverse side weld is shown in Fig. 17.

While this investigation was in progress, the opportunity to set up welding procedures on several types of joints in cupro-nickel employing procedures similar to those used in the production of the test plates was encountered.

Some typical examples of these applications are shown in Figs. 18 through 24.

Figure 18 shows a weld in a 3/8-in. 90–10 cupro-nickel plate in which a butt joint was employed and complete penetration of the joint was required. Face and root welds were made with the gas-shielded metal-arc process without edge preparation and the following welding

Etchant: 1 part Precision No. 1, 1 part Etch No. 4, 1 part water. Magnification: X 5.

Fig. 13 Cross section of weld GSMA 82 made between 3/8-in. 70–30 cupro-nickel on the right and 90–10 cupro-nickel on the left of the joint using the gas-shielded metal-arc process. This weld was made employing a 60-deg included angle and was completed in four passes

Etchant: 1 part Precision No. 1, 1 part Etch No. 4, 1 part water. Magnification: X 5.

Fig. 14 Cross section of weld GSMA 84 made in 3/8-in. 90–10 cupro-nickel on the right side and mild steel on the left side of the joint using the gas-shielded metal-arc process. This weld was made employing a 60-deg included angle and was completed in four passes

Etchant: 1 part Precision No. 1, 1 part Etch No. 4, 1 part water. Magnification: X 5.

Fig. 15 Cross section of weld GSMA 83 made in $^3/_8$-in. 70–30 cupro-nickel on the left side and mild steel on the right side of the joint using the gas-shielded metal-arc process. This weld was completed in four passes. (Reduced by $^1/_2$ upon reproduction)

procedure details were employed:

Joint design, square butt
Backer, none
Welding current, 400 amp
Arc voltage, 30
Gas shield, argon, 30 cfh
Filler wire, $^1/_{16}$-in. diam 70–30 cupro-nickel
Welding speed, 24 ipm

The welding gun was attached to a variable speed travel carriage to accurately control the welding speed and the weld was made semiautomatically in one pass from each side.

Figure 19 shows four different joint designs which were required to fasten $^1/_4$- and $^1/_2$-in. shell sections to a $1^1/_4$- by $1^1/_2$-in. bolt ring.

The base metal is 90–10 cupro-nickel. Weld No. 1 is a 60-deg groove weld, No. 2 is a fillet weld between the $^1/_4$-in. shell and the $1^1/_4$- by $1^1/_2$-in. bolt ring, No. 3 is a 130-deg fillet weld and No. 4 is a 50-deg fillet weld.

These welds were made with the gas-shielded metal-arc process and the following welding procedure details:

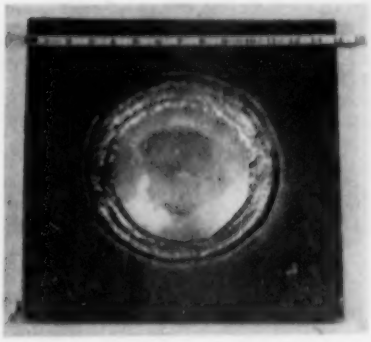

Fig. 16 Restrained weld between $^1/_2$- x 7-in. diam 90–10 cupro-nickel plate and $1^1/_2$- x 14- x 14-in. steel. Magnification X 0.2 (Reduced by $^1/_3$ upon reproduction.)

Fig. 17 Cross section of weld shown in Fig. 16 prior to the application of a reverse pass. Magnification X $2^1/_2$ (Reduced by $^1/_2$ upon reproduction.)

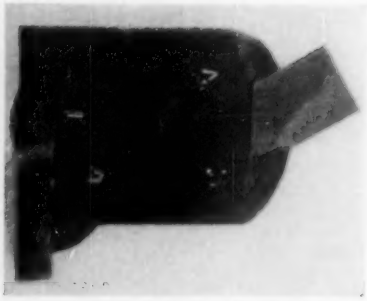

Etchant: 1 part Precision No. 1, 1 part Etch No. 4, 1 part water. Magnification: X $1^1/_2$.

Fig. 19 Cross section of multiple joints made to join $^1/_4$- and $^1/_2$-in. shell sections to $1^1/_4$- x $1^1/_2$-in. bolt ring. (Reduced by $^1/_2$ upon reproduction)

Weld No. →	*1*	*2*	*3*	*4*
Joint design	60-deg included angle	90-deg included angle	130-deg included angle	50-deg included angle
Welding current, amp	300/310	300/310	300/310	300/310
Arc voltage, v	28	28	28	28
Gas shield	Argon 30 cfh			
Filler wire	$^1/_{16}$-in. diam 70–30 cupro-nickel			
Welding speed, ipm/pass	18	18	12	18
Passes	2	1	1	1

Travel speed was automatically controlled.

Figure 20 shows another application and joint design in which the use of the gas-shielded metal-arc process and the 70–30 cupro-nickel filler wire successfully made a good weld between $^1/_4$-in. thick 90–10 cupro-nickel base metal and a $^1/_8$-in. thick 90–10 cupro-nickel backing strip.

The requirements for this joint were that it have a backing strip of the same material (90–10 cupro-nickel) as the base metal and the weld be made in a butt joint with penetration of the weld into the backing strip since it was impossible to reweld from the reverse side.

The second pass in this application is not shown so that visual examination of the penetration of the filler metal into

Etchant: 1 part Precision No. 1, 1 part Etch No. 4, 1 part water. Magnification: X 5.

Fig. 18 Cross section of weld made in $^3/_8$-in. 90–10 cupro-nickel using the gas-shielded metal-arc process. This weld was made without edge preparation and was completed in one pass from either side. (Reduced by $^1/_3$ upon reproduction)

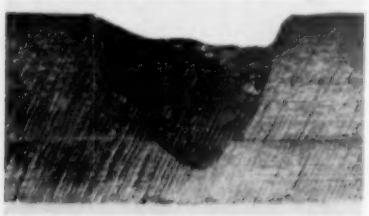

Etchant: 1 part Precision No. 1, 1 part Etch No. 4, 1 part water. Magnification: X 5.

Fig. 20 Cross section of the first pass of a weld made in $^1/_4$-in. thick 90–10 cupro-nickel against a $^1/_8$-in. thick 90–10 cupro-nickel backing bar using the gas-shielded metal-arc process. This weld was made employing a 60-deg included angle and was completed in two passes. Note the good penetration into the backing strip. (Reduced by $^1/_3$ upon reproduction)

Etchant: 1 part Precision No. 1, 1 part Etch No. 4, 1 part water. Magnification: X 3.

Fig. 21 Cross section of a tee joint in $^3/_8$-in. thick 90–10 cupro-nickel using the gas-shielded metal-arc process. Weld was made without edge preparation and was completed in one pass on each side of the upright member of joint (Reduced by $^1/_2$ upon reproduction)

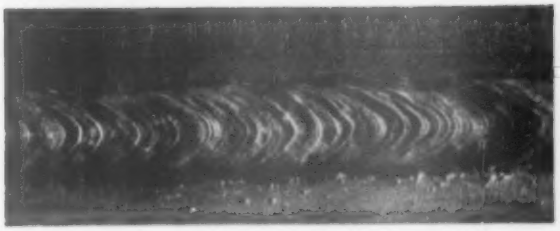

Fig. 22 A view of the typically uniform appearance of the completed weld shown in Fig. 21. Magnification: X $2^1/_2$ (Reduced by $^1/_2$ upon reproduction)

the backing strip can be more easily observed.

The welding procedure details for this application are as follows:

Travel speed was automatically controlled.

Joint design, square butt with $^1/_8$-in. root space
Backer, $^1/_{16}$-in. 90–10 cupro-nickel
Welding current, 310/320 amp
Arc voltage, 28/29 v
Gas shield, argon, 30 cfh
Filler wire, $^1/_{16}$-in. diam 70–30 cupro-nickel
Welding speed, 25 ipm/pass
Passes, 2

Figure 21 shows the use of a tee joint in 90–10 cupro-nickel plate $^3/_8$-in. thick. The cross section of the tee joint shows the good penetration of the base metal.

Figure 22 shows the typically uniform appearance of the completed welds.

The gas-shielded metal-arc process and the following welding procedure details were employed to make these fillet welds:

The travel speed was automatically controlled.

Joint design, tee
Welding current, 290/300 amp
Arc voltage, 30 v
Gas shield, argon 30 cfh
Filler wire, $^1/_{16}$-in. diam 70–30 cupro-nickel
Welding speed, 12 ipm
Passes, 1

A further example of the advantages of gas-shielded metal-arc welding and the adaptability of equipment is shown in Fig. 23. This shows a 90–10 cupro-nickel tube sheet ready for welding to a steel bolt flange.

In this case the gas-shielded metal-arc equipment was mounted on a cutting machine which employs a magnetic follower and a pattern to do shape cutting. This joint was similar to the joint used in the circular or restrained joint previously described and was automatically welded in a similar manner requiring four passes as before.

Figure 25 is an exograph of a one-pass weld in $^3/_{16}$-in. 70–30 cupro-nickel which was made by the gas-shielded metal-arc process employing fully automatic equipment. This test plate was made in $^3/_{16}$-in. 70–30 cupro-nickel without edge preparation.

The following procedure details were employed:

Welding current, 300 amp
Arc voltage, 26–28
Shielding gas, argon 30 cfh
Welding speed, 36 ipm

Discussion

During the course of this investigation of the 70–30 cupro-nickel welding wire, employing either of the gas-shielded arc processes, it was ascertained through the successful production of the 11 test welds that this is a satisfactory filler metal for welding the 70–30 and 90–10 cupro-nickels.

Table 5 shows the more than satisfactory tensile strengths usually obtained from these test welds. However, it should be pointed out that tensile strength attained in specimens GSTA 102 and GSMA 86 are lower than required under ASME Boiler and Pressure Vessel Code Welding Qualifications.

However, since the failure occurred in the base metal outside of the weld or fusion line, which makes a tensile

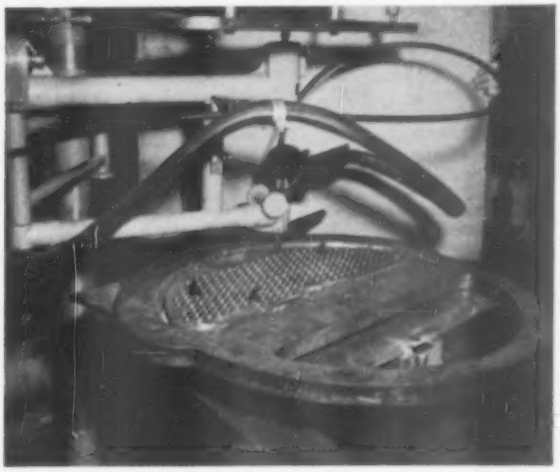

Fig. 23 Manner in which the equipment was employed to automatically weld a joint of irregular shape

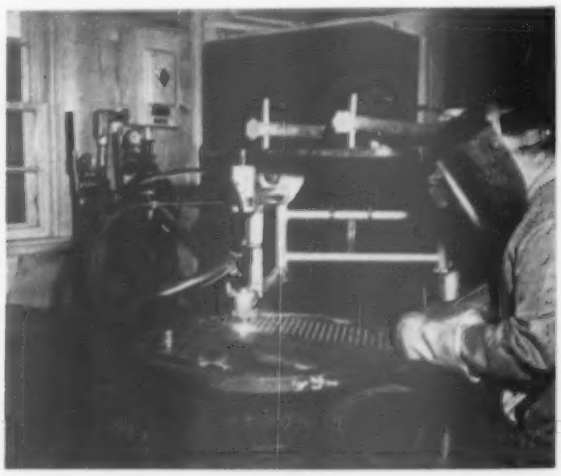

Fig. 24 Welding in progress

strength of not more than 5% below the minimum tensile strength of the base metal satisfactory for qualification, the strengths obtained are acceptable.

Inasmuch as the minimum tensile strength required of the 70–30 cupro-nickel is 50,000 psi and the permissible 5% below that figure would make the minimum tensile requirement 47,500 if failure occurs in the base metal, GSTA 102 at 48,800 psi and GSMA at 48,600 psi would easily qualify.

The $^1/_8$-in. gage cupro-nickel in all test welds consistently produced tensile strengths lower than comparable test welds in the $^3/_8$-in. cupro-nickel. It is, therefore, believed that the wider area of dendritic structure and possible grain growth in the $^1/_8$-in. cupro-nickel caused by the greater heat dissipation into the porportionately wide weld in the thinner material resulted in rapid necking down of the tensile specimens in this dendritic area accompanied by consistently lower tensile strengths than those obtained in the $^3/_8$-in. cupro-nickel.

Fig. 25 View of an exograph of a weld in 70–30 cupro-nickel using the gas-shielded metal-arc process. This weld was made without edge preparation and was completed in one pass

Conclusions

1. Filler metal of substantially the chemical composition shown in Table 2 will produce sound welds having good mechanical properties when used with either of the inert-gas-shielded arc processes.

2. This filler metal will produce equally satisfactory welds in either 70–30 cupro-nickel or 90–10 cupro-nickel. It is also suitable for welding these alloys to each other and will produce satisfactory joints between either of these alloys and mild steel.

3. No special techniques are required; therefore, welding procedures used with this filler metal are uncomplicated.

4. Restrained joints can be satisfactorily executed between cupro-nickel and mild steel employing this filler wire.

Acknowledgment

The writers wish to express their appreciation for the cooperation of the following Research Department personnel who contributed their efforts to the development of the information contained in this report: A. P. Tomeo and A. P. Lane, metallographic examination; R. P. Destito, mechanical testing; R. H. VanDeMark, photography; and R. H. Hahn, chemical analyses.

BULLETIN SERIES *(Continued from page 400-s)*

No. 15 **Slag-Metal Interaction in Arc Welding,** *by Nils Christensen and John Chapman, January 1953. $1.00.*

No. 16 **Ship Structure Research, Part I—The Third Technical Report of the Ship Structure Committee; Part II—Research Under the Ship Structure Committee,** *by Capt. E. A. Wright, Finn Jonassen and H. G. Acker, November 1953. $2.00.*

No. 17 **A Critical Survey of Brittle Failure in Carbon Steel Structure Other Than Ships,** *by M. E. Shank, January 1954. $2.00.*

No. 18 **Testing of Stainless-Steel Weldments,** *by Helmut Thielsch, September 1954. $1.00.*

No. 19 **Review of Welded Ship Failures,** *by Harold G. Acker, November 1954. $1.00.*

No. 20 **High-Strength, Low-Alloy Steels; Analytical Chemistry Fosters Progress in Steelmaking; Steel Quality;** *by Charles M. Parker, January 1955. $1.00.*

No. 21 **Coating Moisture Investigations of Austenitic Electrodes of the Modified 18–8 Type,** *by K. P. Johannes, D. C. Smith and W. G. Rinehart, February 1955. $1.00.*

No. 22 **Welded Tee Connections,** *by A. G. Barkow and R. A. Huseby, May 1955. $1.00.*

No. 23 **Cracking of Simple Structural Geometries,** *by S. T. Carpenter and R. F. Linsenmeyer, July 1955. $1.00.*

No. 24 **Nickel and High-Nickel Alloys for Pressure Vessels,** *by R. M. Wilson, Jr., and W. F. Burchfield, January 1956. $1.00.*

No. 25 **Bibliography on The Welding of Stainless Steels, 1926–1955 with Author Index,** *by Katherine Janis, March 1956. $1.00.*

No. 26 **Investigation of the Influence of Deoxidation and Chemical Composition on Notched-Bar Properties of Ship Plate Steels,** *by F. W. Boulger, R. H. Frazier and C. H. Lorig, April 1956. $1.00.*

No. 27 **Mechanical Properties and Weldability of Six High-Strength Steels,** *by R. D. Stout and J. H. Gross; Economic but Safe Pressure-Vessel Construction, by J. J. Murphy, C. R. Soderberg, Jr., and D. B. Rossheim, May 1956. $1.00.*

No. 28 **Aluminum and Aluminum Alloys for Pressure Vessels,** *by Marshall Holt, June 1956. $1.00.*